

**İZMİR KATİP ÇELEBİ UNIVERSITY ★ GRADUATE SCHOOL OF SCIENCE AND
ENGINEERING**

**DESIGN AND DEVELOPMENT OF A COLLIMATOR MECHANISM THAT
WILL BE UTILIZED IN RADIATION THERAPY**

M.Sc. THESIS

Mustafa Volkan YAZICI

Department of Mechanical Engineering

Thesis Advisor: Assist. Prof. Dr. Erkin GEZGİN

JANUARY 2018

**İZMİR KATİP ÇELEBİ UNIVERSITY ★ GRADUATE SCHOOL OF SCIENCE AND
ENGINEERING**

**DESIGN AND DEVELOPMENT OF A COLLIMATOR MECHANISM THAT
WILL BE UTILIZED IN RADIATION THERAPY**

M.Sc. THESIS

**Mustafa Volkan YAZICI
(Y150105006)**

Department of Mechanical Engineering

Thesis Advisor: Assist. Prof. Dr. Erkin GEZGİN

JANUARY 2018

İZMİR KATİP ÇELEBİ ÜNİVERSİTESİ ★ FEN BİLİMLERİ ENSTİTÜSÜ

**RADYOTERAPİDE KULLANILMAK ÜZERE KOLİMATÖR MEKANİZMASI
TASARIMI VE GELİŞTİRİLMESİ**

YÜKSEK LİSANS TEZİ

**Mustafa Volkan YAZICI
(Y150105006)**

Makine Mühendisliği Bölümü

Tez Danışmanı: Yrd. Doç. Dr. Erkin GEZGİN

OCAK 2018

Mustafa Volkan YAZICI, a M.Sc. student of İzmir Katip Çelebi University Graduate School of Science and Engineering student ID **Y150105006**, successfully defended the thesis entitled “**DESIGN AND DEVELOPMENT OF A COLLIMATOR MECHANISM THAT WILL BE UTILIZED IN RADIATION THERAPY.**”, which he prepared after fulfilling the requirements specified in the

Thesis Advisor: **Assist. Prof. Dr. Erkin GEZGİN**
İzmir Katip Çelebi University

Jury Members: **Assist. Prof. Dr. Fatih Cemal CAN**
İzmir Katip Çelebi University

Assoc. Prof. Dr. Mehmet İsmet Can Dede
İzmir Institute of Technology

Date of Submission: 20 December 2017
Date of Defense : 05 January 2018

to my family,

FOREWORD

First of all, I would like to thank my supervisor Assist. Prof. Dr. Erkin Gezgin who taught, supported and believed to me.

I also would like to thank each member of Mechatronics Engineering Department to let me study in the laboratories throughout the research.

I would like to thank my family who supported me every time.

This collaboration project between İKCU İzmir Katip Çelebi University and DGIST-Daegu Gyeongbuk Institute of Science & Technology was funded by DGIST. I would also like to thank DGIST for their collaboration and support in this project.

January 2018

Mustafa Volkan YAZICI

TABLE OF CONTENTS

FOREWORD	ix
TABLE OF CONTENTS	xi
ABBREVIATIONS	xiii
LIST OF TABLES	xv
LIST OF FIGURES	xvii
SUMMARY	xxi
ÖZET	xxiii
1. INTRODUCTION	1
1.1 Basic Concepts: Radiation Therapy	1
1.1.1 Treatment principle	1
1.1.2 Cell cycles	1
1.1.3 Effects of radiation therapy on healthy tissue	3
1.1.4 Purpose of radiation therapy	3
1.1.5 Decision factors for radiation therapy method.....	4
1.1.6 Types of radiation therapy	4
1.2 Field Blocking and Shaping Devices	5
1.2.1 Type of collimators	5
1.2.2 Advantages and disadvantages of collimators	10
1.2.3 Beam delivery problems	10
1.2.4 Radiation therapy manipulators	15
1.2.5 Multileaf collimators-MLCs	19
1.2.6 Working principles of collimators and linear accelerators.	19
1.3 Statement of Research.....	24
1.4 Literature Survey.....	25
2. DESIGN AND DEVELOPMENT OF COLLIMATOR MECHANISM	29
2.1 Research Constraints and Goals.....	29
2.2 Preliminary Design.....	32
2.3 Preliminary Kinematic Analysis	35
2.4 Modified Design.....	37
2.5 Modified Kinematic Analysis	43
2.6 Prototype Manufacturing	44
3. MODIFICATION OF THE COLLIMATOR PROTOTYPE	47
3.1 Modification Reasons.....	47
3.2 Modified Design.....	48
3.3 Prototype Manufacturing	61
4. SELECTION OF ACTUATORS	65
4.1 Design Constraints	65
4.2 Calculations.....	68
5. PROTOTYPE TRIALS	73
6. THEORETICAL MODIFICATION OF LOWER JAW DESIGN	77

6.1 Kinematic Synthesis	81
6.1.1 Types of kinematic synthesis	81
6.1.2 Types of approximations.....	95
6.2 Integration of the Function Generation Synthesis into Design of a Collimator Mechanism	110
7. CONCLUSION.....	117
REFERENCES.....	119
CURRICULUM VITAE	123

ABBREVIATIONS

2DXRT	: Conventional External Beam Radiation Therapy
CTV	: Clinical Target Volume
EBRT	: External Beam Radiation Therapy
HI	: Homogeneity Index
IMRT	: Image Guided Radiation Therapy
LINAC	: Linear Accelerator
MLC	: Multileaf Collimator
PTV	: Planning Target Volume – Planning Tumor Volume
RF	: Radio Frequency
SAD	: Source to Isocenter Distance
SSD	: Source to Skin Distance
SBRT	: Stereotactic Body Radiotherapy

LIST OF TABLES

	<u>Page</u>
Table 1.1 : Comparison of delivered MU and treatment time.. ..	9
Table 4.1 : Difference in physical properties between first and second design of collimator mechanism.	63
Table 7.1 : Defined structural parameters of the collimator.	115
Table 7.2 : Precision point sets and calculated parameters.	116

LIST OF FIGURES

	<u>Page</u>
Figure 1.1: Cell Cycle	2
Figure 1.2: Illustration of beam radiation therapy.	5
Figure 1.3: Leaf arrangement examples of MLCs.	5
Figure 1.4: Fixed collimators and collimator housing.	6
Figure 1.5 : Iris variable aperture collimator.	7
Figure 1.6 : Detailed view of the multileaf collimator’s leaf banks.	8
Figure 1.7: Transverse view of dose distributions of IRIS and MLC.....	9
Figure 1.8 : Illustration of (a) end leaf transmission, (b) leaf transmission and (c) interleaf transmission... ..	11
Figure 1.9 : Illustration of the penumbra	12
Figure 1.10 : Illustration of transmission penumbra and its reason.	12
Figure 1.11: Illustration of the geometrical penumbra.	13
Figure 1.12 : Illustration of scatter.....	14
Figure 1.13 : Gamma Knife beam delivery system	16
Figure 1.14 : C-Arm beam delivery system.....	16
Figure 1.15 : Tomotherapy beam delivery system.....	17
Figure 1.16 : CyberKnife ® beam delivery system.	17
Figure 1.17 : Vero® beam delivery system	18
Figure 1.18 : ViewRay ® concept beam delivery system.....	18
Figure 1.19 : Standard MLC	19
Figure 1.20 : Illustration of LINAC	20
Figure 1.21 : Components of LINAC head.....	22
Figure 2.1 : Four Degrees of Freedom Robot Manipulator.	33
Figure 2.2 : Working Principle of Four Degrees of Freedom Robot Manipulator (Position and Shape Change of Rectangular Window Opening in Front of the Beam Tube).....	33
Figure 2.3 : Various versions of target treatments. a) Without collimator mechanism, b) Collimator with a fixed gateway window that can be positioned, c) Collimator with variable shape gateway window that can be positioned. ...	34
Figure 2.4 : Illustration pattern generation with rectangular and circular window... ..	35
Figure 2.5 : Collimator mechanism that is placed in front of the beam tube that is positioned on the center of the target.	36
Figure 2.6 : Illustration of difference between cartesian coordinate and cylindrical coordinate mechanism.	37
Figure 2.7: Four Degrees of Freedom Modified Robot Manipulator.	38
Figure 2.8 : Working Principle of Four Degrees of Freedom Modified Robot Manipulator (Position and Shape Change of Rectangular Window Opening in Front of the Beam Tube).....	38
Figure 2.9 : 3D models of jaws.	39

Figure 2.10 : R-Guide rails connection with upper jaws a) Inside view b) Outside view behind the transparent base wall.	39
Figure 2.11 : Linear bushing assembled into the linear jaw.	40
Figure 2.12 : Ball Screw used in Collimator mechanism.....	40
Figure 2.13 : Upper jaw actuation scheme.....	41
Figure 2.14 : Position and shape change of rectangular window opening in front of the beam tube.	42
Figure 2.15 : Isometric view of collimator mechanism.	43
Figure 2.16 : Collimator section cut.....	43
Figure 2.17 : Modified Collimator Mechanism with Circular Jaws.	44
Figure 2.18 : Some of the bulk materials, Pre-Manufacturing.....	45
Figure 2.19 : Some of the machined parts.....	45
Figure 2.20 : Assembly period from top.	45
Figure 2.21 : Assembly period, close up, stabilizers and circular rails are visible. ..	46
Figure 2.22 : Assembly period, isometric view, actuator mounts are visible.	46
Figure 3.1 : Jaw arrangement of Collimator mechanism.	49
Figure 3.2 : Motion transfer through upper jaw.	50
Figure 3.3 : Circular motion guide and its assemble.....	50
Figure 3.4 : Divided upper jaw and rail-track assemble.	51
Figure 3.5 : Assembly of track and first peace of jaw.	51
Figure 3.6 : Upper jaw assembly.....	52
Figure 3.7 : Lower jaw and linear bushing assemble.....	52
Figure 3.8 : Lower jaw and wall connection.	53
Figure 3.9 : Linear actuator connection.	54
Figure 3.10 : Upper section and lower section of collimator mechanism.....	54
Figure 3.11 : Holes on the wall that allows to reach lower jaw.	55
Figure 3.12 : Connection of walls.	55
Figure 3.13 : Connection of DC motor to the wall and motion transfer to the jaw. ..	56
Figure 3.14 : Stabilization bars on assembly.	57
Figure 3.15 : Parts manufactured by rapid prototyping devices.	58
Figure 3.16 : Collimator mechanism inside the cylindrical tube.	58
Figure 3.17 : Isometric view of the Collimator mechanism.....	59
Figure 3.18 : Front view of the Collimator mechanism.	59
Figure 3.19 : Top view of the collimator mechanism.	60
Figure 3.20 : Side view of the collimator mechanism.	60
Figure 3.21 : Rapid prototyping simulation and manufacturing of the upper jaw actuator connector.	61
Figure 3.22 : CNC machining of jaw rod.....	62
Figure 3.23 : Assembling of the jaws and walls.	62
Figure 3.24 : Collimator mechanism.....	63
Figure 3.25 : Three different positions and dimensions of opening.	64
Figure 4.1 : Rigid connections of upper jaw actuator.	66
Figure 4.2 : Rigid coupling mounted to actuator.	66
Figure 4.3 : Fixing of actuator.....	66
Figure 4.4 : Actuator of lower jaw and its connection.....	67
Figure 4.5 : Stripped lower jaw assembly to simulation.....	68
Figure 4.6 : Lower jaw actuator force requirement.....	69
Figure 4.7 : Stripped upper jaw assembly to simulation.....	70
Figure 4.8 : Upper jaw actuator force requirement.	70
Figure 5.1 : Prototype trial setup.....	73

Figure 5.2 : Lower jaw motion pose 1.	74
Figure 5.3 : Lower jaw motion pose 2.	74
Figure 5.4 : Lower jaw motion pose 3.	74
Figure 5.5 : Upper jaw motion pose 1.....	75
Figure 5.6 : Upper jaw motion pose 2.....	75
Figure 5.7 : Upper jaw motion pose 3.....	75
Figure 6.1 : Scattering regions of the point source and their variations for different positions of the collimator leaves.	78
Figure 6.2 : Proposed collimator with vertically layered multi leaf stacks, and reduced scattering regions.....	79
Figure 6.3 : Multiple slider crank mechanisms on both sections of the collimator. Leaves that are formed by the sliders on individual sections are controlled by single input.....	80
Figure 6.4 : Four-bar mechanism represented with its closed-loop parameters.	82
Figure 6.5 : Error graph of three precision points synthesis.	85
Figure 6.6 : Modified four-bar mechanism with respect to four precision points. ...	86
Figure 6.7 : Error graph of four precision points synthesis.	89
Figure 6.8 : Comparison between three and four precision points synthesis errors.	89
Figure 6.9 : Modified four-bar mechanism with respect to five precision points.....	90
Figure 6.10 : Error graph of five precision points synthesis.	94
Figure 6.11 : Comparison between three, four and five precision points synthesis errors.	95
Figure 6.12 : Illustration of output of Chebyshev approximation.....	95
Figure 6.13 : Expected first result of Chebyshev approximation.	98
Figure 6.14 : Derivative of objective function.....	99
Figure 6.15 : Error graph of Chebyshev approximation's first solution.....	101
Figure 6.16 : Derivative of objective function.....	102
Figure 6.17 : Error graph of first iteration.	102
Figure 6.18 : Derivative of first iteration's objective function.	103
Figure 6.19 : Error graph of second iteration.....	104
Figure 6.20 : Derivative of second iteration's objective function.	104
Figure 6.21 : Error graph of third iteration.	105
Figure 6.22 : Error graph of least square approximation.	109
Figure 6.23 : Combined error graph.....	110
Figure 6.24 : Multiple slider crank mechanisms on both sections of the collimator. Leaves that are formed by the sliders on individual sections are controlled by single input.....	111
Figure 6.25 : Offset of the second collimator layer ($a_2=a_1+t$).	113
Figure 6.26 : Construction and variable parameters of the second layer.....	114
Figure 6.27 : Modelled collimator and its motion through three configurations....	116

DESIGN AND DEVELOPMENT OF A COLLIMATOR MECHANISM THAT WILL BE UTILIZED IN RADIATION THERAPY

SUMMARY

This thesis focuses on a Multileaf Collimator design that can shape the beam contour to fit the shape of target geometry and its design improvements. Main purpose of this design is lowering the number of leaves on the multileaf collimator and making the system easier to be controlled. As the Collimator devices undertake the most important point of the beam shaping procedure, ease of control and precision of collimator devices are the major points of operation.

As the radiation therapy is one of the most complex and vital medical operations, this thesis started with the deep literature survey that formed the main constraints and goals of the study. Additional constraints and goals were formed after the examination of commercial purpose collimators with respect to their advantageous and disadvantageous sides. Collimator devices either primary or secondary are integratedly used with Linear accelerators thus, linear accelerator devices were taken as another important factor that formed the constraints of design.

First design of the collimator mechanism was started with the type and number synthesis. After this procedure, collimator mechanism was decided to be four degree of freedom decoupled manipulator that works in Cartesian coordinate system. After the main design was finished, study of the kinematic analysis of the decoupled mechanism was performed.

Due to the fact that radiation therapy robot manipulators carry the collimator mechanisms and motion of the overall system may generate high inertia forces, weight of the collimator mechanism and footprint of the collimator mechanism were also aimed to be reduced.

After the first design, upper jaws were modified to be work in polar coordinates instead of cartesian coordinate system. This modification was not only reduced footprint of the device but also reduced scattering issues caused from angular relation between beam and leaf side surface. This modification followed by manufacturing of the first prototype. Examination of the first prototype gave the final shape to the constraints and goals to the collimator design as further advancing in weight and footprint reduction. By using these final constraints second modification was performed to the system and second prototype was manufactured.

İŞİN TEDAVİSİNDE KULLANILMAK ÜZERE ÇOK YAPRAKLI KOLİMATÖR TASARIMI

ÖZET

Bu tez ışın kontürünü hedef geometriye uyduracak olan çok yapraklı kolimatör tasarımını ve iyileştirmelerini sunmaktadır. Tasarımın ana amacı çok yapraklı kolimatörün yaprak sayısını azaltmak ve cihazın kontrolünü basitleştirmektir. Kolimatör cihazı ışının şekillendirilmesi prosedüründe en önemli noktayı üstlendiği için kolimatörün kontrol kolaylığı ve hassasiyeti operasyonun önemli bir noktasıdır.

Işın tedavisi medikal operasyonların en karmaşık ve hayati olanlarından biri olduğu için kolimatör tasarımının kısıtlarını ve hedeflerini şekillendirecek olan derin bir literatür taramasına bu tezde yer verilmiştir. Kolimatörün tasarımı için ilave kısıt ve hedefler ticari maksatlı kolimatör cihazların incelenmesinden elde edilen avantaj ve dezavantajlarla şekillendirilmiştir. Kolimatör cihazı ister ilkil ister ikincil olsun lineer hızlandırıcılara entegre olarak çalıştığından kısıt ve hedeflerin belirlenmesinde bir diğer önemli unsur lineer hızlandırıcılar olmuştur.

Kolimatör cihazının ilk tasarımına tip ve sayısal sentezle başlaşılmıştır. Bu prosedüreden sonra kolimatör mekanizmasının kartezyen koordinat sisteminde çalışacak dört serbestlik dereceli ayrıştırılmış bir manipulator olmasına karar verilmiştir. İlk tasarım tamamlandıktan sonra ayrışık mekanizmanın kinematik analizi yapılmıştır. Kinematik analiz safhasında Wolfram Mathematica yazılımı denklem çözdürücü olarak kullanılmıştır.

Radyasyon terapisi robot manipülatörlerinin kolimatörü taşımasından ve genel sistemin hareketinin yüksek atalet kuvvetleri yaratabilmesinden dolayı iyileştirmeyle, kolimatör mekanizmasının kütlelerinin ve kapladığı alanın azaltılması hedeflendi.

İlk iyileştirmeden sonra üst çeneler kartezyen koordinat yerine polar koordinat sisteminde çalışacak şekilde modifiye edilmiştir. Bu modifikasyon yalnızca kapladığı alanı azaltmamış olup aynı zamanda ışınla çenelerin yan yüzeyi arasındaki açısal ilişkidir kaynaklanan yansıma sorununu da azaltmıştır. Bu modifikasyonları ilk prototipin üretilmesi takip etmiştir. İlk prototipin incelenmesi ağırlık ve izdüşüm alanında daha da gelişme sağlamak için kolimatör tasarımının kısıt ve hedeflerine son halini vermiştir. En son kısıtlar kullanılarak ikinci modifikasyon yapılmış olup ikinci prototip üretilmiştir.

1. INTRODUCTION

1.1 Basic Concepts: Radiation Therapy

Radiation therapy uses high-energy radiation to shrink tumors and kill cancer cells. X-rays, gamma rays, and charged particles are the types of radiation that are utilized for cancer treatment.

There are two types of delivery methods during the treatment. The radiation may be delivered either by a machine positioned outside the body (external-beam radiation therapy), or by a radioactive material placed inside the body near cancer cells (internal radiation therapy, also called brachytherapy) [1,2].

1.1.1 Treatment principle

Radiation therapy kills cancer cells by damaging their DNA (the molecules inside cells that carry genetic information and pass it from one generation to the next). This procedure can be applied either directly or indirectly by creating charged particles (free radicals) within the cells in order to damage the DNA.

Cancer cells whose DNA is damaged beyond repair stop division or die. When these cells die, they are broken down and eliminated by the body's natural processes in time. In order to understand this process, cell cycle should be mentioned clearly to reveal the changes during radiation therapy [1,2].

1.1.2 Cell cycles

Let's consider the regular life cycle of a cell prior to understand radiation treatment. The cell cycle has actually 5 phases and only one of them is the actual cell division. This 5-phase process is controlled by proteins known as cyclin-dependent kinases (CDKs). As they are so important during normal cell division, they too have a number of control mechanisms.

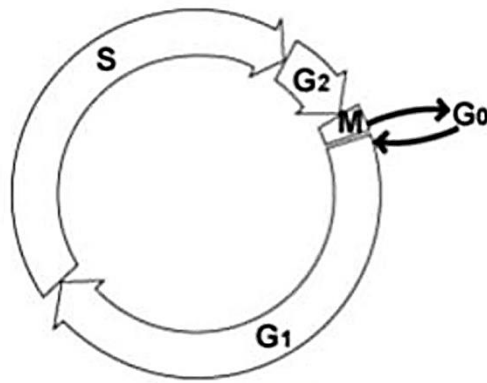


Figure 1.1: Cell Cycle [3]

Figure 1.1 illustrates the normal cell cycle of healthy conditions. In G0 phase Cell rests (it's not dividing) and does its normal work in the body. G1phase which follows G0 phase is the preparation phase for division. RNA and proteins are made for cell division in this phase. S phase represents the synthesis of DNA which is made for new cells. In G2 phase apparatus for mitosis is built. After RNA, proteins, DNA and apparatus for mitosis was built. M phase has been started and in this phase mitosis occurs and the cell divides into 2 cells.

1.1.2.1 Steps of the cell cycle

As represented in figure 1.1 and mentioned earlier, cell cycle includes free steps that are defined and explained below.

G0 phase (resting stage): At this stage cells will not divide and spend much of their lives in this phase by carrying out their day-to-day body functions. Depending on the type of the cells, this stage can last for a few hours or many years. When the cell gets the signal for division, it moves into G1 phase.

G1 phase: At this stage cells get information that determines when they will go into the next phase. They start making more proteins to prepare for division. RNA's needed to copy DNAs are also created in this phase. This phase lasts about 18 to 30 hours.

S phase: In this phase, the chromosomes (which contain the genetic code or DNA) are copied so that both of the new cells formed will have the same DNA. This phase lasts about 18 to 20 hours.

G2 phase: Additional information about proceeding with cell division is gathered during this phase. The G2 phase happens just before the cell starts splitting into 2 cells. This stage lasts from 2 to 10 hours.

M phase (mitosis): In this final phase, which lasts only 30 to 60 minutes, cells divide into two cells that have exactly the same properties.

As it can be clearly seen from the steps radiation therapy focuses on interrupting cell division cycle so that cancer cell division and population growth will be interrupted.

1.1.3 Effects of radiation therapy on healthy tissue

Radiation therapy can also damage normal healthy cells, leading many side effects. Thus, doctors usually take precaution to prevent potential damage to these cells by planning a safe course of radiation therapy. Due to the fact that the amount of radiation that normal tissue can safely receive is known for all parts of the body, this information is issued by the doctors to plan treatment procedure (External radiation therapy section) [2].

1.1.4 Purpose of radiation therapy

Radiation therapy is sometimes used for curative intent with the hope that the treatment will cure cancer, either by eliminating a tumor, preventing cancer recurrence, or both. In such cases, radiation therapy may be used as sole treatment or in combination with surgery, chemotherapy, or both. Radiation therapy may also be used for palliative intent. Palliative treatments are not intended to cure. Instead, they relieve symptoms and reduce the suffering caused by the cancer [1,2].

Some examples of palliative radiation therapy are:

- Radiation treatment on the brain to shrink tumors formed from cancer cells that have spread to the brain from another parts of the body (metastases).
- Radiation therapy to shrink a tumor that is pressing to the spine or growing within a bone, which can cause excessive pain.
- Radiation therapy to shrink a tumor near the esophagus, which can interfere with a patient's ability to eat and drink.

1.1.5 Decision factors for radiation therapy method

Similar to the other types of the treatment methods, cancer treatment also needs some changes depending on patient's or disease's situation. These differences affect the selected radiation therapy method that will be applied to the patient [2].

The main factors that affect the treatment decision can be listed as,

- Type of the cancer.
- Size of the cancer area.
- Cancer's location inside the body.
- Cancer proximity to normal tissues that are sensitive to radiation.
- Travel distance of the radiation beam.
- The patient's general health and medical history.
- Patient's treatment history.
- Other factors, such as the patient's age and other important medical conditions.

1.1.6 Types of radiation therapy

As mentioned before there exists two types of radiation therapy method as internal radiation therapy and external radiation therapy.

1.1.6.1 Internal radiation therapy (Brachytherapy)

Brachytherapy is an advanced cancer treatment. Radioactive seeds or sources are placed inside or to the areas near the tumor, giving a high radiation dose to the related tumor while reducing the radiation exposure in the surrounding healthy tissues. The term "brachy" comes from Greek for short distance. Brachytherapy is radiation therapy given at a short distance: localized, precise, and high-tech [4].

1.1.6.2 External radiation therapy (Beam radiation therapy)

External beam radiation therapy (EBRT) directs a beam of radiation from outside the body to the cancerous tissues inside the body figure 1.2. It is a cancer treatment option that uses enough doses of radiation to destroy cancerous cells and shrink tumors. Examples of EBRT include 3D conformal radiation therapy, IMRT, IGRT, TomoTherapy and stereotactic radiosurgery [1]

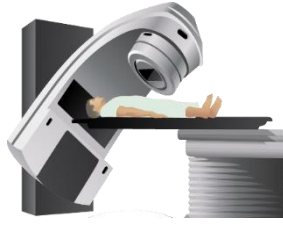


Figure 1.2: Illustration of beam radiation therapy.

As mentioned before, regions exposed to radiation therapy during the treatment include not only cancer cells but also healthy tissues. Due to this situation there exist a need for additional mechanism called field blocking and beam shaping devices (figure 1.3). In external radiation therapy, these devices are used for shaping the linear accelerated particles path and cross-sectional area [2].

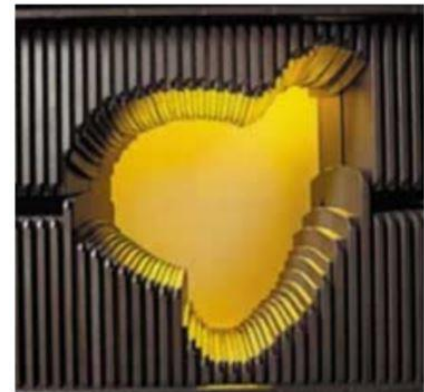
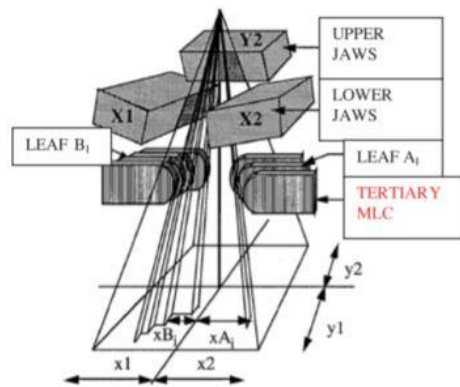


Figure 1.3: Leaf arrangement examples of MLCs [5,6].

1.2 Field Blocking and Shaping Devices

In order to prevent healthy tissue radiation exposure during the treatment, there exist many design utilizing shielding blocks, custom blocks, asymmetrical jaws and multileaf collimators. These collimators act as deflectors and guides for the beam to reach its target by minimal healthy tissue exposure.

1.2.1 Type of collimators

Prior to beam treatment operation additional criterias should also be examined in order to select the correct method and equipment. In the light of this, collimator selection plays an important role that will affect the duration and increase the success

rate of the operation. In this section, collimators are examined in three titles in terms of their structures.

- Fixed Collimators
- Iris Variable Aperture Collimator
- Multileaf Collimator

It should be noted that collimators listed above are secondary collimators. This section of radiation therapy devices is located at end of the system where the beam exits for the target. Some systems use multiple secondary collimator sizes that can be changed automatically or manually during the treatment to deliver beams as defined by the procedural plan.

1.2.1.1 Fixed collimators

Some systems are supplied with fixed secondary collimators (figure 1.4) delivering circular field sizes ranging from 5mm to 60 mm diameter at 800mm SAD (Source to isocenter distance- axis of gantry rotation) These collimators can be changed to vary the beam size as defined by the treatment plan. For each fixed collimator, the manipulator traverses a separate path with respect to a different treatment plan [7].

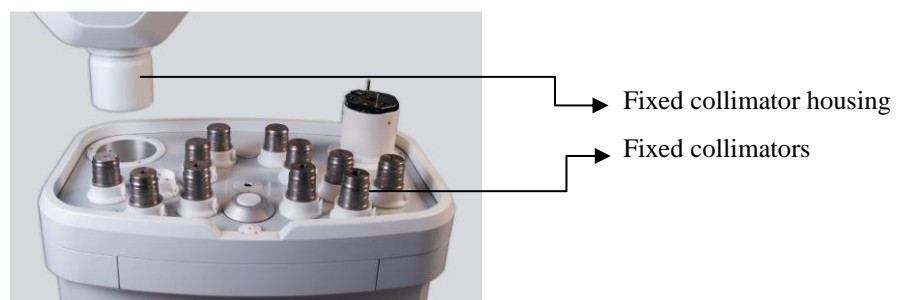


Figure 1.4: Fixed collimators and collimator housing [7].

1.2.1.2 Iris™ variable aperture collimator

The Iris Variable Aperture Collimator (figure 1.5) creates beams with characteristics virtually identical to those of fixed collimators. It consists of two banks of 6 tungsten segments with a hexagonal aperture. As the banks are offset by 30° relative to each other, the design resulting in a dodecahedral (12-sided) aperture when

viewed from one end of the collimator to the other. The Iris Variable Aperture Collimator replicates the existing 12 fixed collimator sizes. The rationale for an iris collimator that allows the field size to be varied during treatment delivery is to enable the benefits of multiple-field-size treatments to be realized with no increase in treatment time due to collimator exchange or multiple traversals of the robotic manipulator by allowing each beam to be delivered with any desired field size during a single traversal [7,8].

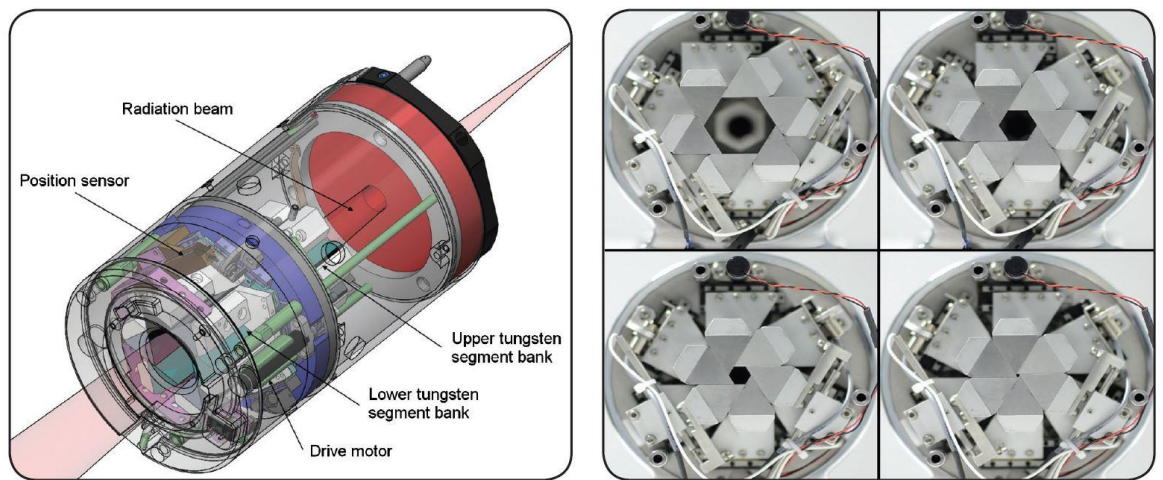


Figure 1.5 : Iris variable aperture collimator [7].

1.2.1.3 Standard multileaf collimator

The Multileaf Collimators (figure 1.6) creates highly conformal beam shapes in relation to the treatment targets and has larger field sizes than the Iris or fixed collimators, enabling the system to treat much larger targets with significantly fewer beams and delivered MU (MU-Monitor unit, a measure of radiation “beam-on” time used for linear accelerators. By convention, one monitor unit equals to one cGy of absorbed in water under specific calibration conditions for the medical Linacs). This results in much faster treatment times and greatly expands the clinical utility of the treatment delivery system [9].

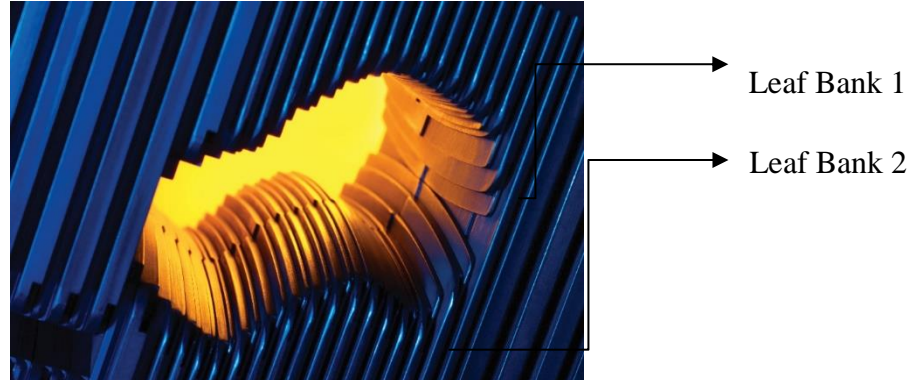


Figure 1.6 : Detailed view of the multileaf collimator's leaf banks [5,6].

All of the mentioned collimators have their own advantages and disadvantages. Thus, selection should be based on the treatment situation. Vindu et al. shares certain comparison about this topic in their study [9].

In fact, their study is the first work of comprehensive comparison between CK's IRIS collimator and InCise MLC for prostate SBRT. When the CTV's (Clinical Target Volume) are small or spherically shaped, advantages of MLC will dissipate since the treatment of these targets can be easily accomplished by using single collimator. In contrary, prostate cancer cases often present relatively consistent PTV (Planning Target Volume, Planning Tumor Volume) and the similar relationship with adjacent risk organs, such as the rectum and the bladder. Therefore, selected prostate cancer without seminal vesicle and extra-capsule invasions is ideal for reliable dosimetric comparison. In this direction their studies indicated that Homogeneity Index (HI is an objective tool to analyze the uniform dose distribution in the target volume) of IRIS plans (1.155) is slightly better than that of MLC plans (1.165) for similar target coverage and conformity indices. This could be attributed to the higher number of beams of IRIS plans, which allows greater flexibility to dose distribution [9].

From figure 1.7, it is apparent that both plans have similar target coverage ($D_{95}^{PTV} = 3625$ cGy, target coverage at planned target volume). It is worth mentioning that the MLC plan has tighter isodose lines (equal dose exposure derivative shells) lines compared to the IRIS plan, which results in a rapid dose falloff beyond the target [9].

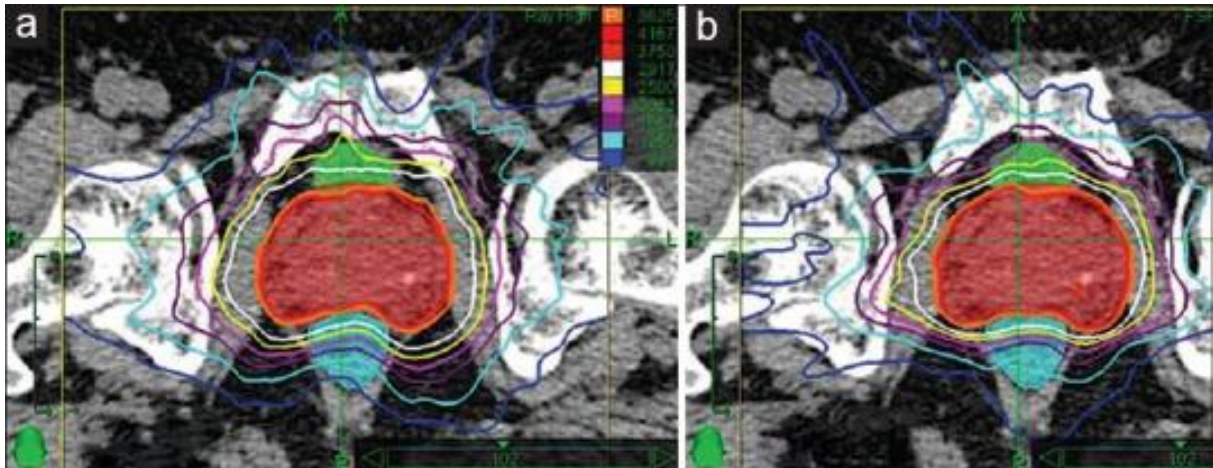


Figure 1.7: Transverse view of dose distributions of IRIS and MLC [9].

The most important finding of their study is the treatment efficiency, which was evaluated based on delivered MUs and treatment time per fraction. The delivered MUs and treatment time per fraction were significantly lower for MLC than IRIS plans [9].

Table 1.1 : Comparison of delivered MU and treatment time [9].

	IRIS	MLC	P
MUs	50.934 ± 8520	29.700 ± 3262	0.002
Treatment time(min)/fraction	45.5 ± 2.5	29.3 ± 1.1	0.006

Data were collected from ten patients. MLC: Multileaf collimator, Mus: Monitor units.

The main advantage of replacing the IRIS collimator with MLC in CK M6™ (CK- Cyber Knife) appears to be the improved efficiency, as demonstrated from the reduction of MUs by 42% resulting to a 36% faster delivery time. Reduced number of MUs per treatment would result in reduced peripheral dose, leading in decreased risk of secondary cancer, which could be an influencing factor for the long-term survival of the patients. Moreover, shorter treatment time would benefit patient comfort and accurate treatment delivery by reducing the patient motion [9].

As seen by the results of the study, each collimator type has its own advantage and disadvantage depending on organs' shape that will be threatened, the distance between critical region, type of cancer etc.

1.2.2 Advantages and disadvantages of collimators

As mentioned before, collimators have both advantages and disadvantages that can be easily summarized below.

Advantages

- Simple and less time-consuming preparation.
- Usage without interrupting the treatment for configurations possibility of field shape correction and change without any effect.
- The therapy expenses are lower because individual shielding blocks are not needed, this also eliminates the need to handle the Wood's alloy (A low melting fusible alloy. There are many alloys that melt at low temperatures. These are called fusible alloys. You may have heard of a famous one, called Wood's Metal. Wood's metal is a mixture of 50% Bismuth, 25% Lead, 12.5% Tin, and 12.5% Cadmium. It melts at a temperature of 158° Fahrenheit. Chemical Name is Bismuth alloy, Chemical Formula is Sn + Pb + Bi + Cd, which is toxic.
- Therapy time reduction (with MLC) so the patient is able to remain still stay during the treatment for shorter periods.
- Other advantages are constant control and continuous adjusting of the field shape during irradiation in advanced conformal radiotherapy [10].

Disadvantages

- Stepping edge effect.
- Radiation leakage between leaves
- Wider penumbra
- Generating complex field shapes
- Island blocking is not possible.
- During the treatment planning different type of x-ray transmission should be considered (through the leaves < 2%, interleaf transmission < 3%, and for jaws <1%.) [9].

1.2.3 Beam delivery problems

Linacs and collimators, as mentioned before, are devices that generate and transfer radiation to the cancerous tissue. During this transfer, there exist some technical problems as beam transmission, penumbra, scattering that causes irregular

dose distribution on the tissue. Engineers and designers have mostly focused on these issues to find efficient solutions.

1.2.3.1 Beam transmission

One of the most important problems occurred during the beam delivery is beam transmission. The beam that comes from the Linac somehow passes from the leaves. This transmission separated into three parts (figure 1.8).

Intraleaf transmission (Leaf transmission): This transmission problem is caused by the beams transmitted through the full height of the leaf.

Interleaf transmission: This transmission problem is caused by the beams transmitted through the surface where adjacent leaves touch each other. Typically, MLCs incorporate an interlocking tongue-and-groove design between adjacent leaves to minimize leakage between leaves.

Leaf end transmission: This transmission is a type of interleaf transmission that occurs between the end of two touching leaves. The place where transmission occurs might be in line contact or surface contact with respect to the end shape of the leaves.

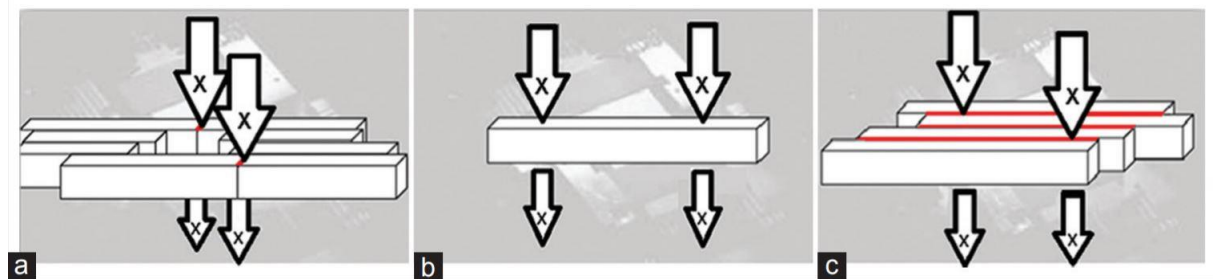


Figure 1.8 : Illustration of (a) end leaf transmission, (b) leaf transmission and (c) interleaf transmission [11].

1.2.3.2 Penumbra:

Radiation beam creates a region where the dose rate rapidly changes as a function of distance from the central axis and there exist dose transitions near the borders of this field. These sections are called penumbra regions (figure 1.9). Dose transitions near the borders of the field, there are three kind of penumbra formations.

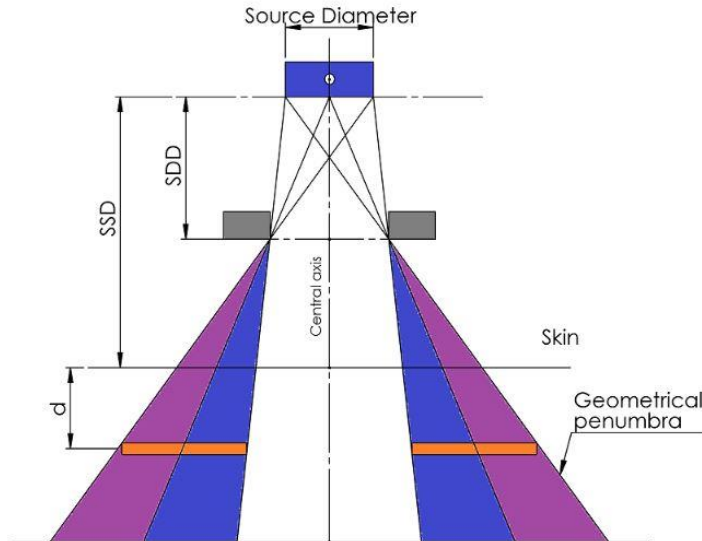


Figure 1.9: Illustration of the penumbra

Transmission penumbra: Variable transmission of beam through non- divergent collimator angle. This occurs due to the beam emerging from the edges of blocks or collimators. It can be decreased by making sure that the shapes of focalized blocks are taken into account considering the beam divergence

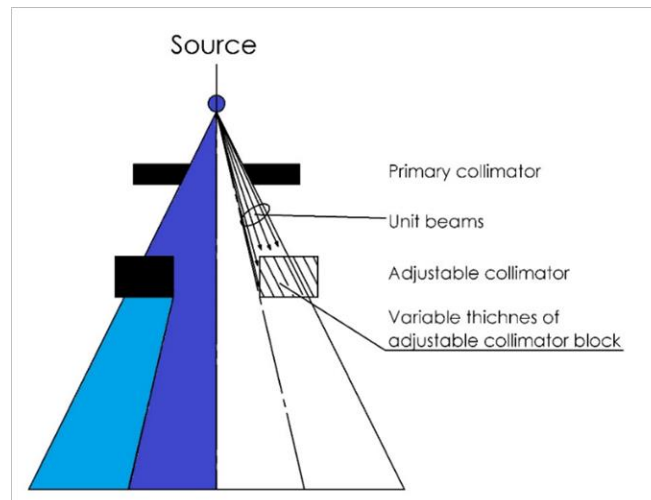


Figure 1.10: Illustration of transmission penumbra and its reason.

Geometrical penumbra: This occurs due to the size of the source; large sources have larger geometrical penumbras. This is the width of the shaded regions of the figure 1.11 at any depth due strictly to the geometry of the setup.

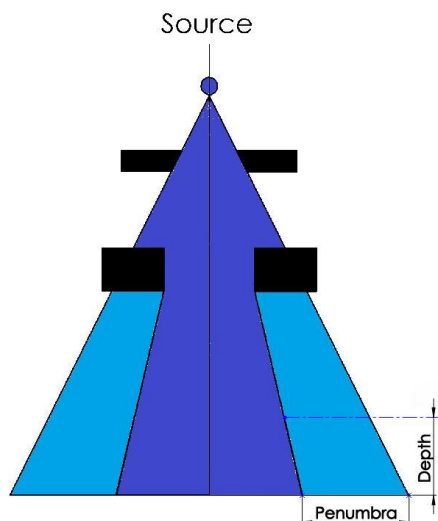


Figure 1.11: Illustration of the geometrical penumbra.

Physical penumbra: the lateral distance between two specified isodose curves at the specified depth (lateral distance between %20-%80).

$$P = \frac{s(SSD + d - SDD)}{SDD} \quad (1.1)$$

This equation gives the amount of penumbra formation at a specified depth.

P: Penumbra

S: Source diameter

SCD=SDD: Source-collimator distance

SSD: Source to skin distance

D=Depth

As seen in figure 1.9 and equation of penumbra, it is easy to understand how penumbra is affected by changes. These factors can be listed as,

Factors that increase the penumbra:

- Increase in SSD
- Increase in focal spot (Source diameter)
- Decrease in SCD

Factors that decrease the penumbra:

- Decrease in SSD
- Increase in SCD
- Energy; Increase in the amount of beam energy is resulted with less scattering so the penumbra region gets smaller.

1.2.3.3 Scattering (Secondary radiation)

Scattered radiation is the particular form of primary radiation directly coming from the source. When the beam crosses with an object or anything that has different properties in terms of transmission of the beam, so-called scattering occurs (figure 1.12). Main problem about this situation is the fact that the secondary radiation may change its direction anywhere. Thus, it causes an uncontrolled dose delivery on the target field and also unwanted dose separation inside the field.

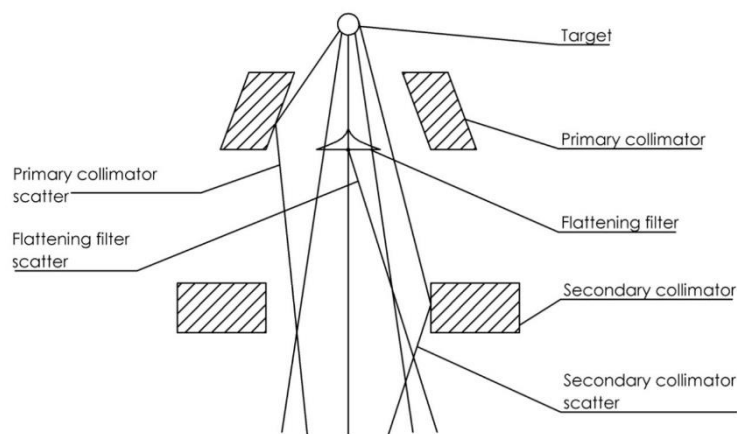


Figure 1.12: Illustration of scatter.

Beam spreading from target can be seen in figure 1.12. Primary collimator scatter and secondary collimator scatter are similar to the reflection of light however flattening filter scattering are not similar to the reflection. Due to the transmission beam divides into two or more parts at the output surface of the flattening filter. Therefore, directions of the divided beams would be different than the input's. This situation is also called as scatter.

Scattered radiation is responsible for uncontrolled dose distribution. Because of this reason it is tried to find out the ways to overcome this scattered radiation. During

the applications, either imaging or radiosurgery-radiation therapy, amount of the dose delivered to healthy tissue is of great importance. Also, as another constraint, amount of dose that will be delivered to the unhealthy tissue must not be over than needed, these are of great importance in terms of chance of operation success.

In imaging, results may not be so critical but quality of imaging, basically in terms of image contrast would be lower than ideal photon delivery condition. This results with lower detailed analysis of that field of body or may yield to a wrong diagnosis. The amount of scattering can be increased under the below conditions,

- Increase in beam energy.
- Increase in thickness where the beam is transferred
- Increase in x-ray field size

1.2.4 Radiation therapy manipulators

Beam delivery operation is carried out by the cooperation of electro-mechanic systems and two main structures of this operations are beam contour shaping and delivery systems. This thesis deals with the design of a collimator mechanism that shape the beam contour to be fit shape of target geometry. In order to understand how this beam is oriented for the target, the examination of the beam delivery systems is crucial. Beam delivery systems are the devices that include all the structure of radiation therapy operation. Types of the well known beam delivery systems are briefly explained below.

1.2.4.1 Gamma knife®

The Gamma Knife® was developed by Lars Leksell and Björn Larsson in 1968 and consists of 201 radioactive Cobalt-60 (^{60}Co) sources which are arranged hemispherical. A gamma ray, which is produced by the Gamma Knife®, has an average energy of 1.25 MeV [12].

A first prefocus of the radiation is done by an inner collimator which is enhanced by an additional collimator-helmet (figure 1.13). This helmet allows to screw in 201 collimator channels with diameters of 4mm, 8mm, 12mm or 16mm. The patient's head is placed in the treatment device with the helmet at a predefined position for treatment. The position is calculated in an earlier treatment planning [13].



Figure 1.13: Gamma Knife beam delivery system [13].

1.2.4.2 C-arm LINAC

Radiation therapy system include a treatment head to emit treatment radiation, a gantry coupled to the treatment head, an x-ray tube to emit imaging radiation, an imaging device to acquire an image based on the imaging radiation, and a C-arm coupled to the x-ray tube, the imaging device, and the gantry [14].



Figure 1.14: C-Arm beam delivery system [15].

1.2.4.3 Helical tomotherapy

Tomotherapy is a method of dynamic beam delivery. The main importance of the method is that the simultaneous motion of treatment table and gantry. While the gantry is rotating the treatment table moves linearly so that spiral shaped movement during the treatment is established.

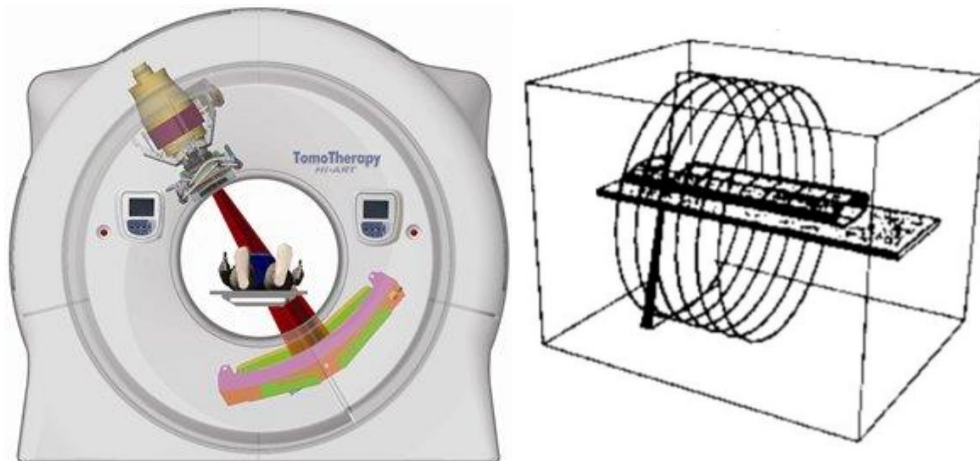


Figure 1.15: Tomotherapy beam delivery system [16].

1.2.4.4 CyberKnife®

The system consists of a small linear accelerator (6 MV, X-Band) that is mounted on a 6-axis industrial robotic arm, a treatment couch that is mounted on a second robotic arm, two X-ray sources, whose rays are arranged perpendicular to each other and two corresponding detector panels (figure 2.16). Thus, a tracking of the accelerator during movements of organs leads to inaccuracy, these movements are analyzed to extract movement patterns which result in a prediction for the position of the organ, and the accelerator can be positioned accordingly [17].



Figure 1.16: CyberKnife® beam delivery system [18].

1.2.4.5 Vero®

Vero® is a treatment delivery device for Stereotactic Body Radiotherapy (SBRT). It consists of a gimbale X-ray head (figure 1.17), two (orthogonal) kilo-volt X-ray tubes and two flat panel detectors that are mounted on an O-ring (figure 1.17). This O-ring can rotate $\pm 185^\circ$ around the patient and can be skewed $\pm 60^\circ$ around its vertical axis.

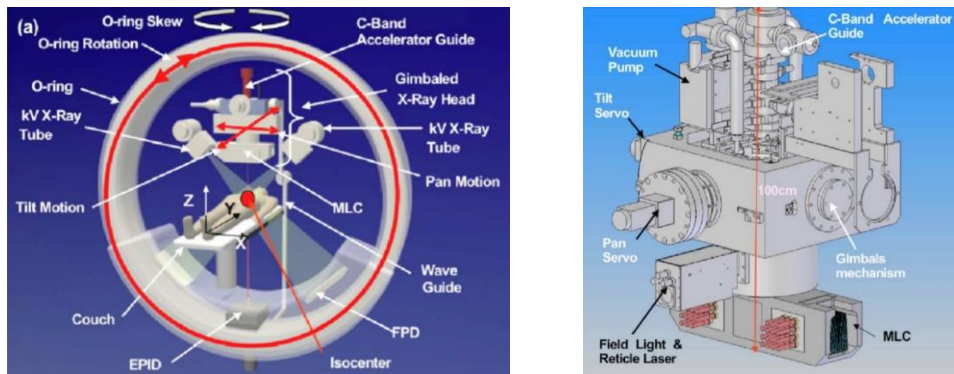


Figure 1.17: Vero® beam delivery system [19].

1.2.4.6 ViewRay ®

Three teletherapy heads that are arranged with multileaf collimators are used in this device. As this is a new hybrid system research and design developments are still cried out.

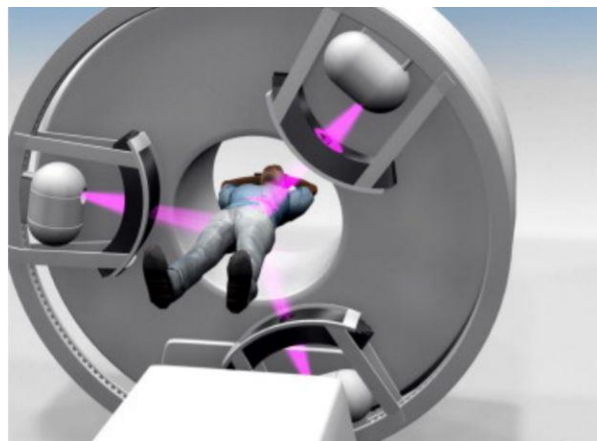


Figure 1.18: ViewRay ® concept beam delivery system [20].

1.2.5 Multileaf collimators-MLCs

Lots of description can be found for MLC systems but rapidly changing technology and science changes these descriptions over time. In a multileaf collimator (figure 1.19) dozens of thin steel blades controlled by computer are adjusted for each patient, matching the irradiating proton beam to the shape of the tumor. The multi-leaf collimator (MLC) was firstly introduced in the early 1990s. Their implementation into the radiation therapy have resulted in promising results and make linear accelerators an effective option for treating cancerous tumors. The most important property of the MLC is their ability to target the beams to a specific contour by sparing normal tissue.

Generally, most of the MLC designs utilize dozens of alloy leaf-blades to create precise contour, which restricts beam's shape on the target.

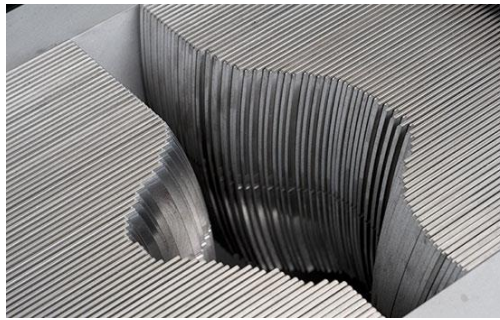


Figure 1.19 : Standard MLC

Although the first explanation of the MLC points out dozens of leaf usage, the main design constraint of these devices is to be able to modify beam center on the target area. Thus, it is not crucial to utilize multiple leaves higher than necessary to form contour precisely. In the light of this it should be noted that the same function can be accomplished by lowering the number of leaves in single section by increasing number of sections (levels).

1.2.6 Working principles of collimators and linear accelerators.

Linear particle accelerators (LINACs) (figure 1.20) generate x-rays and high energy electrons for medicinal purpose in radiation therapy, serve as a particle injector for higher-kinetic energy accelerators, and are used directly to achieve the highest kinetic energy for electrons and positrons.

LINACs are the type of particle accelerators that greatly increase the kinetic energy of subatomic particles or ions by subjecting the charged particles to a series of

oscillating electric potentials along the beam line. Basic sections of the Linacs are described below in detail.

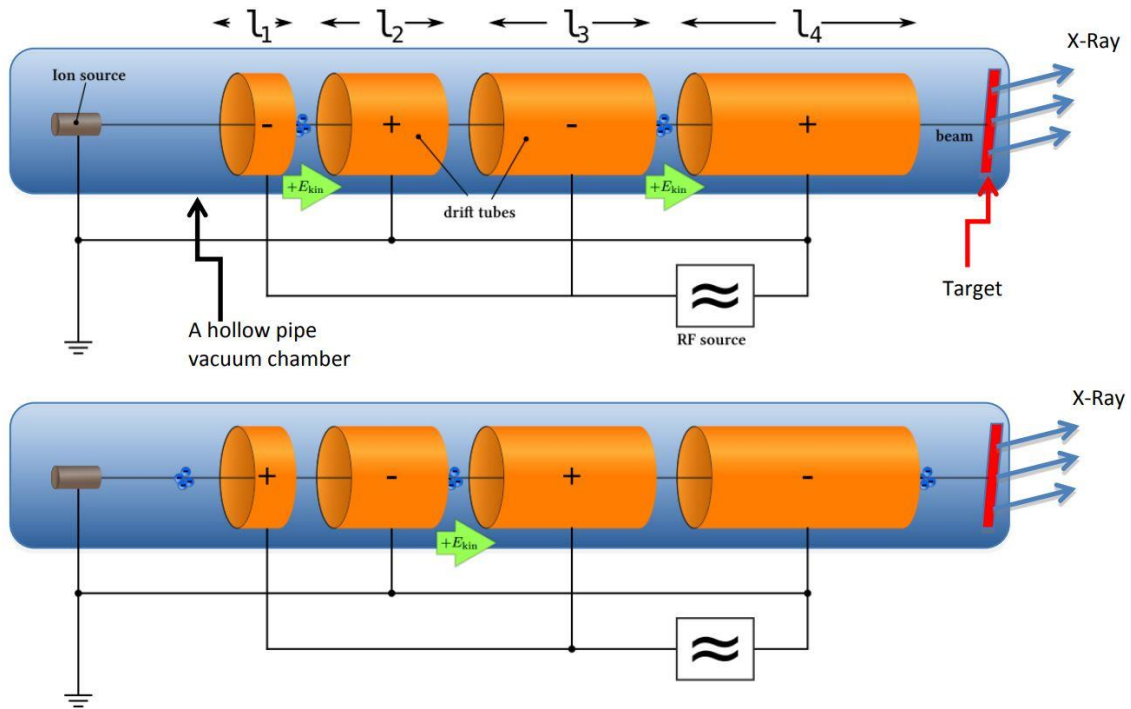


Figure 1.20: Illustration of LINAC [21].

The particle source (Ion source): The design of the source depends on the particle that is being accelerated. Electrons are generated by utilizing a cold cathode, hot cathode, photocathode, or radio frequency (RF) ion sources. Protons are generated in an ion source, that may have different design variations. If heavier particles are to be accelerated, (e.g., uranium ions), a specialized ion source is needed [21].

A high voltage source: It is used for the initial injection of particles [21].

A hollow pipe vacuum chamber: This section of the Linac can be seen as a long hollow tube that carries the electrons inside. The length of the chamber usually varies with respect to the application. If the device is to be used for the generation of X-rays for inspection or therapy the pipe will only 0.5 to 1.5 meters long. If the device is to be an injector for a synchrotron its length becomes be about ten meters long. If the device is to be used as the primary accelerator for nuclear particle investigations, then the length increases to several thousand meters long [12]. As mentioned before within the chamber, electrically isolated cylindrical electrodes (“drift tubes”) are placed, the length of each tube varies with the distance along the pipe, with shorter segments (“ l_1 ”)

near the source and longer segments (“ λ ”) near the target and it is determined by the frequency and power of the driving power source and the nature of the particle to be accelerated. The mass of the particle has also a large effect on the length of the cylindrical electrodes; for instance, an electron is considerably lighter than a proton, thus it will generally require smaller section of cylindrical electrodes to be accelerated very quickly. Similarly, as its mass is so small, electrons have much less kinetic energy than protons at the same speed. Due to the electron emission possibility from highly charged surfaces, the voltages used in the accelerator have an upper limit, so the acceleration procedure is not accomplished as simple as just increasing voltage to match increased mass [21].

One or multiple sources of radio frequency energy (“RF source”) are used to energize the cylindrical electrodes. A high-power accelerator will use as a source for each electrode. The sources must be operated at precise power, frequency and phase that are appropriate to the particle type to be accelerated in order to obtain maximum device power. If electrons are accelerated to generate X-rays then a water-cooled tungsten target is being used. Various target materials are being used when protons or other nuclei are accelerated, depending upon the specific investigation. For particle-to-particle collision investigations the beam may be directed to a pair of storage rings, keeping the particles within the ring by magnetic fields. The beams may then be extracted from the storage rings to create head on particle collisions. Additional magnetic or electrostatic lens elements might be included to ensure that the beam remains in the center of the pipe and its electrodes. Very long accelerators may maintain a precise alignment of their components through the use of servo systems guided by a laser beam [21].

Radiosurgery can be performed by using linear accelerator systems. By definition, radiosurgery is a single session surgical procedure directed by a neurosurgeon and a radiation oncologist. The entire procedure occurs in one day, including immobilization, scanning, planning and the procedure itself. With radiosurgery, the dose of the radiation given in single session is usually less than the total amount of dose that would be given with radiation therapy. Thus, the tumor receives a very high single dose of radiation in radiosurgery, and smaller doses over time with radiation therapy [21].

The best use of LINAC technology may be its ability to target larger brain and body cancer tissues that cannot be treated with single session radiosurgery. Other precise techniques using single session Gamma Knife® machines or single session Linac technology are best utilized within the brain. There exists no visible benefit for fractionated radiation treatments its single session radiosurgery can be performed. Multiple radiation treatments might result in less tumor control and more permanent side effects [21].

Linear accelerator systems are designed to be general-purpose radiation delivery devices and generally it requires modifications to render it usable for radiosurgery or IMRT (intensity modulated radiation therapy). Often, these modifications are the addition of another piece of machinery [21].

Conventional external beam radiation therapy (2DXRT) is delivered via two-dimensional beams using linear accelerator systems. 2DXRT mainly consists of a single beam of radiation that is delivered to the patient from several directions: often front or back, and both sides

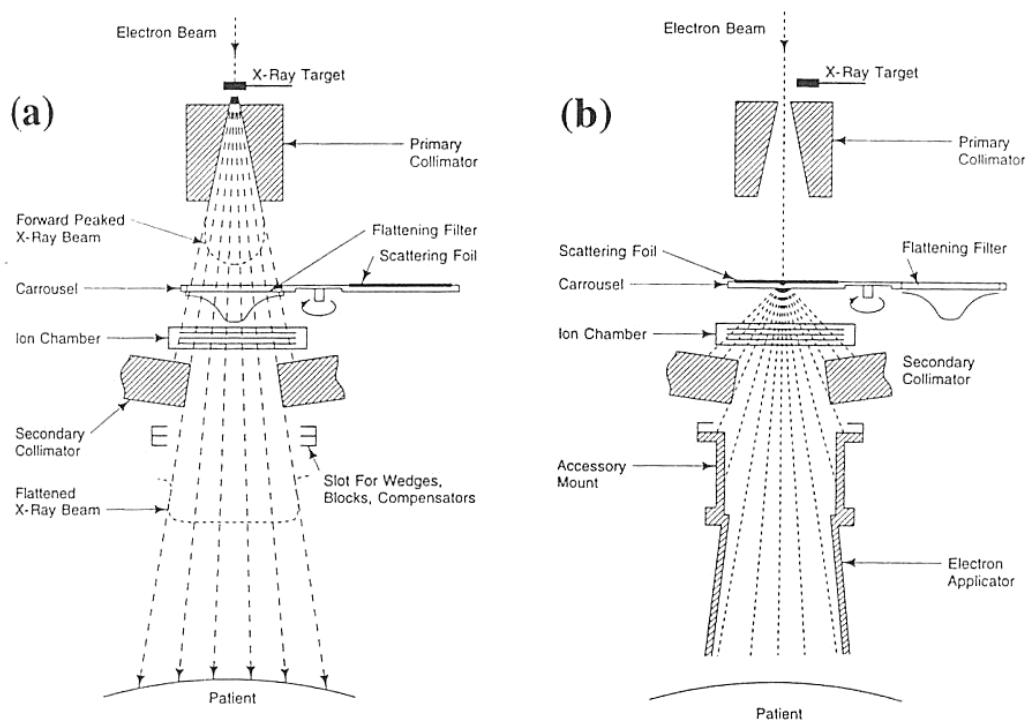


Figure 1.21 : Components of LINAC head.

The generic Linac head contains several components (figure 1.21), which influence the production, shaping, localizing, and monitoring of the clinical photon and electron beams.

In this section x-rays are generated by sending electrons to the x-ray target to be collided that composed of metals that have the higher amount of atomic number like tungsten. Radiation direction of this photon depends on the energy amount of arrival electrons. If electron's kinetic energy is lower than 100 keV its direction of radiation will be approximately equal in all directions. As electrons have the higher amount of energy, x-ray radiation through surface normal will also be increased. When Electrons that have the high amount of energy (in the range of MV) come through one side of the surface target, x-rays are created on the other side.

The head part of a linear accelerator consists of the following parts:

- **Tungsten target** where the electron beam is collided, x-rays are generated by stopping the whole electrons.
- **Circular primary collimator** that affects the diameter of the x-ray beam. It defines the available circular field size and is essentially a conical opening projection into a tungsten shielding block.
- **Flattening filter** is the conical shaped x-ray homogenization part. The photon dose distribution produced by LINAC is strongly forward peaked. To make the beam intensity uniform across the field, a flattening filter is inserted in front of the beam direction. The filter is usually made of lead, tungsten, uranium, steel, aluminum or their combination.
- **Dual Ionization chamber** are used for monitoring the photon and electron radiation beam output as well as for monitoring the radial and transverse beam flatness. The flattened beam is incident on the dose monitoring chambers. The monitoring system consist of several ion chambers or a single chamber with multiple plates.
- **Scattering foils:** clinical photon beams are produced by target and flattening filter combination. Clinical electron beams are produced by the retraction of the target and flattening filter from the electron pencil beam. This procedure happens by either scattering the pencil beam with a single or dual scattering foil or deflecting and scanning the pencil beam magnetically to cover the field

size required for electron treatment. Un this procedure special cones (applicators) are used to collimate the electron beams.

Each clinical photon beam has its own target/flattening filter combination. The flattening filters and scattering foils (if used for electron beams) are mounted on a rotating carousel or sliding drawer for ease of mechanical positioning into the beam, as required.

- **Secondary collimator**, consists of four blocks, two of them forms the upper and remaining form the lower jaws. It provides rectangular field at the LINAC isocenter. This part usually made of lead or tungsten.
- **Multileaf collimator (Optional)**: Multileaf collimators (MLCs) are a relatively recent addition to Linac dose delivery technology. In principle, the idea behind an MLC is simple; however, building a reliable MLC system presents a substantial technological challenge. The number of leaves in commercial MLCs is steadily increasing and there exists models with 120 leaves (60 pairs) covering fields up to $40 \times 40 \text{ cm}^2$ and, requiring 120 individually computer-controlled motors and control circuits. MLCs are becoming invaluable in supplying intensity-modulated fields in conformal radiotherapy either in step-and-shoot mode or continuous dynamic mode. Miniature versions of MLCs (microMLCs) projecting 1.5 to 6 mm leaf-widths and up to $10 \times 10 \text{ cm}^2$ fields at the Linac isocenter are also currently available commercially. They may be used in radiosurgery as well as head and neck treatments

1.3 Statement of Research

Perhaps one of the most important and most dangerous diseases of our time is cancer. Therefore, scientists have always worked on how to find a most effective method to diagnose and treat this disease. As stated in the previous sections there are lots of operation methods and equipment developed by these scientists. External beam therapy can be given as one of the most used technics to the treatment of this disease. External beam therapy devices consist of lots of parts and they are controlled by specific software also it is known that precision and quality of the devices increases the chance of treatments. Therefore, on this study it has been decided to develop a multileaf collimator mechanism that is precise and easy to be operated to control beam

blocking contour. At the beginning of the project, it is decided to use as few as possible leaves to achieve the desired goals of precision and ease of control. Thus, the problems, scattering, penumbra, leakage, operation time, and heavy structures, etc. could be reduced. Generally used MLCs consists of 2 sets of opposing leaves. Each set includes multiple leaves. The treatment field, which is the projected view of the target volume, must fit best to the contour created by the collimator device and treatment plan. This contour is created by changing the position of these opposing leaves. To create a contour, the system must actuate dozens of leaves. When the number of leaves increases within the system due to the high beam leakage from their connections, uncontrolled dose delivery becomes an issue through of the system. Also with the increased leaf number, payloads of the system proportionally increase too. This reduction in the number of leaves might be achieved by using not only just one axis but also two independent axes for the motion of the leaves. In this way, there will be no need to use may leave to provide flexibility in 2 axes. As seen in the previous works, using small leaves will also cause to an increase in the not only the number of leaves but also the complexity of the mechanism. Thus, it would be better to use big but optimal leaves to create precise contour. This reduction of the number of leaves might be achieved by using not only one axis but also two axes to the motion of leaves. By this way as the mechanism getting smaller it will be lighter. It should be noted that lighter collimator devices cause reduction in terms of inertia and lower inertias are advantages for robot manipulators which carry the collimator head. Also, fewer leaves will reduce the amount of the beam transmission from the surface where leaves in one bank touches each other.

1.4 Literature Survey

Considering the technological advancements, vital contributions and efficiency of the robotic systems in radiotherapy on the field of medical science cannot be unseen. As these systems formed by many different structural sections including the manipulator itself, linear accelerator and the collimator, each improvement on these sections contributes to the overall treatment efficiency. From the time when the idea of manipulating not only the robot manipulator but also the gap between the beam and the target during the treatment has emerged, number of studies and new patents related with collimators throughout the literature has increased. Addition of the collimators to

the robotic systems not only facilitates the controllability of the beam area on the target but also improves the radiation leakages and penumbra formation that are dependent on collimator structure.

Throughout the literature various authors have studied on the parameter optimization and performance evaluation of collimator designs for different applications. Weinmann et al. [22] optimized a novel conical slant hole collimator design for molecular breast imaging (MBI) by utilizing Monte Carlo simulations. In their study authors derived the initial design parameters from an existing parallel hole collimator and by varying five parameters during simulations they have optimized the design for application feasibility. Talat et al. [23] proposed a new approach in the optimization of a breast specific parallel hole collimator. In their study Monte Carlo simulations were utilized along with the response surface methodology. Si et al. [24] studied on the design and optimization of a multipinhole collimator for improved medical imaging. During their study authors achieved valuable improvements on imaging resolution and detection efficiency. Molazadeh et al. [25] evaluated the target dose absorption characteristics during dynamic multi-leaf collimator usage by the help of diode detector and film measurements. In their study collimator characteristics were determined by using Monte Carlo simulations. Fixed collimator is the type of collimator that has a simple structure and will be used with a secondary collimator in the future. This collimator can be described as a device which has a hole throughout its height. Traditionally, these collimators are used to shape x-ray beam on radio surgery. Such collimators have very low collimator transmission, sharp penumbra and perfect field size reproductivity [The design, physical properties and clinical utility of an iris collimator for robotic radiosurgery]. Zhou et al. [26] introduced their paper on the leaf end shape optimization by utilizing tangent-secant theorem. The authors also verified their approach by the help of Monte Carlo simulations and ray tracing algorithm. In their research penumbra evaluation, beam characteristics, surface of beam interference and intensity variations were also investigated. Zhang et al. [27] introduced the development of a high speed multi leaf collimator design along with its performance evaluation. In their design linear actuators were preferred instead of rotary actuators in order to drive the collimator leaves. During the evaluation phase they have utilized Monte Carlo simulations, camera based measurements and target tracking experiments for various motion characteristics.

Aside from the optimization studies, there exist multiple patents on the structural design of various collimators. Bohn [28] proposed a system that focused mainly on the actuation of the leaves. Similar to the existing collimator systems, their design utilizes dual opposing leaf sets. The main design advantage of the proposal is the usage of piezo electric actuators to generate linear motion. Ciscato et al. [29] introduced a collimator system that has different structure. Unlike the reciprocal motion of dual leaves in basic commercial multi-leaf collimator systems, adjustable beam gap of this design is created by the help of two block pairs that are assembled vertically so that one pair stays on top of another. As the width of the gaps between each block pair is constant and the pairs are able to move linearly on an axis perpendicular to each other, two degrees of freedom system was obtained to adjust the position of the formed rectangular beam gap. Pastry et al. [30,31] designed two different multi-leaf collimator devices with distinct working principles. Authors' earlier design consists of dual opposing sets of leaves that are able to move on a circular path. Unlike other existing systems, rack-like gear mechanism was used in their design to actuate the leaves. Design includes a circular arc-shaped guiding slot with a constant radius. Circular movement of the leaves ensure that the ray coming from the beam source stays parallel to the slope of the leaf contact surface. Authors' other design consists of dual sets of linearly moving leaves that are actuated by using specially arranged actuators. Power transmission between the actuators and the leaves are carried out by flexible elements. In order to provide better adaptation between the beam and the slope of the leaf surface Swerdloff et al. [32] utilized circular leaves in their collimator design. The system has dual collimating sections that are assembled vertically. Lower portion of the collimator includes multiple leaves arranged as a partial cylinder with a specific fixed radius that depends on the distance between the beam source and the leaves to ensure minimal scattering due to the parallelism between the beam path and the leaf surface. Ji et al [33] proposed a simple two degrees of freedom collimator design, where the geometry of the beam gap is adjusted prior to the operation by the help of horizontal leaf arrays. In order to carry out this adjustment, an acrylic plate for the gap formation that includes the template of the planned geometry was manufactured with respect to the treatment protocols and target form. Prior to the operation this template plate is used to fix the contour form of the beam gap. The leaves of the design are also designed with a special coupling structure to

prevent leakages between the leaves. One of the oldest collimator patents was proposed by Green et al. [34]. The working principle of their design is based on the vertical layers that include four leaves on them. During the operation the beam gap can be adjusted by the help of leaf motions. Nunan et al. [35] mostly focused on the slope of the beam travelling through the beam gap up to the target area for scattering issues. In their design, considering also the slope of the beam, the desired contour on the target is adjusted by the help of multiple vertical collimator layers. In addition to the structural design, radiation-resistant lubrications have been applied to the interleaf spaces to reduce the friction and leakages on the system. In the multi-leaf collimator design of Kasper et al. [36], there exist dual sets of multiple leaves that are moving linearly towards each other to form a beam gap with specific geometry. These leaves are designed to protect healthy tissue by creating this specific contour that best fits the target area during the treatment operation to deliver the necessary dose.

As seen in the literature, there exist various studies and patents regarding with the structural collimator design and parameter optimization. In order to contribute to the area this study tries to integrate function generation kinematic synthesis into the design of a vertically stacked multi-leaf collimator in order to reduce scattering issues in radiotherapy applications. In the light of this, the problem is modelled and simplified as two degrees of freedom planar mechanism that will be considered for contour adjustment in a single plane. Throughout the study synthesis procedure will be described in detail along with the structural design

2. DESIGN AND DEVELOPMENT OF COLLIMATOR MECHANISM

In the light of rapid technological developments in recent history, as in the most of other areas there has been an increase in robot usage in medical treatments. Although there are wide ranges of areas inside medical robotics, robotic radiology can be given as one of the most important and advanced branch of the field. Usage of robots in radiotherapy not only increases the chances of recovery but also increases the reliability, precision and treatment efficiency.

Considering the importance of the field, this thesis focused on the radiotherapy robot manipulators. Throughout this work four degrees of freedom decoupled mechanism was designed as a collimator for the linear accelerator of the novel radiotherapy manipulator. As the proposed manipulator has fixed isopoint, addition of the collimator to the system will increase the possibilities of the treatment by allowing the focus position to be adjusted on the target and the precision of the linear accelerator that will affect overall manipulator positively.

2.1 Research Constraints and Goals

Design of Collimator mechanism not only require to engineering science but also biomedical and medical science. Therefore, infrastructure for special information of radiation therapy and radiation therapy devices should be ensured. After the short literature survey, investigation of the collimator designs, and discussions by the professionals in the area, working principles and constraints of the collimators have been analyzed (This information can be seen in chapter 1). Afterwards, main design constraints of the manipulator were decided as below:

- Structure of the manipulator should be as simple as possible to reduce the control difficulties.

- By the help of the collimator mechanism, the fixed isopoint of the linear accelerator should be adjusted through the target area (Importance of this subject mentioned in chapter 1).
- By the help of the collimator mechanism, the geometry of the beam on the target should be adjusted in order to cover non-symmetrical targets. Thereby, it is aimed to reduce the unwanted dose delivery to healthy tissue.
- As the precision is the highest priority, number of components on the manipulator should be as few as possible to reduce errors due to joint clearances and manufacturing errors.
- As the collimator is carried and positioned by the help of Linac, collimator mechanism should be lightweight as possible as. Thus, the effect of inertia of the collimator itself to the Linac could be reduced.

With respect to the proposed manipulator needs and constraints type synthesis was carried on, where the manipulator type was decided as a decoupled serial modular manipulator. Following type synthesis, structural synthesis of the desired manipulator was carried out and the overall mobility was decided to be four, where the manipulator structure is composed of double two degrees of freedom serial modular sections on top of each other. As the manipulator structure is decoupled kinematic analysis of the system was concluded easily. Due to the fact that manipulation speeds are low in a relatively small area, dynamics of the system was only considered during the selection of actuators. Prior to the prototype manufacturing, designed manipulator would be constructed in computer aided design software and its capabilities would be tested in a simulation environment.

After the definition and examination of the constraints the goals of the project, Collimator mechanism design, was started to study. The goal identification season has been carried carefully because of the expectation to decide most accurate time schedule. The goals would shape the time schedule and basic form of the preliminary design. In this regard the study has begun with literature survey. Short but detailed literature survey was carried out in order to check the current advances on the radiotherapy manipulators and the collimators used in them. In this way, some technical issues related to the radiation therapy was examined and tried to understand

relation between problem and its solution. There were various of designs ranging from fixed openings that are manually mounted to the beam exit of the linear accelerator during the treatment, multi-leaf systems that are changing the radius of the beam tube to overcome manual labor so that doses or focus points can be adjusted and other multi-leaf systems that are used to change the shape of the projected beam on to the target area in order to protect other healthy areas. Some designs consist of dozens of leaves with different leaf thickness, and there were also some designs consist of few leaves. As each of the design has their own advantages and disadvantages, by analyzing all of them with respect to current project goals some design targets have been set as follows;

- In order to reduce complexity by reducing the number of total actuators, previously proposed radiotherapy robot manipulator has been designed as a spherical mechanism that has a fixed isopoint that is positioned at the center of a sphere of the manipulator work envelope. Although it has several advantages in terms of increased precision and easy control scheme, treatment of the large non-uniform tumor shapes has chance to result in a difficult procedural routine. In the light of this a collimator that is to be designed throughout this study should help to overcome this disadvantage by not only adjusting beam cone shape but also directing the beam to a point other than just isopoint. This can be only possible to construct a gateway in front of the beam and manipulate its position so that the allowed beam through the gateway can be directed to the target.
- The collimator should dynamically adjust itself during the treatment with respect to the planned routines so that it should be mobile robotic system rather than a cartridge that can be manually changed in the treatment period. As a result, treatment period and manual labor will be reduced as much as possible while patient comfort will increase during the treatment and also errors caused from human faults would be reduced.
- As it is still important to preserve the simplicity, the number of actuators that will be used in the collimator should be as few as possible for the ease of control.
- Although not a primary requirement, overall collimator manipulator should be

as compact as possible due to preserve space in the radiotherapy robot manipulator head. As mentioned before this requirement can reduce overall radiation therapy system's loads and dimensions. This is not only a mechanical requirement but also requirement that may affect patient's psychologic situations when he or she on the radiation therapy season.

- Collimator mechanism should be designed such a way that will make easier its assembling and disassembling of any part changing requires.

2.2 Preliminary Design

Considering project goals that are mentioned in the previous section, four degrees of freedom decoupled robot manipulator was decided to be designed. As seen in figure 2.1 considered manipulator has two sections (red and yellow) on top of each other that are responsible for decoupled x and y motions of the jaws that will help to direct the beam. Radiation therapy deliver the required dose onto the two-dimensional projection of the target volume. Therefore, decoupled x and y motions would be enough to describe the two-dimensional shape by capability of the isocenter change of collimator. In each axis there is an additional degree of freedom that adjusts the gap between the jaws on the same axis. By this way it is not only possible to move the rectangular window opening that will guide the beam in x and y direction but also possible to adjust the shape of the rectangular window opening in two dimensions (figure 2.2). The ability of changing dimensions of the window opening can give advantageous in terms of the precision when non-symmetrical shapes are being radiated. Also, additional degree of freedom in each axis make possible dynamic collimation, mentioned in chapter 1.

It should be noted that the black circle on the figures shows the tube where the beam exits the linear accelerator. Due to the fact that the manipulator behaves as a gateway, the beam is only allowed to pass through the window as the remaining part of the beam will be blocked by the jaws of the manipulator. In other word the dose that would be delivered to the target would be in form of this opening, if scattering and penumbra is neglected.

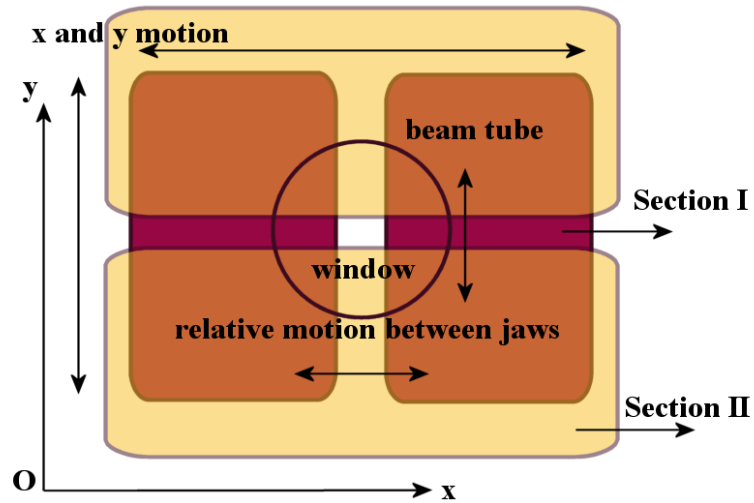


Figure 2.1: Four Degrees of Freedom Robot Manipulator.

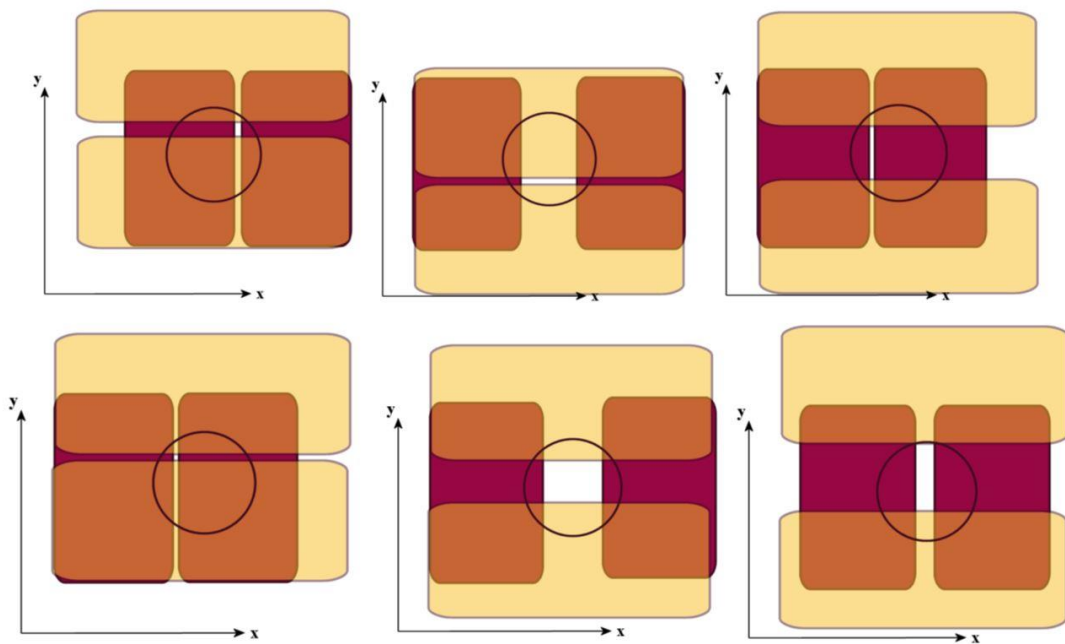


Figure 2.2: Working Principle of Four Degrees of Freedom Robot Manipulator (Position and Shape Change of Rectangular Window Opening in Front of the Beam Tube).

It can be easily seen in figure 2.3 the advantages of the shape adjustment of the gateway window. Consider a target with a rough geometrical shape that is positioned in front of the beam cone that is focused on it (Figure 2.3a). As its overall area is smaller than the projection of the beam, some portions of the healthy zones will also

be affected by the beam during the treatment. (Side effects of the healthy tissue exposure to the radiation therapy mentioned in chapter 1) Next consider a collimator with a fixed gateway window with rectangular shape that can be positioned in front of the beam (Figure 2.3b). Using this idea, the target can be scanned during the treatment with less harm to the healthy zones on the borders however the treatment time will be increased as it is needed to cover all the area of the target with a fixed geometrical shape and it will cause to more complex radiation treatment plan. Finally consider a collimator with a gateway window that can be both positioned and adjustable in shape (Figure 2.3c). By this way, while leaving the healthy zones free of radiation as much as possible, the target can easily be scanned by using few passes that will also affect the time of the treatment positively. Adjustable position and shape give an advantage in terms of the precision of the treatment. Because as the thickness or height of the opening getting smaller the possibility of the alternative treatment plan increases. On the other hand, doing so will increase the time required for the treatment period. As a result, treatment should be carefully preplanned with respect to the treatment period and the healthy tissue exposure amount.

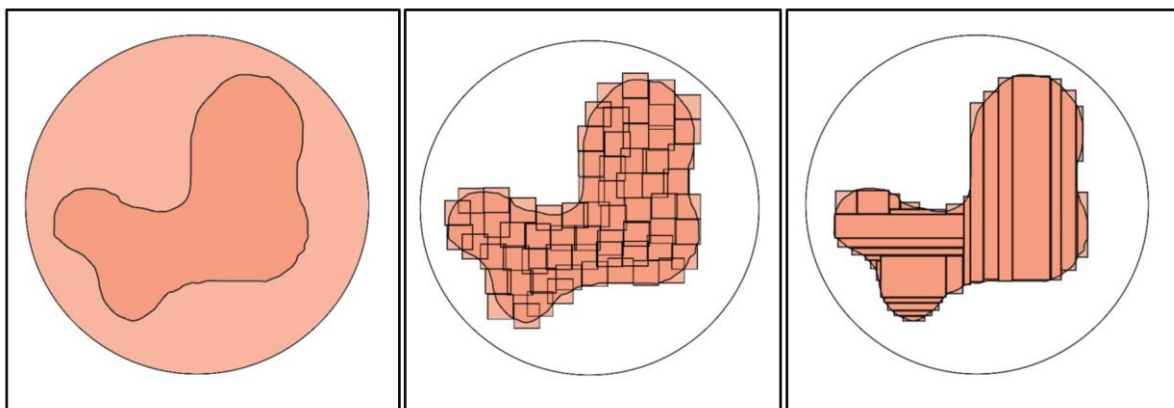


Figure 2.3: Various versions of target treatments. a) Without collimator mechanism, b) Collimator with a fixed gateway window that can be positioned, c) Collimator with variable shape gateway window that can be positioned.

As mentioned in the design goals and constraints, number of the actuators in the final design should be as few as possible. Although collimating actuators can be carried out by using three degrees of freedom circular shape window (two translations for planar positioning + dimensional radius change of the window), it is not a suitable. Due to the structural compatibility of the rectangular window and its more suitable

geometrical surface covering ability. Rectangular window shape is more ideal to pattern generation. Rectangular shape contacts with each other by line contact on contrary to circles that contact with each other by point contact. Difference between covering a surface with a rectangular window and a circular window is illustrated in figure 2.4. In figure non-symmetrical contour is patterned with rectangular and circular window. Rectangular window is able to generate a pattern that is not coincident with each other inside the target but circular shape because of its point contact cannot generate a pattern without causing empty space between them. When the three circles touched each other, an empty area middle of them. In order to fulfill this empty area there should be a circle usage that is coincident with contact points of these three circles. In this regard there would be additional unwanted dose delivery to the intersecting areas of circles.

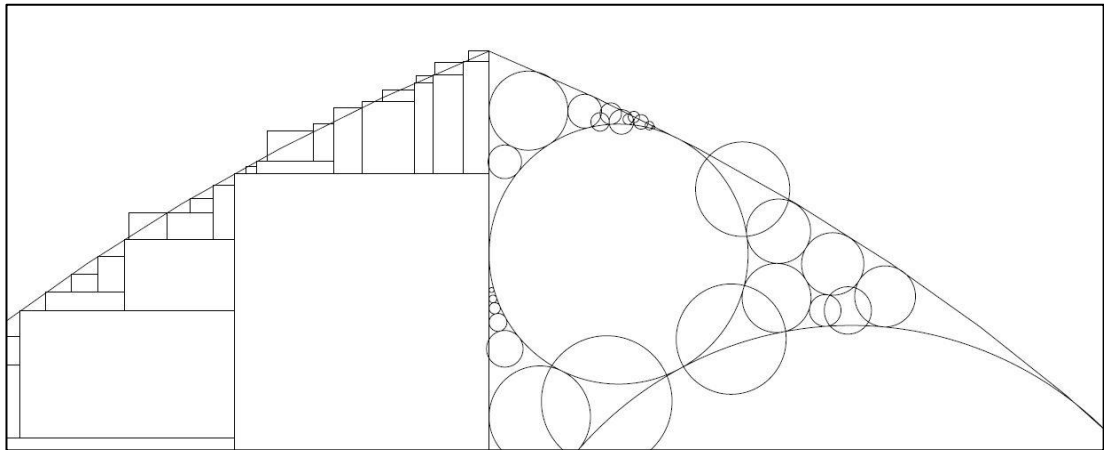


Figure 2.4: Illustration pattern generation with rectangular and circular window.

2.3 Preliminary Kinematic Analysis

The main purpose of the collimator that needs to be designed in this study is to direct the beam into a valid position on target with a specified rectangular geometry as mentioned chapter 2.2, so it is important to extract the mathematical models of its motion to obtain ability to control opening. Consider a collimator mechanism that is placed in front of the beam tube with a radius r illustrated in figure 2.5.

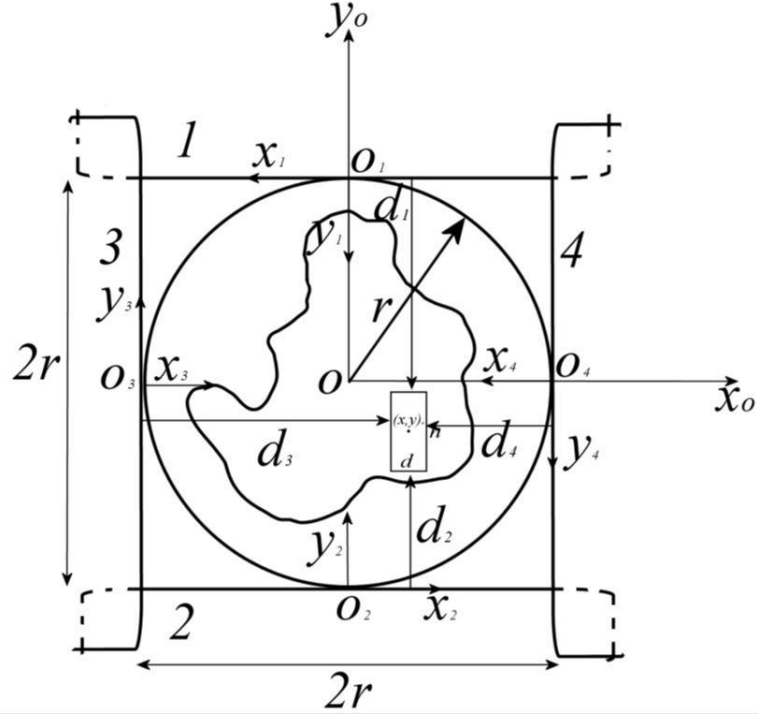


Figure 2.5: Collimator mechanism that is placed in front of the beam tube that is positioned on the center of the target.

The system consists of four independently actuated jaws (the "jaw" can be seen as the "leaf" in other documents, because of its geometry and difference in this mechanism the components so-called "leaf-leaves" will be called as jaw in this thesis), and the maximum workspace of each jaw will be determined by the radius of the beam tube as $2r$. As seen in figure 2.5, each jaw has an individual coordinate system where their centers (o_1, o_2, o_3, o_4) are fixed to the global coordinate frame at $o_1(0, r), o_2(0, -r), o_3(-r, 0), o_4(r, 0)$. If the task is to form a (dxh) rectangular opening at the target (x, y) , kinematic analysis problem will become to find the individual translation amounts of the jaws (d_1, d_2, d_3, d_4) .

$$\begin{aligned}
 d_1 &= r - \left(y + \frac{h}{2}\right), & d_2 &= r + \left(y - \frac{h}{2}\right), \\
 d_3 &= r + \left(x - \frac{d}{2}\right), & d_4 &= r - \left(x + \frac{d}{2}\right)
 \end{aligned}
 \tag{2.1}$$

It should also be noted that the first action should be taken by the radiation therapy manipulator in such a way that the center of the beam tube will be positioned on the center of the target (o) as illustrated in figure 2.3a.

2.4 Modified Design

Although the design concept explained so far was suitable for most of the project goals after concept 3D models has been created, it was decided that the design in its cartesian form will consume a larger volume inside the linear accelerator. As one of the goals is focused on the compactness of the system as much as possible, it was decided that the design should be modified.

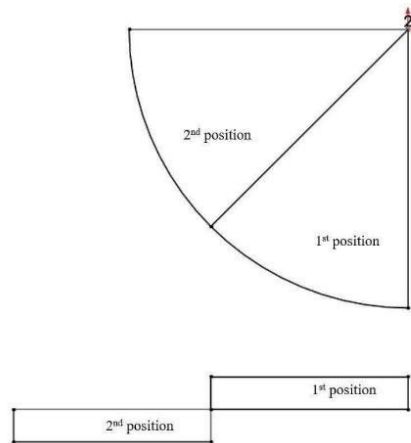


Figure 2.6: Illustration of difference between cartesian coordinate and cylindrical coordinate mechanism.

One of the sections was modified so that it will work in polar coordinates instead of cartesian coordinates. As a result of the modification, working envelopes of two jaws will be dramatically reduced without affecting the working principle of the proposed four degrees of freedom robot manipulator. It can be seen in basic illustration above, figure 2.6. Jaw at the upside of the figure represents the jaw that moves on the polar coordinates and the other jaw at the downside of the figure represents the jaw that moves on the cartesian coordinates. The first and second positions of these jaws are illustrated and it is easy to see the differences between projection areas needed for these mechanisms to obtain equal opening as one of them is translated and the other one is rotated. After the structural modification, the coarse manipulator design was modelled in a 3D simulation environment. This modification also affects the penumbra

dimension-rate on the target (Penumbra and problems caused by it mentioned in chapter 1). Rotational motion of the upper jaw ensure that the surface of this jaw would be aligned to beam parallelly thus the beam pass through its surface parallelly and no beam transmission occurs. In previous design beam has to come with an angle to the side surface of this jaw and this beam has passed from corner of jaw that has triangular shaped irregular thickness on beam path. As seen in figure 2.7, the first section of the manipulator includes cylindrical jaws that have two rotational degrees of freedom instead of translational and the second section of the manipulator includes two translational degrees of freedom cylindrical jaws instead of flat ones.

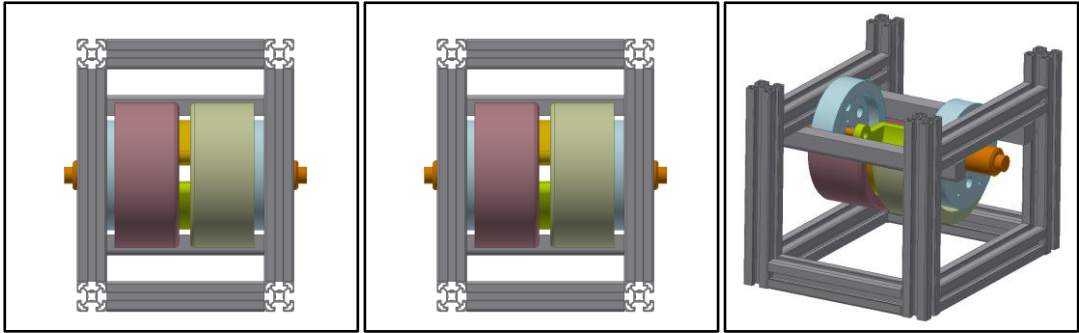


Figure 2.7: Four Degrees of Freedom Modified Robot Manipulator.

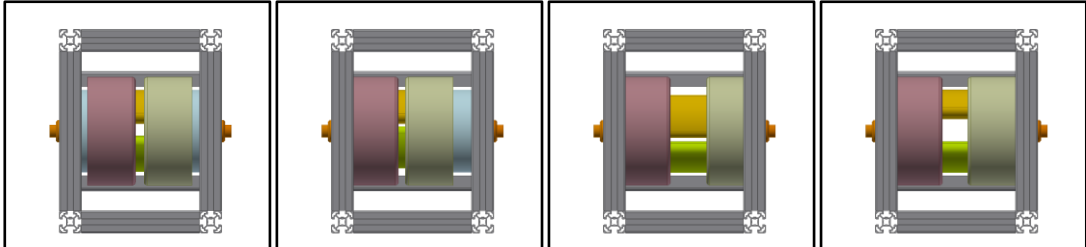


Figure 2.8: Working Principle of Four Degrees of Freedom Modified Robot Manipulator (Position and Shape Change of Rectangular Window Opening in Front of the Beam Tube).

When figure 2.2 and figure 2.7 are compared, it can be easily seen that the working principles of two different designs are the same. After the simulation runs are completed, the overall manipulator was modelled so that it will be ready for manufacturing. 3D design of the prototype and 3D models of the individual parts can be seen in following pages.

Dimensions of the jaws were decided with respect to the workspace requirements and basic shapes of jaws were decided at the beginning of the design as seen in figure 2.9. Support problem of jaws when they were moving was solved. The proposed solution is use to circular guides which is mostly used in biomedical systems because of their precision. Linearly translated jaws were supported by the linear bushing which can precisely supports the load when it was moving. These parts can be seen in figures below.

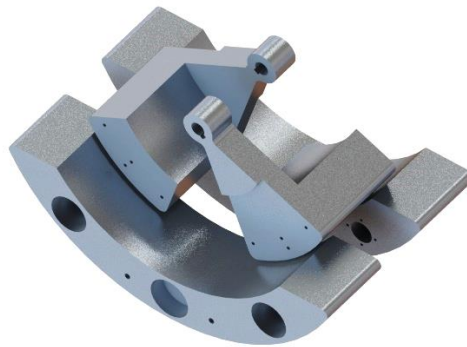


Figure 2.9: 3D models of jaws.



Figure 2.10: R-Guide rails connection with upper jaws a) Inside view b) Outside view behind the transparent base wall.

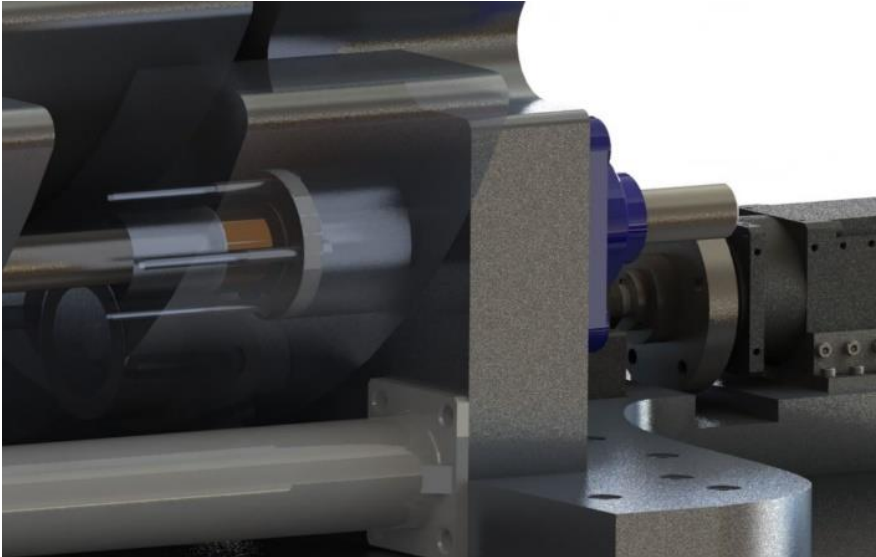


Figure 2.11: Linear bushing assembled into the linear jaw.

Actuators that would provide the required motion to the jaws can be examined into two groups in terms of their connection to the system. Each of the jaws are actuated by rotary actuators but only upper jaws in other words rotating jaws do not need any change in this motion but lower jaws that are translationally moving need to mechanical motion converter to change the type of the motion from rotary motion to the linear motion. This necessity supplied by motion converter so-called ball screw. Motion generated by the actuator is transferred to jaw by ball screw and a tube-shaped part that connects the ball screw's nut and jaw to each other. As motion transferring component, ball screw selected because of their high precision motion transfer. These components mostly used in biomedical systems, machining systems and defense industry. Location where and how ball screws are assembled can be seen in figure 2.12.

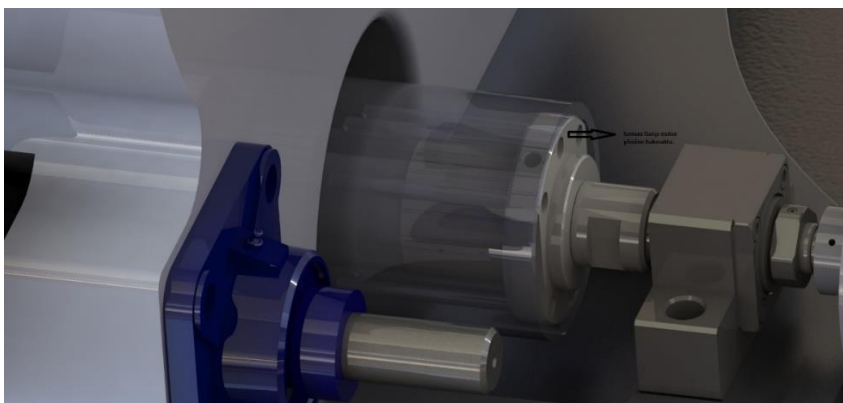


Figure 2.12: Ball Screw used in Collimator mechanism.

Upper jaws change the either dimension or position of the opening by rotating thus rotary motion should be accurate to obtain precise dose delivery thus there is no mechanical motion converter assembled between actuator and jaw. This is why motion was transferred directly by rod and key on it. Upper jaw motion transfer system can be seen in figure 2.13. The actuator placed on the wall where R-Guide also assembled on it. Therefore, compact mechanism was tried to be obtained by lowering the component number. It should be noted that as the number of components getting fewer, clearances and un-wanted dimensional offsets getting smaller.

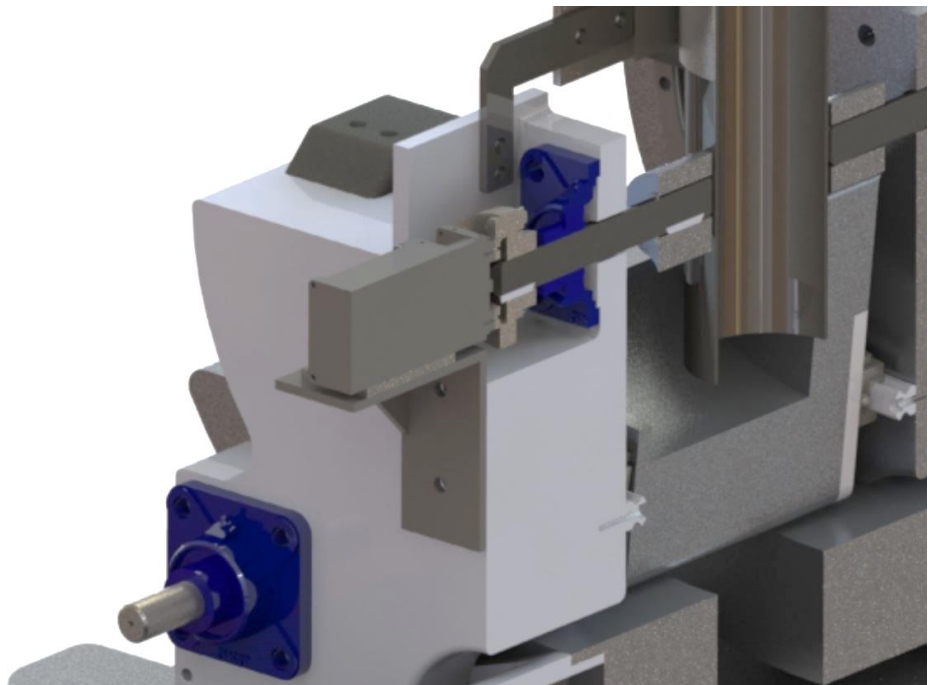


Figure 2.13: Upper jaw actuation scheme.

As mentioned previously main purpose of designed collimator mechanism is to change position and dimension of the rectangular shaped opening where beam would be transferred. This is illustrated in figure 2.2 and figure 2.8. After the 3D modelling and simulation of the collimator mechanism illustrations proofed by final designed and it can be seen in image 2.14.

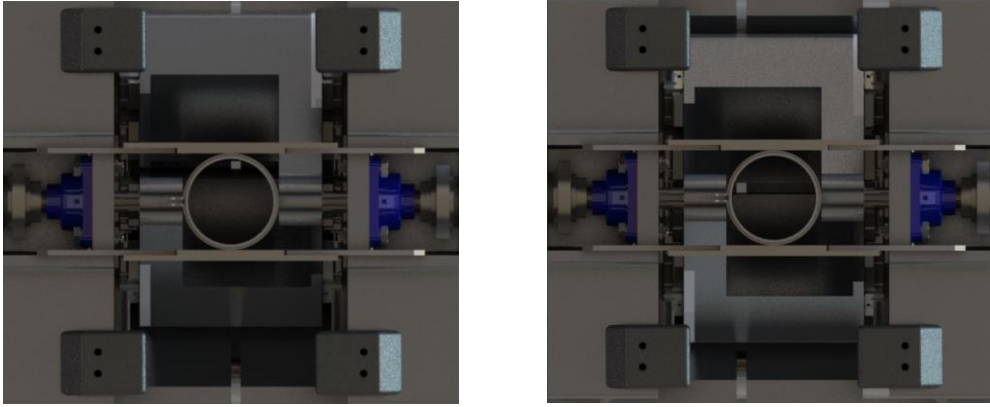


Figure 2.14: Position and shape change of rectangular window opening in front of the beam tube.

Main components are mentioned up to now. Other parts and connections will be mentioned basically and everything can be seen detailly in figures in next pages. After the actuation and supporting systems of the jaws another important thing about the design of collimator mechanism is to obtain precise assembling. Therefore, actuators and bearings were connected directly to a rigid base. Rigid base and the walls at the two sides connected each other by bolt and nut. And positional accuracy between them achieved by groove at the touching surface of each other. The R-Guide supporting upper jaws should be positioned correctly and another important issue about these components is to achieve accurate distance between two rails set which assembled opposed walls. Therefore, metal bars which have a “O” shaped cross-section placed between these two walls. In this way walls have been prevented to wrong dimensional positioning and the force generated from center of mass of walls transferred through these bars not on upper jaws and r-guides.

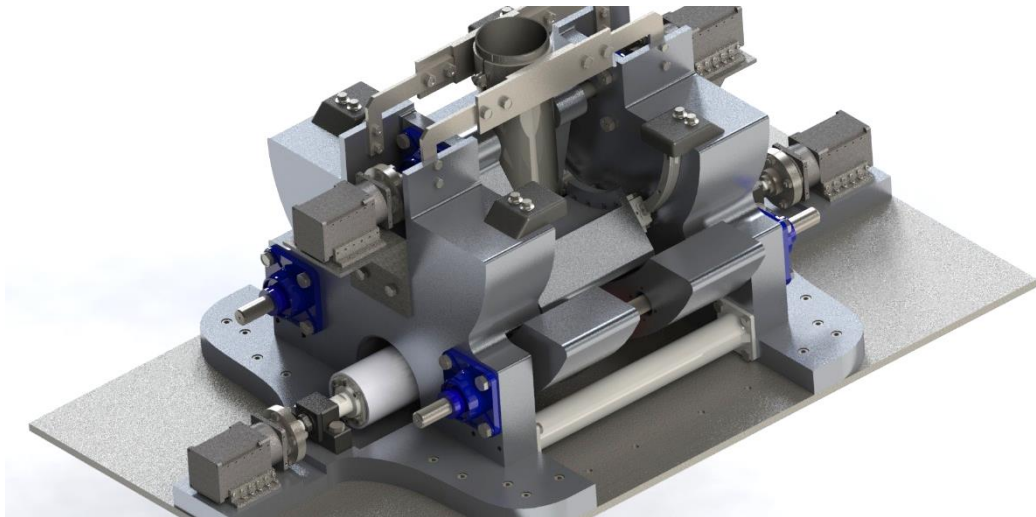


Figure 2.15: Isometric view of collimator mechanism.

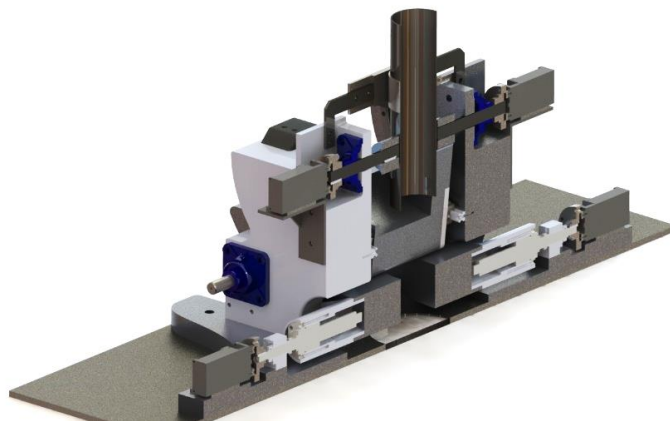


Figure 2.16: Collimator section cut.

2.5 Modified Kinematic Analysis

In order to position the modified circular collimator jaws to the desired configuration, θ_1 and θ_2 should be defined as functions of d_1 and d_2 respectively (figure 2.17).

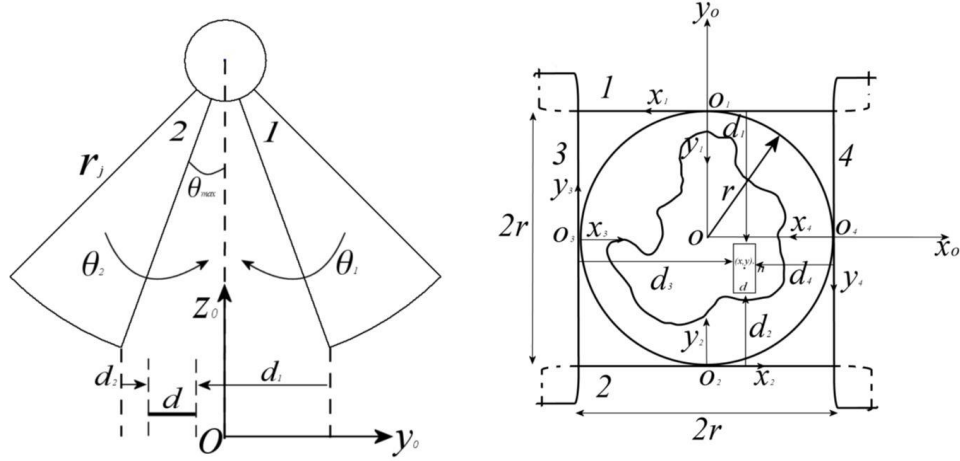


Figure 2.17: Modified Collimator Mechanism with Circular Jaws.

Using geometrical tools θ_1 and θ_2 variables in terms of d_1 and d_2 could be calculated as below,

$$d_1 = r - r_j \sin(\theta_{\max} - \theta_1), \quad \theta_1 = \theta_{\max} - \sin^{-1}\left(\frac{r - d_1}{r_j}\right) \quad (2.2)$$

$$d_2 = r - r_j \sin(\theta_{\max} - \theta_2), \quad \theta_2 = \theta_{\max} - \sin^{-1}\left(\frac{r - d_2}{r_j}\right)$$

Combining equation 1 and 2, new equations for the actuation variables for a given target will become,

$$\theta_1 = \theta_{\max} - \sin^{-1}\left(\frac{y + \frac{h}{2}}{r_j}\right), \quad \theta_2 = \theta_{\max} - \sin^{-1}\left(\frac{\frac{h}{2} - y}{r_j}\right), \quad (2.3)$$

$$d_3 = r + \left(x - \frac{d}{2}\right), \quad d_4 = r - \left(x + \frac{d}{2}\right)$$

2.6 Prototype Manufacturing

CAD / CAM software were frequently used throughout the project to make the most precise production and design possible. For this reason, CNC machines were preferred during the production process. Aluminum 7075 was used in the production of many parts as it was decided before the design to obtain a light construction higher radiation emission rate.



Figure 2.18: Some of the bulk materials, Pre-Manufacturing.



Figure 2.19: Some of the machined parts.



Figure 2.20: Assembly period from top.



Figure 2.21: Assembly period, close up, stabilizers and circular rails are visible.



Figure 2.22: Assembly period, isometric view, actuator mounts are visible.

3. MODIFICATION OF THE COLLIMATOR PROTOTYPE

Design and development of the collimator mechanism were mentioned in the previous chapter. Each step of the assembly process gave new ideas about collimator's design. After the whole of the Collimator system assembled, collimators real-life characteristics was examined and it is tried to find better solutions for each section of it. During these examinations and the studies, some problems are noted. In this section, the reasons behind designing a modified version of the collimator and differences between new and previous design would be mentioned.

3.1 Modification Reasons

It should be known that there should be no change in the system's workspace and general concept.

In section 2.1 some research goals have been mentioned. These are basically; compactness, ease of assembly, fixed isopoint,etc. There was one topic that was tried to be solved at the beginning of the project, high volume of the collimator (in section 2.4 the changes can be seen). Most of the constraints and goals defined in chapter 2 were successfully provided but there were some ideas formed during assembly to design improved one by means of earned experiences. Some of the reasons and constraints behind improved design can be seen below.

- All of the previous constraints should be consistent with the modified manipulator.
- Kinematic Structure of the manipulator should stay the same by preserving its overall mobility and its decoupled nature.
- Utilizing geometrical approaches footprint of the modified collimator should be reduced as much as possible.
- High volume of the Collimator mechanism is a problem in terms of the assembling of it to the linear accelerator. As its volume getting higher the assembling of its to the to the Linac head would be harder. There is also another

point of view to this topic, psychological effects of the huge mechanical systems on the patients. These patients already under pressure in terms of the danger of the disease and side-effect of radiation therapy by this reason everything or every step should be make them feel in safe.

- It was realized that some parts of the design couldn't be assembled easily thus this problem should be solved in next design.
- Particularly jaws (leaves) and some of the other components were heavy. There was no possibility to solve this problem by changing material of them. Because if a component would have been manufactured by using the low-density material it would result in the increase in the thickness of these components where beam passes through. By this reason it is decided to change design of jaws and some parts in order to obtain light weight structure. Also, one more problem related to the heavy structure was that of the force and torque requirements to make them move. If heavy structure problem would be solved it would probably decrease the actuators capacity, cross-section of some parts which supports the loads, types of bearings and number of connectors.
- Compactness was another goal tried to be ensured to Collimator mechanism. It was obtained in terms of the components but it couldn't in terms of the connectors. Also shape of some components made Collimator mechanisms structure somewhat complex. It was another problem which was worth to be dealt.
- Footprint of the modified collimator should be circular in geometry as it will be inserted to the cylindrical casing.

With respect to the considered manipulator needs and constraints all of the assembly parts proposed design were analyzed and modified by generating a novel design. As always prior to the prototype manufacturing, designed manipulator was constructed in computer aided design software and its capabilities were tested in a simulation environment.

3.2 Modified Design

Modification of the Collimator mechanism has started with the jaws modification. Both first and second design has been started with the design of jaws in

order to obtain necessary workspace. After the jaws have been designed, their supports as bearings, bushings, liner&circular rails, rods and bases were designed. Most important thing is to find effective dimensions and shapes for the jaws so that jaws would be able to block beam by its lighter and smaller design. As blocking the beam jaws should also be efficient in terms of beam transmission, penumbra, and scattering. After jaws were designed, the forces and torques generated by their loads and motions should be carried and transferred by the mechanical components therefore, these components were designed with respect to jaws characteristic. Final design of the jaws which are driven by decoupled mechanism is shown in figure 4.1 and jaw arrangement can also be seen clearly. It is easy to realize the difference between figure 2.9 and figure 3.1.

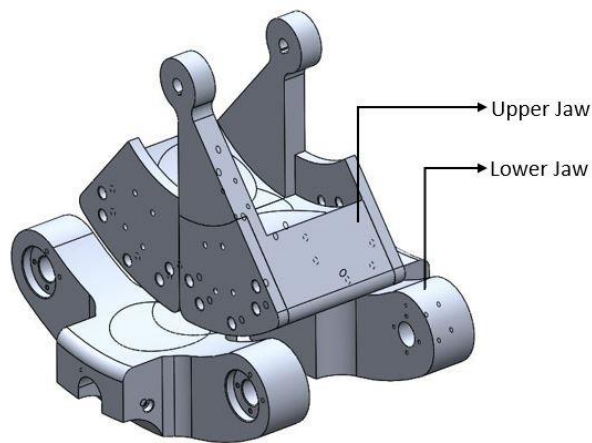


Figure 3.1: Jaw arrangement of Collimator mechanism.

Upper jaws rotate to adjust dimensions of the opening in a single axis where the beam allowed to pass through. This rotation motion generated by a rotary actuator and transferred by a rigid rod and key assembled between them. To ensure precise motion transfer from actuator to jaw there exist a rigid-clutch and rigid rod. Axis of the output of the actuator is collinear with that of the Jaw's. There was another idea for this placement which is placing them vertically to each other. But this time additional motion transfer mechanism should be used to change the direction of rotation. Thus, there would additional clearance between the actuator and jaw thus, the axis placed collinear to each other. This principle can be seen in figure 3.2.

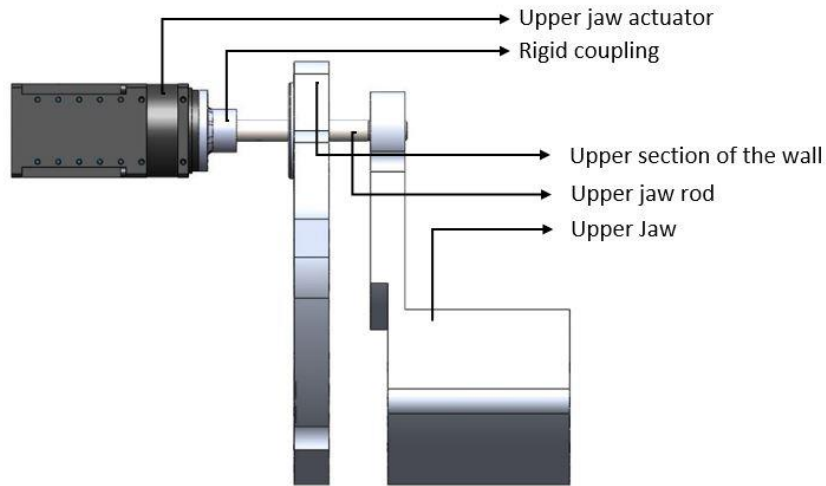


Figure 3.2: Motion transfer through upper jaw.

As seen in the figure 3.2 rotation of the jaw needs to be supported by an additional mechanical component. This component should be responsible for carrying the loads of the jaw and ensure precise circular path for its motion. The circular motion of the upper jaw is on the 150 mm circle with 120° angle. THK HCR 15-A circular motion guides selected to handle these issues. This component and its connections on the system can be seen in figure 3.3.

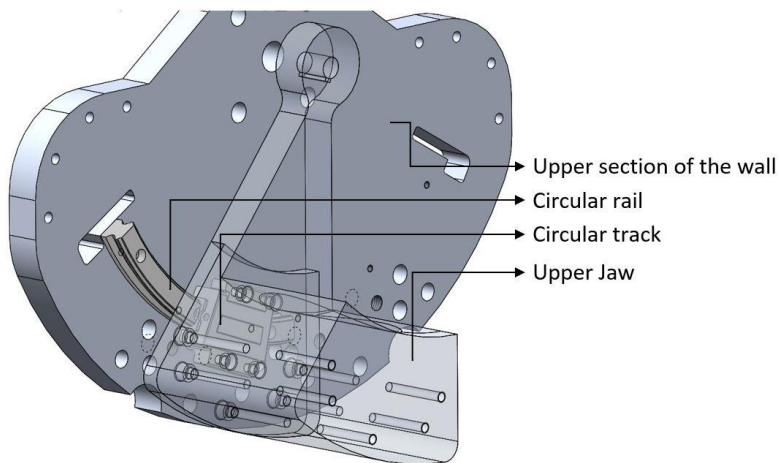


Figure 3.3: Circular motion guide and its assemble.

Circular motion guide consists of two components one of them is track and another is rail. The rail was assembled to the wall with a constant radius, the huge gray part in figure 3.3, and tracked to the jaw. Because of the tracks own design, it was impossible to assemble it to the jaw directly. Therefore, the jaw was divided into three

parts to make assembly possible and efficient. The main problem was the fact that the screws could not be placed between the track and the jaw.

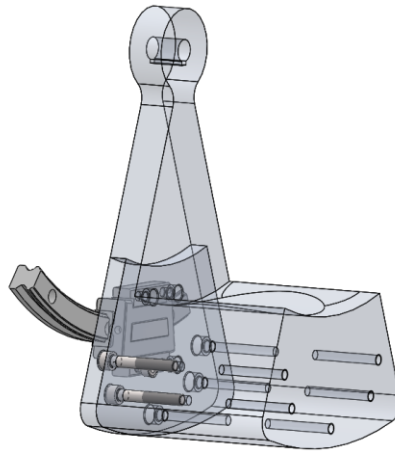


Figure 3.4: Divided upper jaw and rail-track assemble.

Hexagonal socket screw's head as seen in the figure below, placed into the part thus, way it become possible to be assembled.

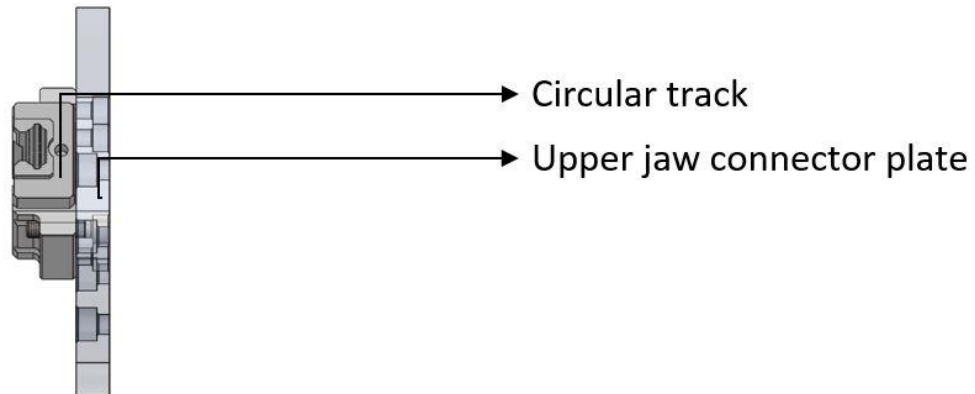


Figure 3.5: Assembly of track and first peace of jaw.

After the track and the first peace of the jaw was assembled, this sub-assembly should be assembled to the main body of the jaw. At the end there were rotatable jaw assembly ready to be connected with the walls.

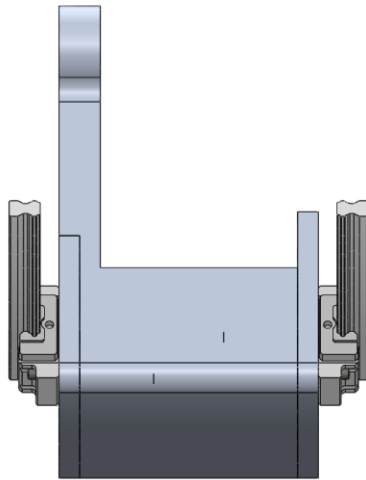


Figure 3.6: Upper jaw assembly.

Linearly moving lower jaws need to be supported by such a component that can carry the load of it and able to ensure precise linear motion. Linear motion of lower jaws was supported by THK LMF 12 M linear bushing. Lower jaws were machined to mount this component and the structure of the connection between bushing and jaw design to make connection between them at the center of mass. This jaw moves on a steel rod that was hardened to prevent bending. In case of bending surfaces of the jaws cannot block the beam efficiently. Another problem related to the bending is that the surface contact between two opposing lower jaw turn into line contact, therefore, beam transmission would be higher at this contact area. The surface of the rod was also grinded to ensure as smooth as possible contact between the linear bushing and its own contact surface.

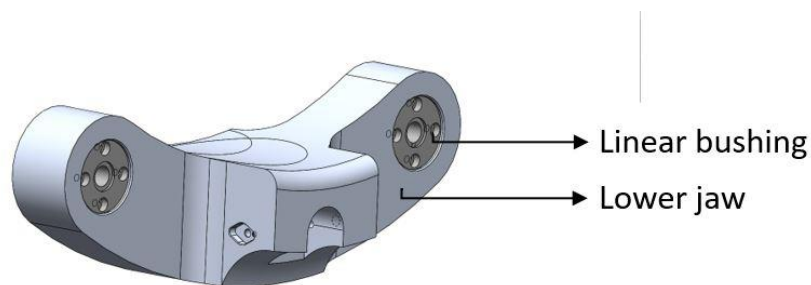


Figure 3.7: Lower jaw and linear bushing assemble.

Linear bushing was mounted to this jaw as seen in figure 3.7. After first tests of sub-assemblies of collimator mechanism, it was distinguished that the linear motion

of the lower jaw was not straight enough because of the clearance of linear bushings. The number of linear bushing mounted on lower jaw was increased to three and the condition of the linear motion has been improved. Lower jaws were also connected to the wall by means of the rod and rod-wall connection supported by SKF FY 15 TF bearing unit which allows three rotational degrees of freedom by means of its spherical bearing surface and spherical housing surface. These bearing units were chosen not to damage the collimator mechanism if any unexpected impaction occurs during the assembly.

Like upper jaw, lower jaw's shape was massively changed to lower its weight and alter its dimensions. It can easily be seen if figure 2.9 and figure 3.7 are compared.

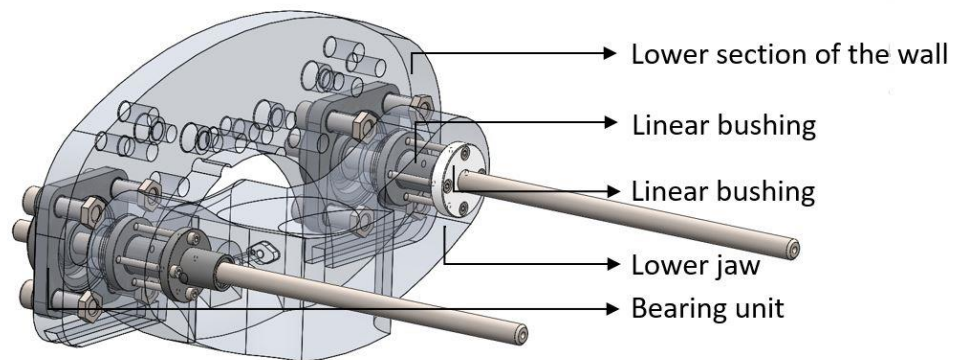


Figure 3.8: Lower jaw and wall connection.

On the previous design actuation of the lower jaw has been provided by rotary motor and the direction of motion has been changed by utilizing THK ball-screw. Thus, the previous design was complex in terms of the actuation of the lower jaws because there were more than one part related to transfer motion and additional mechanical components needed because of ball-screw. The second disadvantage was the dimension of this system. Ball screw itself cause an increase in the dimension on one axis. Due to the reasons actuator system was modified.

Linear actuator was used in the new design instead of rotary actuator and ball-screw thus system became very compact.

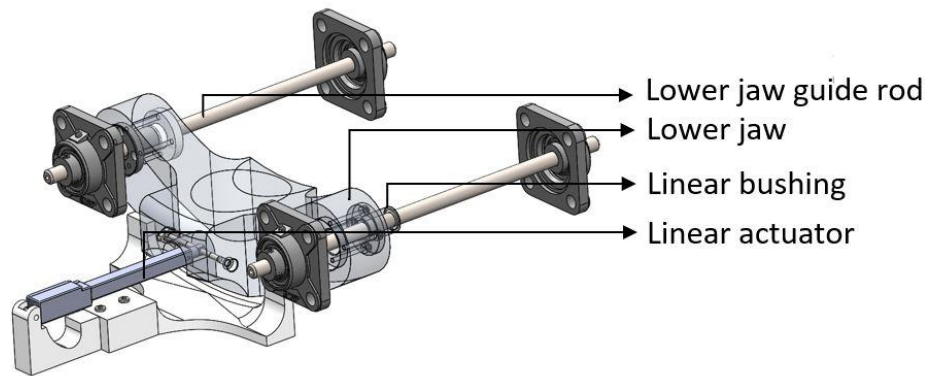


Figure 3.9: Linear actuator connection.

While one end of the linear actuator was connected to the base platform other end was connected to the mobile lower jaw. Lower and upper jaws can be assembled separately to examine the systems behavior to check if there exist any problem or not. Compactness of the system gave an advantage in this regard. While overall system would be assembled the step of connections can be different, most successful method is assembling lower section of collimator and upper section of the collimator separately finally each section would be connected to each other. This method can be seen in figure below.

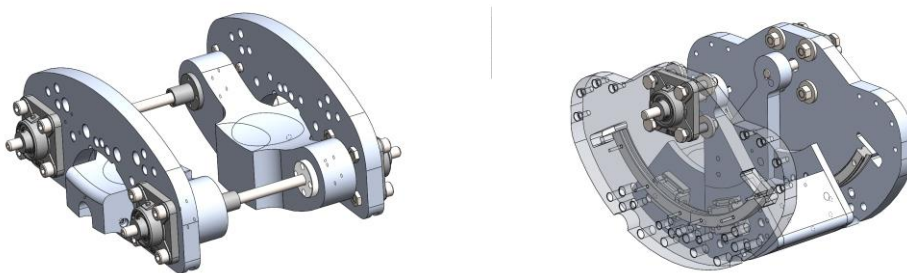


Figure 3.10: Upper section and lower section of collimator mechanism.

These sections would be connected by holes drilled on walls. The difference between walls of previous design and this design can be seen easily by comparing figure 2.15 and figure 3.11. Connection of upper and lower jaw is illustrated below. Previous design was a little bit complex in terms of the screw connections and tightening these screws was also problem because of the location of them. In this

reason wall was designed with holes on them which allows to tighten screws from outside of the collimator mechanism (figure 3.11).

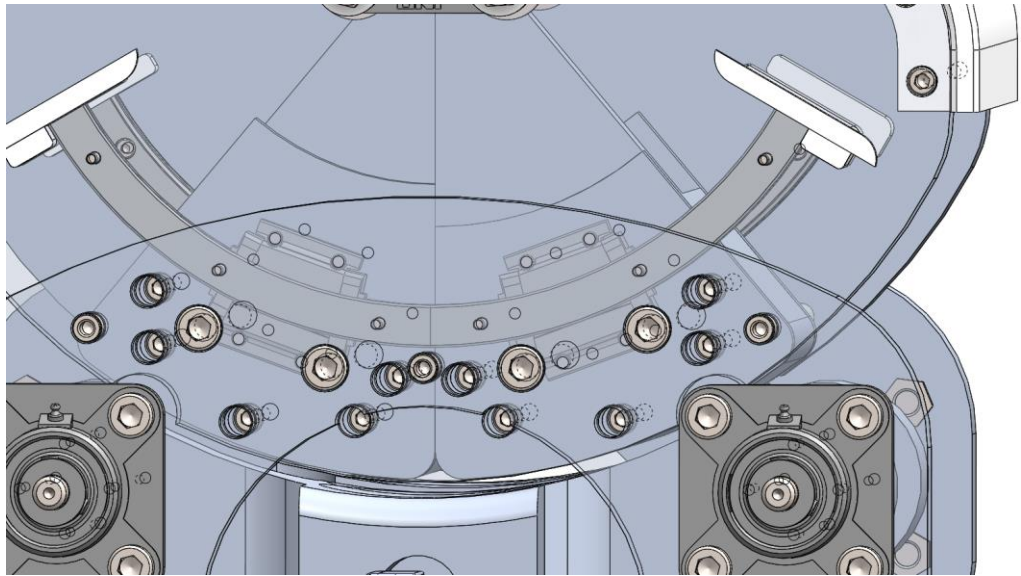


Figure 3.11: Holes on the wall that allows to reach lower jaw.

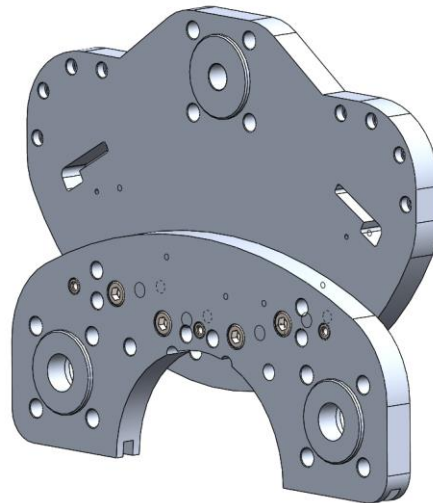


Figure 3.12: Connection of walls.

These walls were connected by screw-nut and the accurate positioning on each other was provided by three pins. Lower jaw actuation system and its assembly mentioned before. Now actuation system of the upper jaws will be mentioned. In previous design a DC motor coupled to the jaw directly by coupling and DC motor connected to steel sheet platform manufactured by weldment. Sheet platform connections between walls was not efficient in terms of the clearances and problem

caused from welding. These problems made us change the design of motion transfer system of upper jaw and its mounting to the wall. Final and most effective design idea about this issue using a part that will connect the DC motor to the wall and the coupling would be placed into this system. While mounting connector part to the wall form closed design procedure was followed to prevent clearances, unless clearances was prevented the error would be directly transferred to the upper jaw. As the mechanism designed for radiation therapy that sort of failures will not be tolerated in terms of the success and importance of the operation (Importance of dose delivery to the target tissue was mentioned in chapter 1).

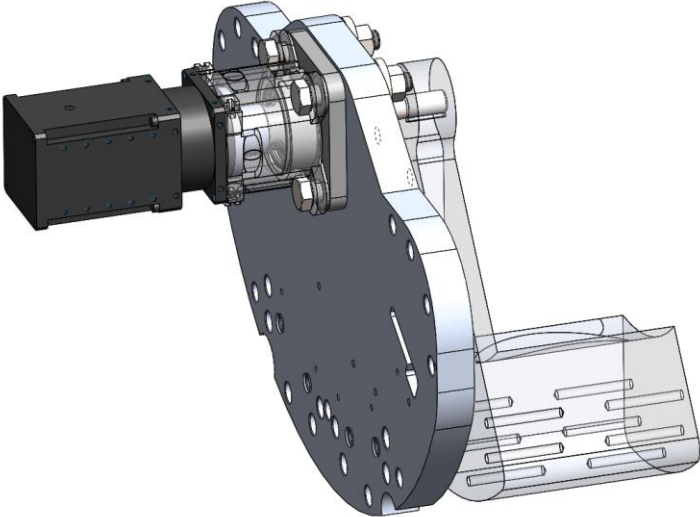


Figure 3.13: Connection of DC motor to the wall and motion transfer to the jaw.

Another component was changed in second design is the bars which was used to hold the huge walls at an exact distance from each other and which used to compensate forces caused from the center of mass point of old walls, this problem was mentioned in chapter 2 and can be seen in figure 2.15. These bars with “O” shaped cross-section was heavy and caused to a problem in terms of the hardness of assembling and disassembling of lower parts of the previous collimator mechanism. In second design these bars transferred to upper section of the Collimator and re-designed to abolish problems (figure 3.14).

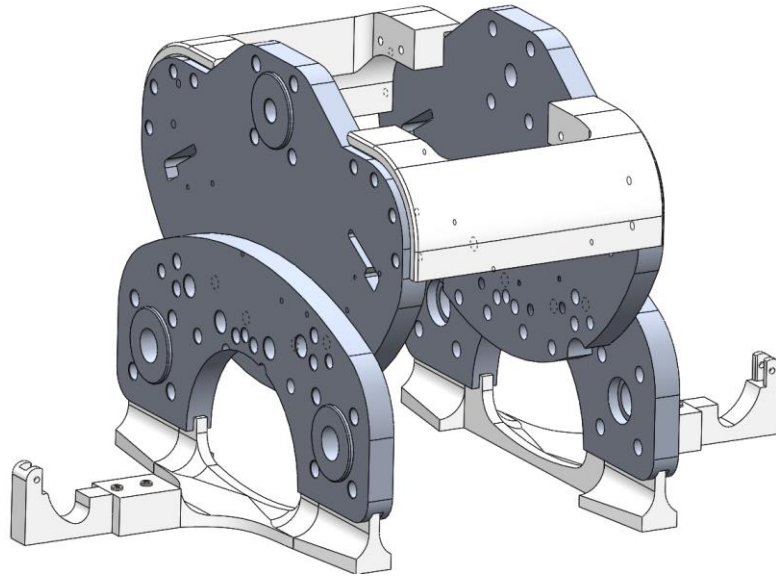


Figure 3.14: Stabilization bars on assembly.

The second design is not as rigid as first design thence, lower section of the system should be strengthened like upper section in order to prevent elasticity of construction. The lower section of the system was connected to the ground so as to hold walls at an exact distance from each other. Thus, either of upper and lower sections of the walls has been supported not to allow bending or twisting. Stabilization components need to be design flexibility to create most effective component. As described in goals and constraints of the project there was an expectation to obtain the light-weight structure. These two reasons gave an idea of manufacturing these components by 3D rapid prototyping devices so-called 3D printers. After the selection of suitable rapid prototyping material and devices it became possible to design and manufacture most efficient design for these components. There are also two more components that were manufacturing by using rapid prototyping devices. One of them is stopper designed for the safety of circular guide and track. This provides not to pull out track from rail. Another component is the circular part mounted behind the linear bushings on the lower jaw. These components responsible for preventing penetration of the dust in where linear bushings mounted. These two components can be seen in figure 3.15.

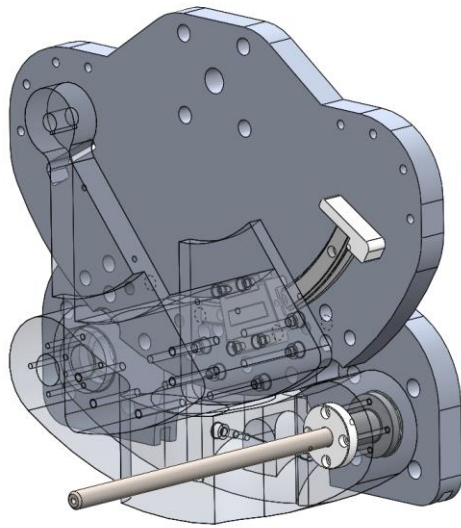


Figure 3.15: Parts manufactured by rapid prototyping devices.

As mentioned before the second design collimator mechanism would be mounted inside the linear accelerator head which is cylindrical thus, collimators dimensions and shape should be fit these criteria. End of the assemble on 3D simulation environment it was proofed and can be seen in figure 3.16.

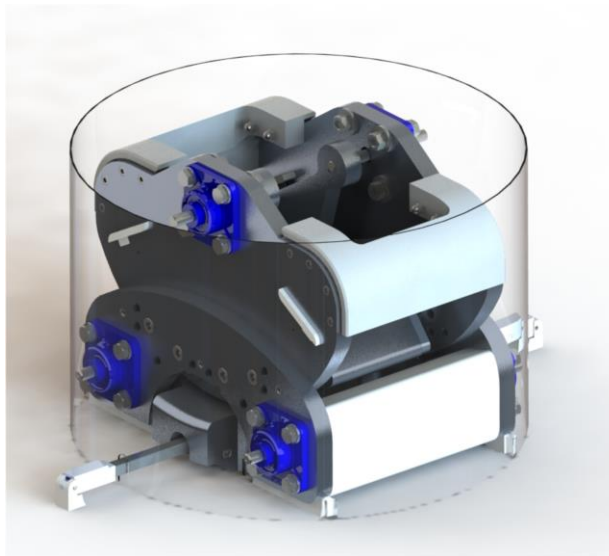


Figure 3.16: Collimator mechanism inside the cylindrical tube.

Some 3D images are given below for better understanding of the system.

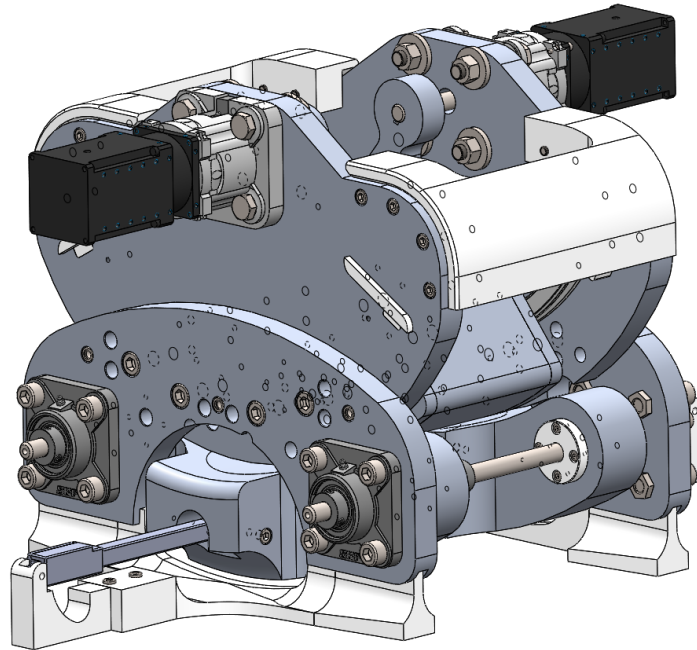


Figure 3.17: Isometric view of the Collimator mechanism.

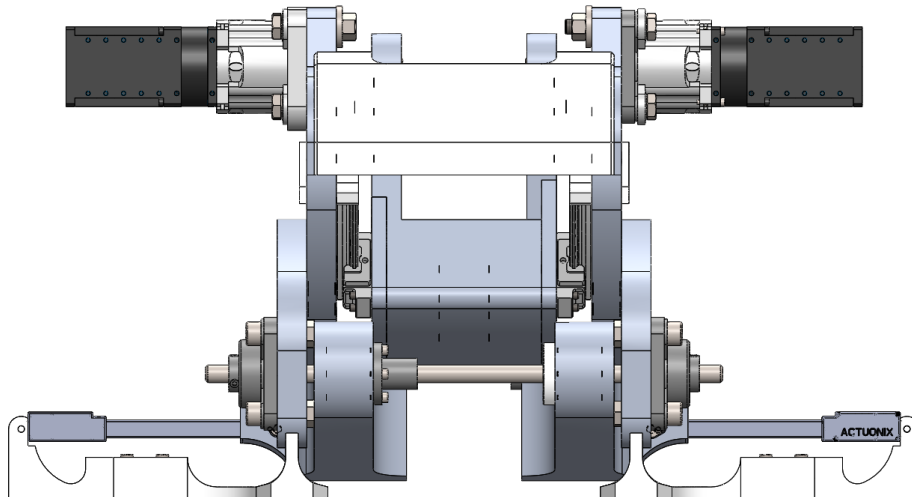


Figure 3.18: Front view of the Collimator mechanism.

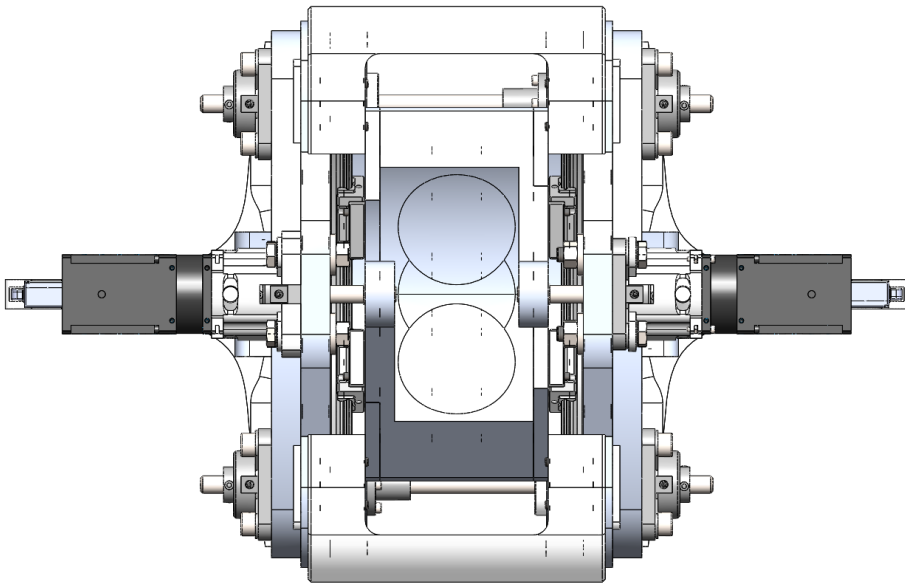


Figure 3.19: Top view of the collimator mechanism.

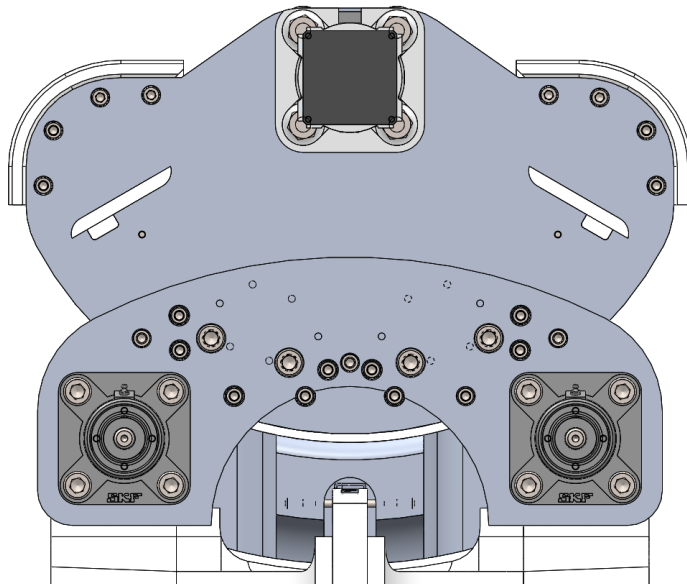


Figure 3.20: Side view of the collimator mechanism.

3.3 Prototype Manufacturing

Collimator mechanism as mentioned before in chapter 1, chapter 2 and chapter 3 needs to be designed and manufactured carefully due to the goals and constraints. As the precision of the mechanical system of the Collimator getting improved the success of the radiation therapy which this collimator used would be improved. Thus, after the 3D design and simulation of the Collimator have been done only think can be done to improve the precision of the mechanism is qualified manufacturing. During manufacturing process CNC (Computer numerical control) machines and rapid prototyping so-called 3D printers were used for the purpose of precise manufacturing. After each component manufactured each one of them measured and controlled in terms of suitability of form and dimensional tolerances stated in technical drawings and mechanical strength expectations gathered from calculations and simulations.

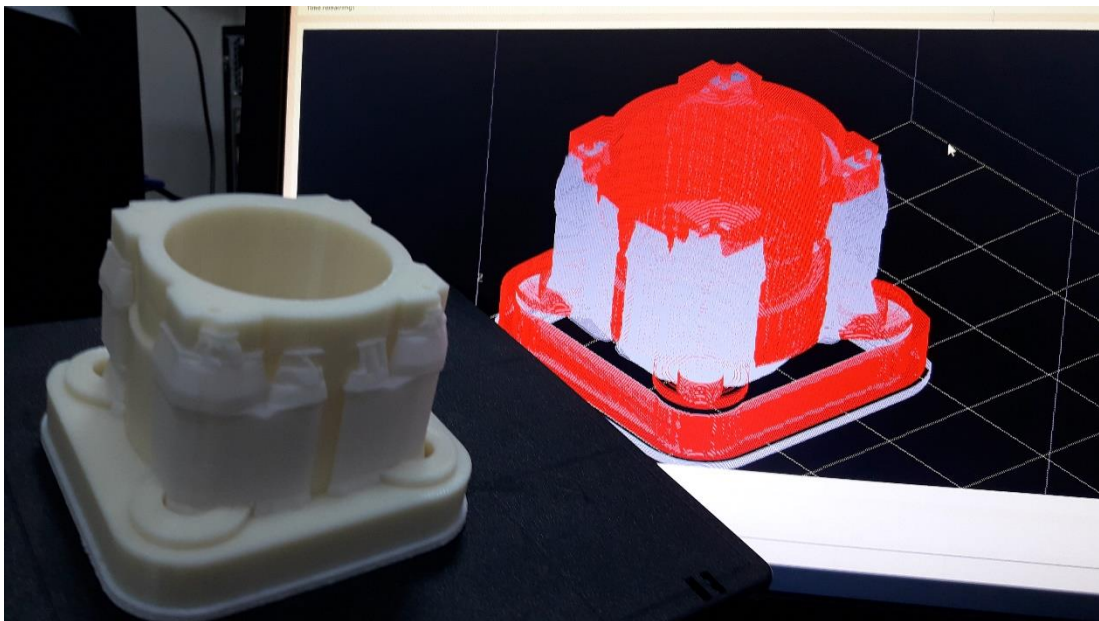


Figure 3.21: Rapid prototyping simulation and manufacturing of the upper jaw actuator connector.

All of the metal components were manufactured by experts and after the visual examination, each component of the Collimator mechanism examined and tested with respect to pre-prepared control scheme. These operations were carried out at the Biomedical-Robotics laboratory of our department. Rapid prototyping part of the manufacturing was carried out at the Prototyping and Manufacturing laboratory of our department.

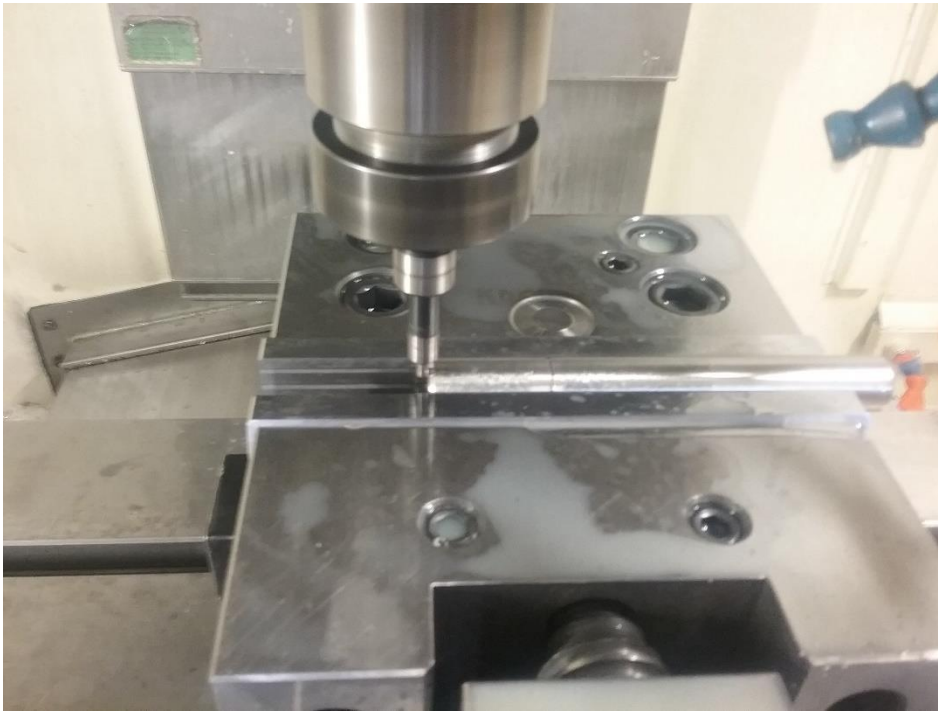


Figure 3.22: CNC machining of jaw rod.

After the examination of all parts had finished, assembling of the overall system has started. During assembling of the system each part mounted in the order of the pre-prepared assembling scheme.



Figure 3.23: Assembling of the jaws and walls.

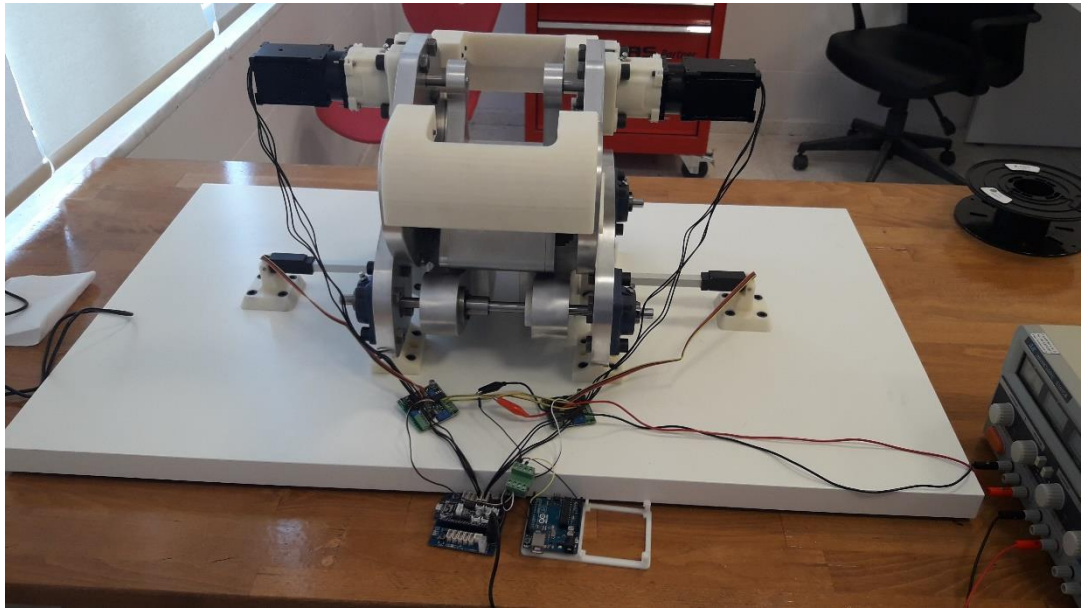


Figure 3.24: Collimator mechanism.

To give better understanding about what has been changed in second design there is a table below.

Table 3.1: Difference in physical properties between first and second design of Collimator mechanism.

	First Design	Second Design	Difference
Upper Jaw Mass	5.15 [kg]	3.37 [kg]	1.78 [kg]
Lower Jaw Mass	10.9 [kg]	3.51 [kg]	7.39 [kg]
Wall Mass	21.87 [kg]	5.58 [kg]	16.29 [kg]
Total Mass	147.39 [kg]	30.68 [kg]	116.71 [kg]
Total Volume	42984.6 [cm ³]	13402.45 [cm ³]	29582.15 [cm ³]
Footprint	6000 [cm ²]	1675.94 [cm ²]	4324.06 [cm ²]

After assembling of the collimator mechanism was finished, opening where beam pass through generated by moving four jaws and figure 3.25 can be compared with figure 2.2 and figure 2.14.



Figure 3.25: Three different positions and dimensions of opening.

4. SELECTION OF ACTUATORS

4.1 Design Constraints

Collimator mechanism is designed to generate and manipulate the so-called opening where beam allowed to pass directly without any absorption to the target area on the patient. The dose delivered to the target area is decided by radiotherapy expert with radiation therapy plan. In this plan the location and dose amount that would be delivered to the patient should be mentioned clearly because radiation therapy methods have side effects (Mentioned in chapter 1) as most of the other treatment methods. These side effect may be very crucial in terms of the health of the patients. One of the most dangerous cases is the possibility of the generation of cancerous tissue on healthy area. This case happens when the dose rate out of tolerance is delivered to healthy tissue. To avoid this sort of side effects it is important to deliver exact amount of beam to the target area by delivering minimum amount of dose to the healthy zone. In previous chapters, it is mentioned that the main design criteria of the collimator is to be able to achieve the most precise and easy controllable structure. In the light of this are of the main important factors that affects the precision of collimator mechanism is the actuators. Study on actuators which rotate and translate the jaws was examined in two ways.

- Connections of actuators.
- Selection of actuators.

Connections of actuators are important in terms of the transferring of motion. Motion generated by actuators should be transferred without loss. The loss of motion can be caused by elastic components used to connect driven components to the source of motion, for example, elastic couplings. These components can store the small amount of energy caused by torsional loads and it would cause to inequality between input and output motion rate. This drawback can be compensated by feedback control system but it would conflict with one of the goals which is ease of control.

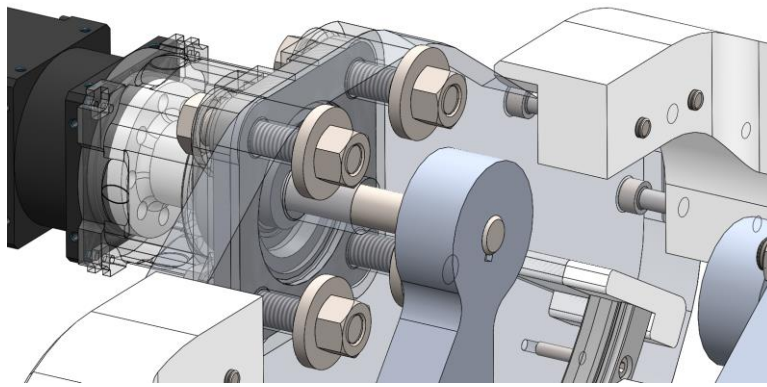


Figure 4.1: Rigid connections of upper jaw actuator.

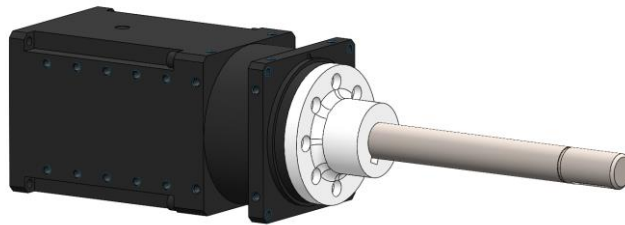


Figure 4.2: Rigid coupling mounted to actuator.

As seen figures in above, rigid connection is the one of rigid coupling which is mounted to actuator to transfer motion to rod and other one is the key on the rod to transfer rotary motion from rod to upper jaw. By this way error that cause from connections is tried to be minimized. This actuator should also be fixed to block its rotation around its own axis.

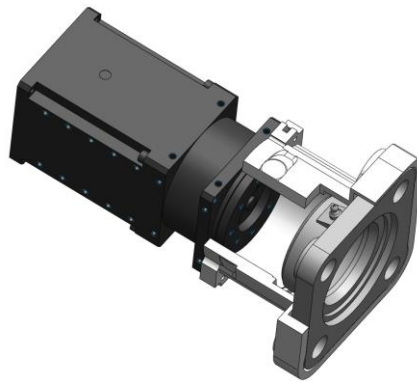


Figure 4.3: Fixing of actuator.

Figure.4.3 shows the fixing method of upper jaw actuator. The white component in figure connects the actuator to the Collimator mechanism and positional accuracy of this component is ensured by geometrically. Geometrically this component is designed to center its axis with that of actuator's and bearing's which is assembled to the wall. Centering ensured by the cutting surface of this component in form of bearing surface.

Another type of actuator used in this mechanism is a linear actuator that linearly moves the lower jaw so that the size and position of the opening can be changed.

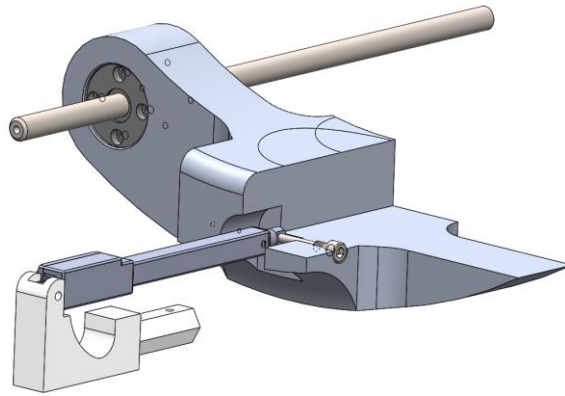


Figure 4.4: Actuator of lower jaw and its connection.

Lower jaw actuator can be seen in figure 4.4. As mentioned in previous design actuator type chosen for lower jaw was the rotary actuator. The rotary motion was converted to linear motion by mechanical ball-screw linear motion component. This component was both an additional mechanical component which causes to complexity in terms of its need of precise assembling and a component which cause to getting the bigger structure. In this regard main differences could be ensured with replacement of heavy ball-screw structure with linear actuator. Actually, this type of electrically powered actuators is not high load class actuators but the differences between loads applied to the upper jaw and lower jaw actuation systems are so different. Upper jaws move against gravitation but lower jaws move perpendicular to its direction.

Therefore, huge portion of the reaction force acted on actuator is generated due to friction and inertial forces of lower jaw.

4.2 Calculations

These reaction forces acted on lower and upper jaws' actuators were obtained by utilizing motion simulation runs on 3D modelling and simulation software SolidWorks. Actuators were selected in the light of simulation data. In this regard correctness of data obtained from simulation results were also checked by engineering calculation methods. After mathematical calculations was verified the simulation data, actuators were selected. There were two important points when actuators were being selected; output torque and precision of actuators. Resultant torque and force of actuators were obtained by multiplication of the simulation results with factor of safety.

Due to the fact that no part of the system out of moving components would affect the simulation results only moving parts inserted to simulation environment in order to lower simulation time.

Simulation input speeds were decided with respect to the necessary time that will spend during the radiation treatment. Each jaw should be able to pass 80mm length of the its full path in 5 seconds. By using this data input motions were given to the jaws.

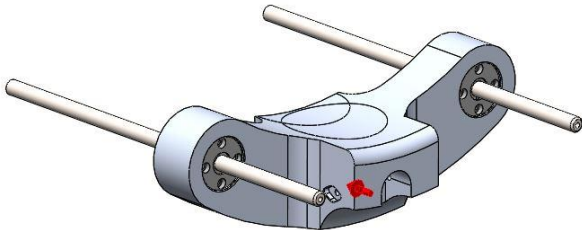


Figure 4.5: Stripped lower jaw assembly to simulation.

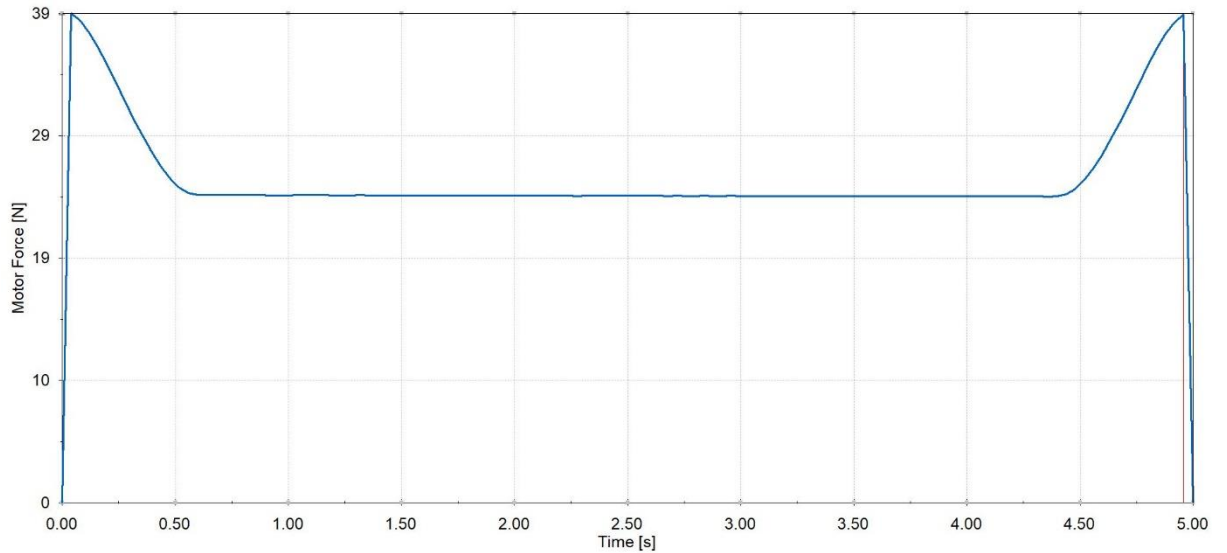


Figure 4.6: Lower jaw actuator force requirement.

Figure 4.6 show us maximum linear force requirement of lower jaw is 39 [N]. Motion of the lower jaw travels its full stroke at 80mm and this motion should be as fast as possible. It is easy to see that the peak point of force requirement graph related with the acceleration and deceleration of the jaw's itself.

$$F_r = F \times s \quad (4.1)$$

F: Peak point of simulation data.

s: Factor of safety.

In this study “s” was chosen as 2.5.

By this way;

$$F_r = 39 \times 2.5 = 97.5 [N]$$

Actuonix L-16 P miniature linear actuator was selected to actuation of lower jaws. By this actuator;

- Ease of assemble
- Ideal dimensions
- Necessary force

were obtained.

Actuator selection for upper jaws was more critical than the lower jaws. If it is neglected that the penumbra and scatter caused from error of the displacement, effect of lower jaw error would be proportional to error of its linear displacement. On the other hand, effect of upper jaw motion error would be proportional to error of the angular displacement and distance between source and target. The distance between source and target would be caused to increase effect of this error on target area. In this regard precision of upper jaw actuator as important as its torque capacity.

As in the lower jaw, no part of the system would affect to the simulation results only moving parts inserted to simulation environment to upper jaw simulation.

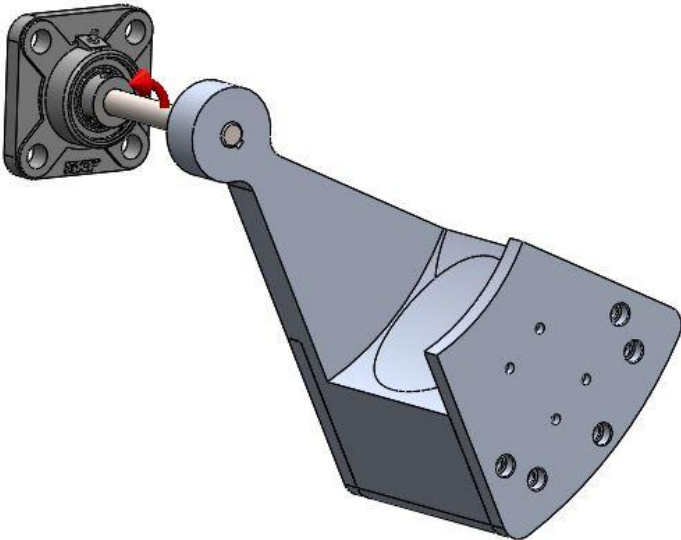


Figure 4.7: Stripped upper jaw assembly to simulation.

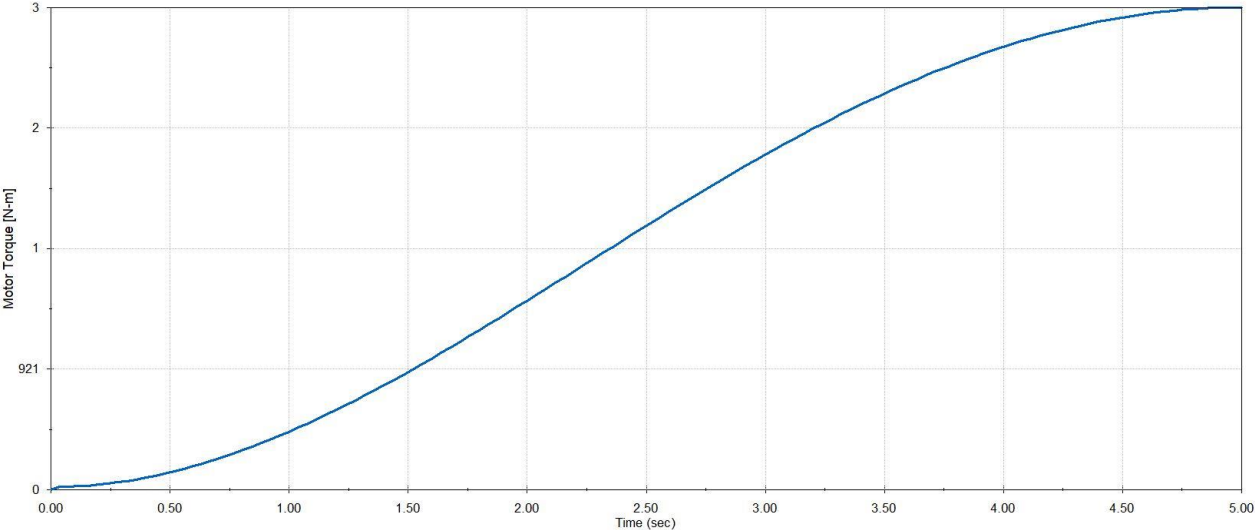


Figure 4.8: Upper jaw actuator force requirement.

Figure 4.8 show us maximum torque requirement of upper jaw is 3.7 [N-m].

$$T_r = T \times s \quad (4.2)$$

T: Peak point of simulation data.

s: Factor of safety.

In this study “s” was chosen as 2.5.

By this way;

$$T_r = 3.7 \times 2.5 = 9.25 [N - m]$$

DYNAMIXEL PRO L54-50-S500-R robot actuator was selected to actuation of lower jaws. By this actuator;

- Ease of assemble
- Ideal dimensions
- Necessary force
- Necessary precision

were obtained

5. PROTOTYPE TRIALS

After the prototype of collimator mechanisms assembling finished mechanical examinations done. Examinations include visual controls, mechanical controls, comparison of structural properties obtained from 3D simulation environment and real-life conditions etc. It is followed by examination of actuator with no load. Actuators had been assembled and prototype trials was begun.

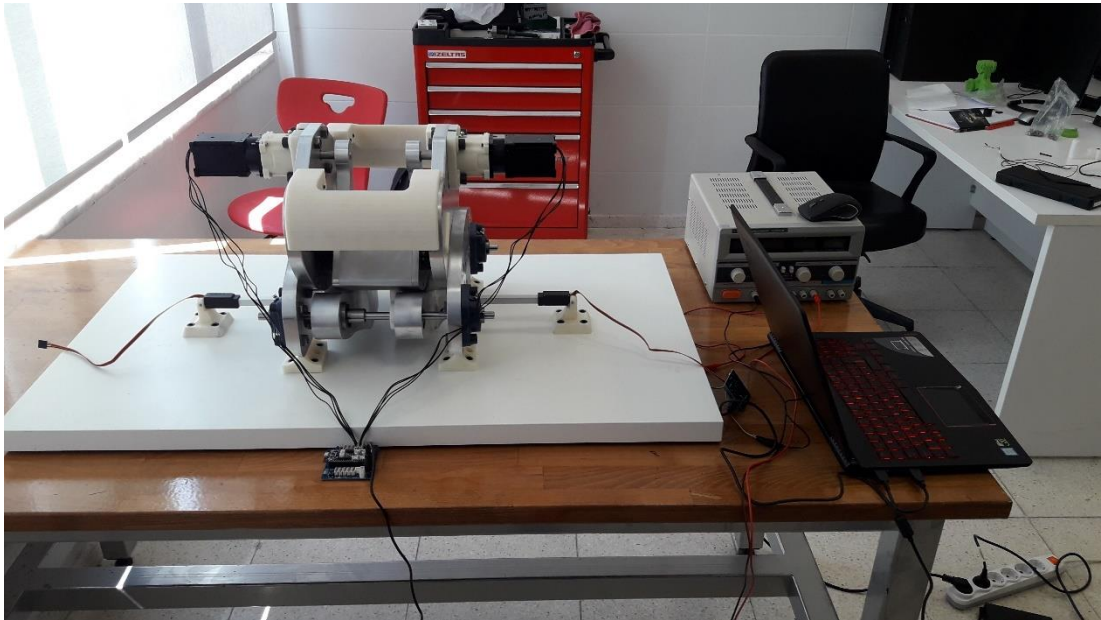


Figure 5.1: Prototype trial setup.

The purpose of trials is comparing the mechanism designed in CAD software and mechanism manufactured and assembled. Most important part of trials is to move jaws so as to generate rectangular opening, changing its dimensions and changing its positions. At first lower jaws motion was observed and recorded so as to catch every detail of motion of lower jaws and its effects on overall system.

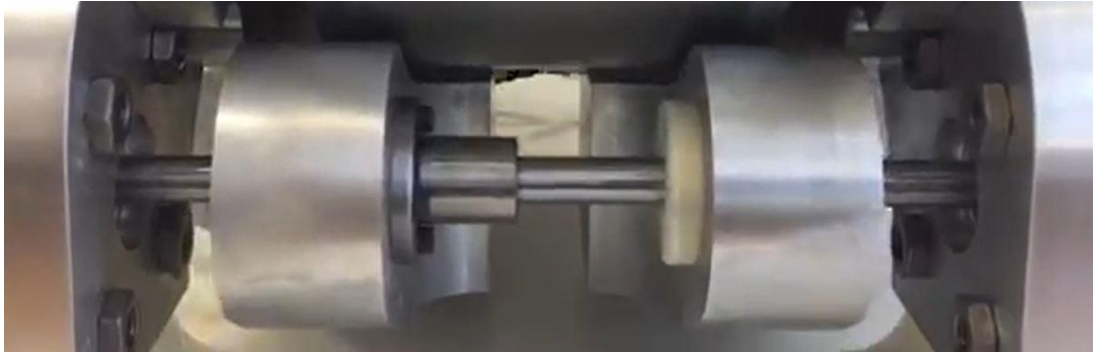


Figure 5.2: Lower jaw motion pose 1.



Figure 5.3: Lower jaw motion pose 2.



Figure 5.4: Lower jaw motion pose 3.

Figure 5.2, figure 5.3 and figure 5.4 shows the closing period of lower jaws at the central axis of Linac.

Same procedure applied to the upper jaws. But this time control applied to the upper and lower jaws at same time because rectangular opening dimension and position would be tried to changed.



Figure 5.5: Upper jaw motion pose 1.



Figure 5.6: Upper jaw motion pose 2.

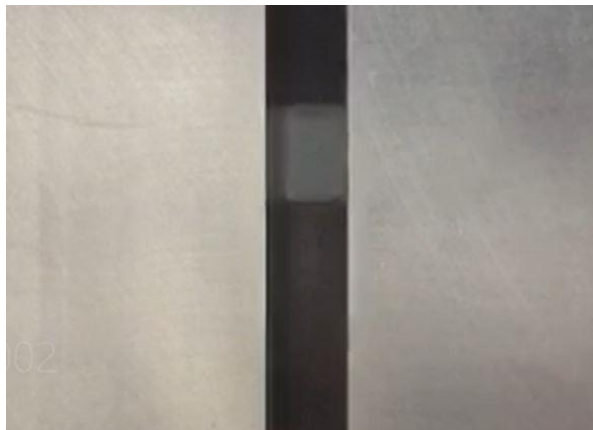


Figure 5.7: Upper jaw motion pose 3.

6. THEORETICAL MODIFICATION OF LOWER JAW DESIGN

As the collimator mechanism would be mounted to Linac devices, body of collimator mechanism in terms of the shape should be appropriate to the Linac head. In next studies this issue is aimed to be involved to design procedure as a major goal. Lower jaw actuators mounted to test setup base due to the fact that Linac head geometry and dimensions is not obvious. When the device would have been decided to be tested with a Linac, the outer geometry of the collimator mechanism would be modified so as to make it possible to be mounted to Linac head. Medical test phase of the project will have been started with this step. Medical test step of the project will include control system and software design to the Collimator mechanism. Also, another idea to improve collimator's performance is to lowering the overall weight by means of lightweight materials. When using light weight material on manufacturing of jaws, surface coating can be solution not to decrease the shielding performance of jaws. During designing and manufacturing of Collimator mechanism, limited manufacturing opportunities was a disadvantageous in terms of the compact design methods. In next studies this problem would be tried to be solved by using new manufacturing approach which provides flexibility in terms of complex geometry formation such as plastic injection, casting, additive manufacturing, etc.

There would be mechanical modification on system. In chapter 2 and 3, it is mentioned that the modification reasons and effect of collimator mechanism. One of the important output of modification is reduced scattering and penumbra due to the circular movement of upper jaw. Collimator trials shows that the linear motion of lower jaw caused to changing alignment angle between beam and contact surface of lower jaws. It improves the rate of scattering issue and penumbra generation. In this regard lower jaws working principle and shape have been decided to be changed.

In order to start design procedures, it is very important to form and understand the design constraints as a first consideration. These constraints are formed with

respect to information gathered by synthesizing of learning outcomes of all of the previous sections. Figure 6.1 illustrates a dual leaf collimator block that is placed in front of a point source for adjustment of opening. Due to the geometry of the collimator blocks, scattering regions are inevitably formed as the beam travels through the collimator opening. Analyzing only the figure, the simplest solution to this problem might be thought as decreasing the thicknesses of the blocks to reduce the amount of scattering (It is assumed that the leaf end shape is flat). However, doing so will render collimators shielding property inefficient for adjustments. This issue is mentioned in chapter 1 as interleaf transmission. Without reducing the necessary leaf thickness another possible solution can be given as the modification of the wall geometry, where beam scattering happens. On the other hand, as collimator leaves are dynamically moving with respect to the adjustment of the beam characteristics on target plane, efficiency of the specific wall geometries on scattering will vary throughout the leaf workspace. Figure 1.12 shows us how occurs this phenomenon.

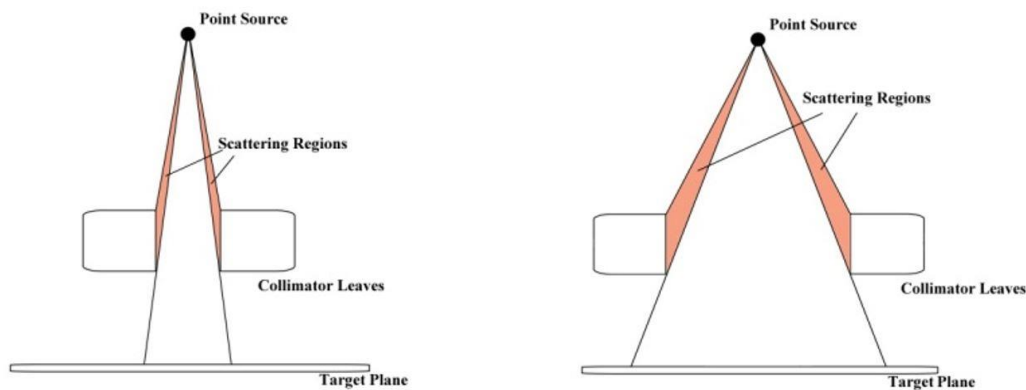


Figure 6.1: Scattering regions of the point source and their variations for different positions of the collimator leaves.

In the light of these, following sets of design constraints have been decided to be considered.

- In order to preserve shielding ability as much as possible, total material thickness in front of the source should be kept intact with the new proposed approach. The relation between shielding ability and jaw thickness can be seen

in chapter 1- figure 1.11, where penumbra formation was mentioned and illustrated.

- Wall geometry of the leaves should be able to be modified continuously in every instantaneous position of the blocks in order to reach reduced scattering fields.
- If the geometry of the leaf walls is to be changed continuously with respect to the leaf positions, motions should be carried out by using minimum number of actuators for cost and control efficiency.

From this point of view, collimator leaves are decided to be designed as vertically stacked layers that are assembled on top of each other (figure 6.2) unlike the common multi-leaf collimator designs that are using horizontal stacking. As seen in figure 6.2, this approach reduces the amount of scattering by preserving the total amount of shielding thickness. This approach provides leaves ends to move as if they rotate around the point source and cause to better angular alignment between wall and beam. Also by increasing the total number of layers, in other words reducing the individual thicknesses of the layers by preserving the overall thickness, finer results can be accomplished. Consequently, decreased individual leaf thickness and dynamic jaw shape was found as the solution of this problem.

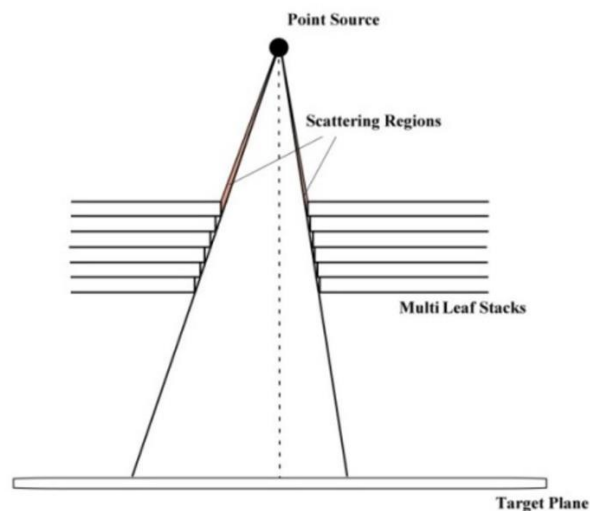


Figure 6.2: Proposed collimator with vertically layered multi leaf stacks, and reduced scattering regions.

As it can easily be seen from figure 6.2, although there exist multiple layers of leaves to be adjusted their motions are dependent on each other as the leaves on both

sides have to be aligned on the hypotenuses of the right and left triangle in order to cause minimal scattering. Due to the fact that right and left sections of the collimator system should be independent, it is possible to control overall motion that is needed to adjust beam opening by utilizing a single actuator for each side. In the light of this, multiple slider crank mechanisms that are driven by a single input are considered to be designed for each collimator sections (Figure 6.3).

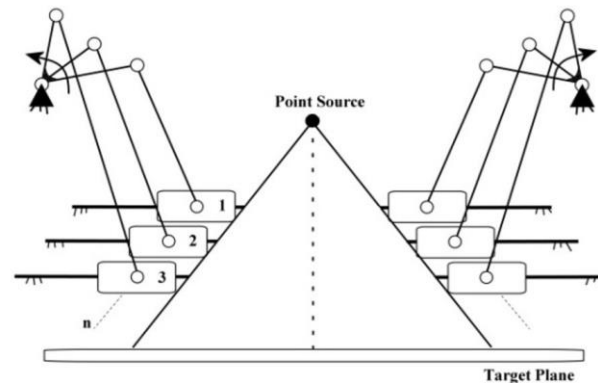


Figure 6.3: Multiple slider crank mechanisms on both sections of the collimator. Leaves that are formed by the sliders on individual sections are controlled by single input.

After the decision on the structural design part of the overall collimator mechanism was made, the only step that is left, can be given as forming a procedure that needs to be followed in order to calculate the construction parameters (fixed parameters) of the mechanism. Due to the fact that the individual shortest vertical distances between the planes of point source and collimator system are always fixed and defined with respect to the dimensions of the radiotherapy manipulator, the geometry of the beam triangle is only defined by the position of the first sliders. Thus, the positions of the remaining sliders can be considered as the functions of the first slider positions. From this point of view, in order to calculate the whole construction parameters, procedure of function generation synthesis will be sufficient precision points is developed for the given mechanism and explained in the following section.

Before the integration of the function generation synthesis into a collimator mechanism, kinematic synthesis studies of a four bar mechanism was done and results were compared.

6.1 Kinematic Synthesis

Motion study of machines and mechanism may be achieved by two methods as analysis and synthesis. They can simply be described as studies that deal with the mechanical systems in order to understand or fulfill their certain motion characteristics. In this chapter of the thesis, kinematic synthesis of the mechanisms that will be explained and the method will take place later in the design of multileaf collimator system. The decision of the kinematic synthesis methods and its procedures are one of the most important steps during the mechanical design, as dimensions of the parts and error characteristics of the designed mechanism are obtained by kinematic synthesis [37].

6.1.1 Types of kinematic synthesis

Basically, there are three types of kinematic synthesis methods to designate the output characteristic of the mechanism as function generation synthesis, body guidance synthesis and path generation synthesis. Due to the fact that it will be utilized throughout the thesis, function generation synthesis will be discussed in this study.

6.1.1.1 Four bar kinematic synthesis with 3 precision points

Function generation synthesis attempts to design construction parameters of the mechanisms to provide a specified function relation between input and output motion.

A simple example can be given by synthesizing a four-bar linkage to generate the function $y = f(x)$. In this case x would represent the motion of the input link so that the motion of the output link will approximate the function y .

In order to carry the function generation of four-bar mechanism loop closure equation should be formed to reach the function of the system.

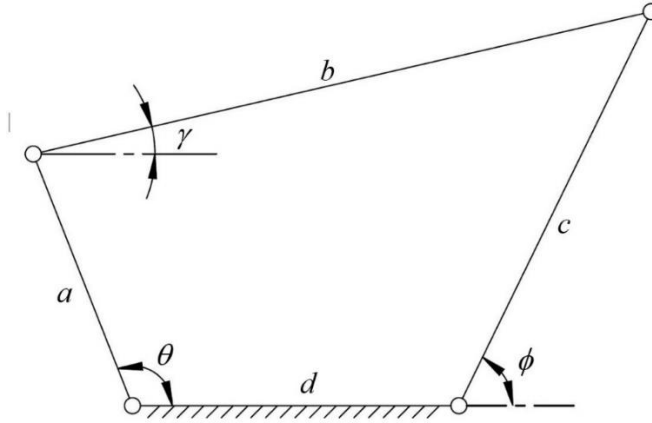


Figure 6.4: Four-bar mechanism represented with its closed-loop parameters.

As seen in the representation of the four-bar in figure 6.4 closed loop equation of the mechanism can be written as,

$$\vec{a} + \vec{b} = \vec{d} + \vec{c} \quad (6.1)$$

$$ae^{j\theta} + be^{j\gamma} = de^{j0} + ce^{j\phi} \quad (6.2)$$

After this step sine and cosine terms of the equations will be represented as $\cos \theta \rightarrow C\theta$, $\sin \theta \rightarrow S\theta$ for the ease of notation. If equation 6.2 is expanded into its imaginary and real components equation 6.3 will be formed.

$$aC\theta + aS\theta + bC\gamma + bS\gamma = d + cC\phi + cS\phi \quad (6.3)$$

Equation 6.3 can be separated into two parts; as

Real terms,

$$aC\theta + bC\gamma = d + cC\phi \quad (6.4)$$

and imaginary terms,

$$aS\theta + bS\gamma = cS\phi \quad (6.5)$$

As mentioned before, function generation synthesis of a mechanism aims to obtain a mechanism that will approximate the input motion to the function of output. It means that input θ of the four-bar mechanism shown in figure 6.1 would be approximated to that of output ϕ . Thus, it is clear that γ should be eliminated from equation 6.3 to left ϕ and θ alone.

$$bC\gamma = d + cC\phi - aC\theta, \quad bS\gamma = cS\phi - aS\theta \quad (6.6)$$

In order to eliminate the terms in equation 6.6 which include γ , two equations are squared and added together. Thus, the terms in the left side is simplified with respect to the Pythagorean formula for sines and cosines, $(bC\gamma)^2 + (bS\theta\gamma)^2 \rightarrow b^2(C^2\gamma + S^2\gamma) = b^2(1)$ (equation 6.7).

$$b^2 = d^2 + c^2C^2\phi + a^2C^2\theta + c^2S^2\phi + a^2S^2\theta + 2dcC\phi - 2daC\theta - 2caC\phi C\theta - 2caS\phi S\theta \quad (6.7)$$

Further simplification results in,

$$b^2 = d^2 + c^2 + a^2 - 2ca(C\phi C\theta + S\phi S\theta) + 2dcC\phi - 2daC\theta \quad (6.8)$$

Where $C\phi C\theta + S\phi S\theta = C(\theta - \phi)$

In order to reduce the number of unknowns in equation 6.8 “d” parameter can be taken as a scaling factor (d=1) as it will not affect input output function relation, (equation 6.9). It should be noted that the results (link lengths) can be scaled up by the desired amount of d later.

$$b^2 = 1 + c^2 + a^2 + 2cC\phi - 2aC\theta - 2caC(\theta - \phi) \quad (6.9)$$

Finally, the objective function in the form of a polynomial can be constructed,

$$0 = \frac{c^2 + a^2 + 1 - b^2}{2ca} + \frac{1}{a}C\phi - \frac{1}{c}C\theta - C(\theta - \phi) \quad (6.10)$$

$$0 = P_0f_0 + P_1f_1 + P_2f_2 - F \quad (6.11)$$

where,

$$P_0 = \frac{c^2 + a^2 + 1 - b^2}{2ca}, \quad P_1 = \frac{1}{a}, \quad P_2 = \frac{1}{c} \quad (6.12)$$

and,

$$f_0 = 1, \quad f_1 = C\phi, \quad f_2 = -C\theta, \quad F = C(\theta - \phi) \quad (6.13)$$

In order to solve equation 6.11, the values of terms θ and ϕ should be given as precision points. As there exist only three unknowns in equation 6.11 (P_0, P_1, P_2) three equations are needed to be formed by three sets of precision points $\phi_i = f(\theta_i) \quad i = 1, 2, 3$ (equation 6.14).

$$\begin{aligned}
P_0 f_0^1 + P_1 f_1^1 + P_2 f_2^1 - F_1 &= 0 \\
P_0 f_0^2 + P_1 f_1^2 + P_2 f_2^2 - F_2 &= 0 \\
P_0 f_0^3 + P_1 f_1^3 + P_2 f_2^3 - F_3 &= 0
\end{aligned} \tag{6.14}$$

Equation 6.14 can be written in matrix form as

$$\underbrace{\begin{bmatrix} f_0^1 & f_1^1 & f_2^1 \\ f_0^2 & f_1^2 & f_2^2 \\ f_0^3 & f_1^3 & f_2^3 \end{bmatrix}}_A \underbrace{\begin{bmatrix} P_0 \\ P_1 \\ P_2 \end{bmatrix}}_P = \begin{bmatrix} F_1 \\ F_2 \\ F_3 \end{bmatrix} \tag{6.15}$$

As seen in equations objective function consists of two types of parameters that are P_i and f_i . P_i 's contains system parameters and f_i 's contains system variables as input and output angles. Each f_i and F_i term can be found by assigning related precision point value to them. In this way now, it is possible to solve equation system and find values of unknown P terms.

$$\begin{bmatrix} P_0 \\ P_1 \\ P_2 \end{bmatrix} = [A^{-1}] \begin{bmatrix} F_1 \\ F_2 \\ F_3 \end{bmatrix} \tag{6.16}$$

After finding values of P_i system construction parameters (a,b,c) can be calculated by using equation 6.12

Example: Design a four-bar mechanism that will generate $\phi = \theta^{1.3}$ function between the input interval $30^\circ < \theta < 70^\circ$

To solve given system, 3 precision points are needed related to form three equations. These points are chosen from input angle interval by using equal spacing.

$$\theta_1^1 = 30^\circ = 0.5236 \text{ rad} \quad , \quad \theta_1^2 = 50^\circ = 0.8726 \text{ rad} \quad , \quad \theta_1^3 = 70^\circ = 1.2217 \text{ rad}$$

Output angles ϕ corresponding to each θ is formed by using constraint equation $\phi = \theta^{1.3}$ as,

$$\phi_1^1 = 0.4312 \text{ rad} \quad , \quad \phi_1^2 = 0.8377 \text{ rad} \quad , \quad \phi_1^3 = 1.2973 \text{ rad}$$

After defining ϕ and θ values, f_i^j and F_j parameters are calculated and put into the equation 6.14. As result of these calculation P_i would be obtained as $P_0 = 1.0117$, $P_1 = 0.0934$, $P_2 = -0.1165$

and the construction parameters will be calculated as

$$a = 1/P_1 , b = \sqrt{a^2 + c^2 + 1 - 2P_0ac} , c = -1/P_2 \quad (6.17)$$

$$a = 10.6971 , b = 1.8249 , c = 8.5780$$

The system found above with resultant link lengths approximate the output angle to the function $\phi = \theta^{1.3}$. This system gives the results with a small error out of precision points. As seen in figure 6.5 at the precision points zero errors are achieved.

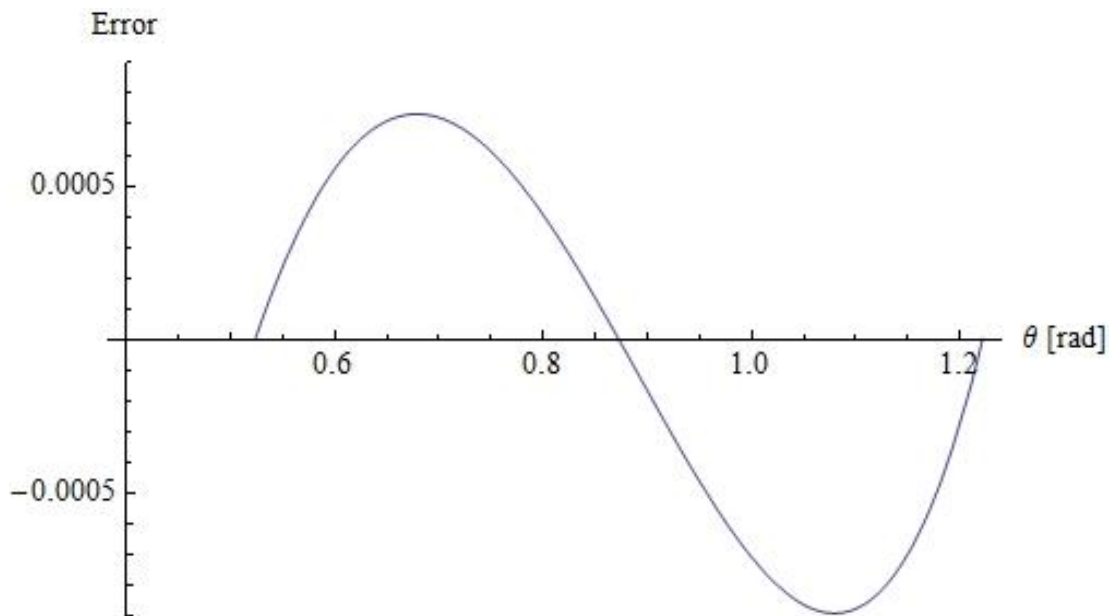


Figure 6.5: Error graph of three precision points synthesis.

6.1.1.2 Function generation synthesis of four-bar with 4 precision points

In order to refine the synthesis procedure and decrease the amount of error, number of precision points can be increased for the procedure. On the other hand as the number of precision points should be equal to the number construction parameters, to increase the amount of precision points by one, another parameter should be introduced to the system.

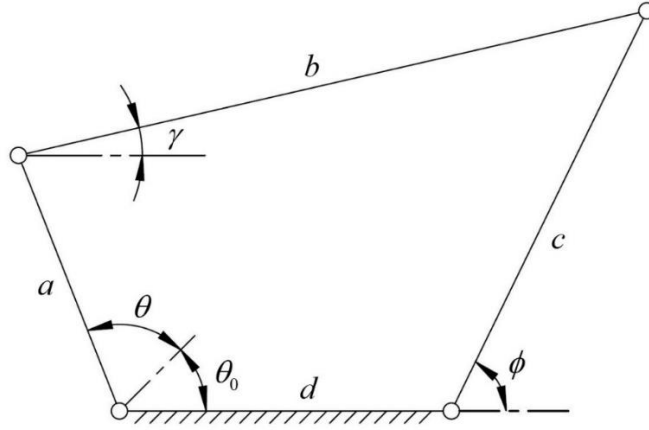


Figure 6.6: Modified four-bar mechanism with respect to four precision points.

As seen in the figure 6.6 usage of the fourth precision point is now possible to be assigned by the addition of θ_0 (input position) to the system. As another parameter is added to the four-bar mechanism, its objective function should also be modified. It is easy to obtain modified objective function by replacing each θ terms in equation 6.10 with $(\theta_0 + \theta)$ as;

$$\frac{c^2 + a^2 + 1 - b^2}{2caC\theta_0} + \frac{1}{aC\theta_0} C\phi - \frac{1}{c} C\theta + \frac{1}{c} \tan \theta_0 S\theta + \tan \theta_0 S(\theta - \phi) - C(\theta - \phi) = 0 \quad (6.18)$$

$$P_0 f_0 + P_1 f_1 + P_2 f_2 + P_3 f_3 + P_4 f_4 - F = 0 \quad (6.19)$$

Where the constant parameters are,

$$P_0 = \frac{c^2 + a^2 + 1 - b^2}{2caC\theta_0}, \quad P_1 = \frac{1}{aC\theta_0}, \quad P_2 = \frac{1}{c}, \quad P_3 = \tan \theta_0, \quad P_4 = \frac{1}{c} \tan \theta_0 \quad (6.20)$$

And variable functions are,

$$f_0 = 1, \quad f_1 = C\phi, \quad f_2 = -C\theta, \quad f_3 = S(\theta - \phi), \quad f_4 = S\theta, \quad F = C(\theta - \phi) \quad (6.21)$$

Inspecting the modified objective function reveal that there exists one non-linear term in the function ($P_4 = P_2 P_3$). After the linearization of this term, synthesis of four-bar mechanism would be possible by using the similar method as the previous example.

Let's represent the non-linear terms as λ where,

$$P_4 = P_2 P_3 = \lambda \quad (6.22)$$

And assume that all of the parameters P_i are linearly dependent on λ as

$$P_i = l_i + m_i \lambda \quad (6.23)$$

The new objective function will be,

$$P_0 f_0 + P_1 f_1 + P_2 f_2 + P_3 f_3 + \lambda f_4 - F = 0 \quad (6.24)$$

When equation 6.23 is inserted into equation 6.24, an objective function in the form of linear and non-linear terms is achieved.

$$(l_0 + m_0 \lambda) f_0 + (l_1 + m_1 \lambda) f_1 + (l_2 + m_2 \lambda) f_2 + (l_3 + m_3 \lambda) f_3 + \lambda f_4 - F = 0 \quad (6.25)$$

After the separation of the equation 6.25 into linear and non-linear parts two equations are formed and it is possible to find l_i and m_i by using these equations along with the precision points.

$$l_0 f_0 + l_1 f_1 + l_2 f_2 + l_3 f_3 = F \quad (6.26)$$

$$m_0 f_0 + m_1 f_1 + m_2 f_2 + m_3 f_3 = -f_4 \quad (6.27)$$

As each equation has four unknowns, it is possible to find them by re-defining known parameters for four precision points.

$$\begin{bmatrix} f_0^1 & f_1^1 & f_2^1 & f_3^1 \\ f_0^2 & f_1^2 & f_2^2 & f_3^2 \\ f_0^3 & f_1^3 & f_2^3 & f_3^3 \\ f_0^4 & f_1^4 & f_2^4 & f_3^4 \end{bmatrix} \begin{bmatrix} l_0 \\ l_1 \\ l_2 \\ l_3 \end{bmatrix} = \begin{bmatrix} F_1 \\ F_2 \\ F_3 \\ F_4 \end{bmatrix}, l_i : i = 0, 1, 2, 3 \quad (6.28)$$

$$\begin{bmatrix} f_0^1 & f_1^1 & f_2^1 & f_3^1 \\ f_0^2 & f_1^2 & f_2^2 & f_3^2 \\ f_0^3 & f_1^3 & f_2^3 & f_3^3 \\ f_0^4 & f_1^4 & f_2^4 & f_3^4 \end{bmatrix} \begin{bmatrix} m_0 \\ m_1 \\ m_2 \\ m_3 \end{bmatrix} = \begin{bmatrix} -f_4^1 \\ -f_4^2 \\ -f_4^3 \\ -f_4^4 \end{bmatrix}, m_i : i = 0, 1, 2, 3$$

After the parameters are calculated non-linear term λ will be found by using equation 6.22 as

$$(l_2 + m_2\lambda)f_2.(l_3 + m_3\lambda) = \lambda \quad (6.29)$$

After non-linear parameter λ is found it is possible to calculate all of the P_i parameters by utilizing equation 6.23 and construction parameters by using equation 6.20

Example: Design a four-bar mechanism that will generate $\phi = \theta^{1.3}$ function between input interval $30^\circ < \theta < 70^\circ$.

Same example can be carried out with four precision points to decrease the overall error.

In order to solve the given system, 4 precision points are needed to form the necessary equation system with four equations.

These precision points are chosen from the input angle interval by using equal spacing.

$$\theta_1^1 = 30^\circ = 0.5236 \text{ rad} , \theta_1^2 = 43.3333^\circ = 0.7563 \text{ rad},$$

$$\theta_1^3 = 56.6666^\circ = 0.9890 \text{ rad} , \theta_1^4 = 70^\circ = 1.2217 \text{ rad}$$

Output angles ϕ corresponding to each θ is found by using constraint equation $\phi = \theta^{1.3}$ as,

$$\phi_1^1 = 0.4312 \text{ rad} , \phi_1^2 = 0.6955 \text{ rad},$$

$$\phi_1^3 = 0.9857 \text{ rad} , \phi_1^4 = 1.2973 \text{ rad}$$

After defining precision point values, l_i, m_i and λ ($i=0,1,2,3$) parameters are calculated to obtain P_i ($i=0,1,2,3$).

by using equation 6.28

$$l_0 = 0.8687 , l_1 = 0.6157 , l_2 = -0.3729 , l_3 = -1.1861$$

$$m_0 = -1.9229 , m_1 = -1.1878 , m_2 = 3.1894 , m_3 = -2.8198$$

$$\lambda_1 = -0.3380 , \lambda_2 = 0.1455$$

If the first result of λ was chosen that the results will be,

$$P_0 = 1.5188 , P_1 = 1.0173 , P_2 = -1.4512 , P_3 = -0.2329 , P_4 = -0.3380$$

After the unknown parameters are computed, construction parameters of the system will be found from equation 6.20 as

$$a = 1 / (P_1 C \theta_0) , b = \sqrt{a^2 + c^2 + 1 - 2P_0 a c C \theta_0} , c = -1 / P_2 , \quad (6.30)$$

$$\theta_0 = \text{Arctan}(P_3)$$

$$a = 1.0093 , b = 0.6602 , c = 0.6890 , \theta_0 = -0.2288 \text{ rad}$$

The system found above with resultant link lengths approximate the output angle to the function. This system gives the results with a small error out of precision points. As seen in figure at precision points zero error values are achieved.

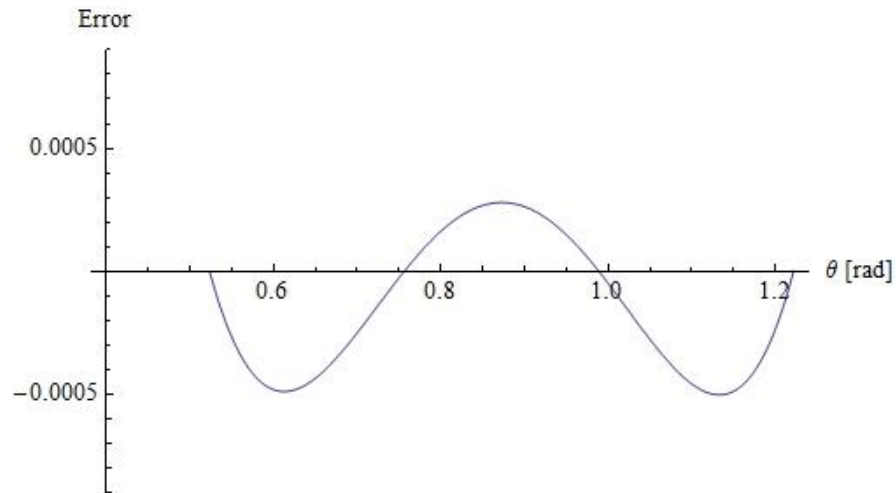


Figure 6.7: Error graph of four precision points synthesis.

Comparison between errors of function generation synthesis of four-bar mechanisms with three and four precision points is shown in figure 6.8. It can easily be seen that errors are referred by increased number of precision points.

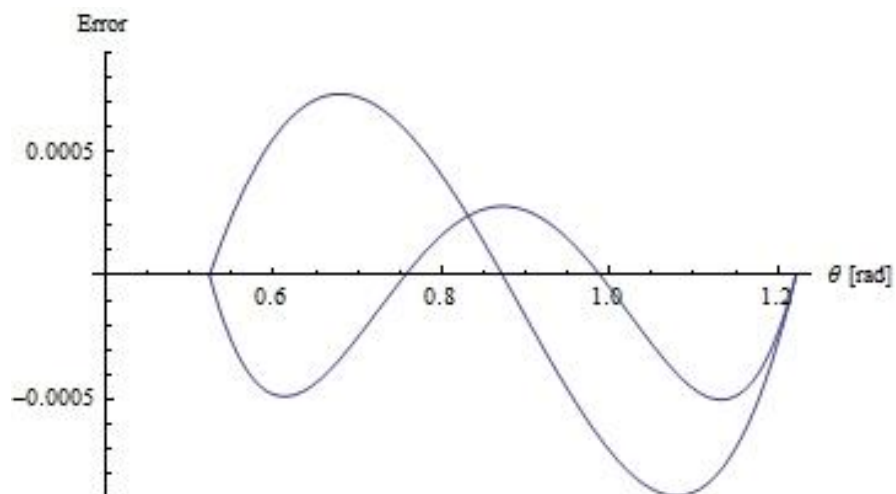


Figure 6.8: Comparison between three and four precision points synthesis errors.

6.1.1.3 Four-bar kinematic synthesis with 5 precision points

Similarly, in order to reduce the error further, additional precision point can also be utilized by addition of another construction parameter to the system. In the light of this information assign an additional precision point system needs to have additional dimensional parameter and it is provided by the addition of an offset angle to the output angle ϕ_0 (figure 6.9).

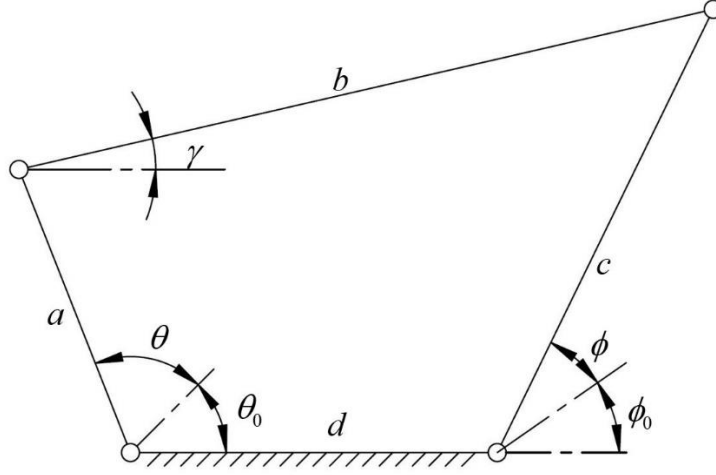


Figure 6.9: Modified four-bar mechanism with respect to five precision points.

Similarly, in order to form modified objective function each ϕ term in equation 6.18 can be replaced with $(\phi_0 + \phi)$.

After the modification, the new objective function can be written as

$$\frac{c^2 + a^2 + 1 - b^2}{2caC\theta_0C\phi_0} - \frac{1}{cC\phi_0}C\theta + \frac{1}{cC\phi_0}\tan\theta_0S\theta + \frac{1}{aC\theta_0}C\phi - \frac{1}{aC\theta_0}\tan\phi_0S\phi \quad (6.31)$$

$$+ (\tan\theta_0 - \tan\phi_0)S(\theta - \phi) - \tan\theta_0\tan\phi_0 - C(\theta - \phi) = 0$$

$$P_0f_0 + P_1f_1 + P_2f_2 + P_3f_3 + P_4f_4 + P_5f_5 + P_6f_6 - F = 0 \quad (6.32)$$

where,

$$P_0 = \frac{c^2 + a^2 + 1 - b^2}{2caC\theta_0C\phi_0}, \quad P_1 = \frac{1}{cC\phi_0}, \quad P_2 = \frac{1}{cC\phi_0}\tan\theta_0$$

$$P_3 = \frac{1}{aC\theta_0}, \quad P_4 = \frac{1}{aC\theta_0}\tan\phi_0, \quad P_5 = (\tan\theta_0 - \tan\phi_0), \quad (6.33)$$

$$P_6 = \tan\theta_0\tan\phi_0$$

and,

$$\begin{aligned} f_0 = 1, f_1 = -C\theta, f_2 = S\theta, f_3 = C\phi, f_4 = -S\phi, \\ f_5 = S(\theta - \phi), f_6 = C(\theta - \phi), F = C(\theta - \phi) \end{aligned} \quad (6.34)$$

As seen in equation 6.31, there exist two non-linear parameters in the modified objective function. As in the first case. Let's represent those parameters as λ_1 and λ_2 where

$$P_5 = \frac{P_2}{P_1} - \frac{P_4}{P_3} = \lambda_1, \quad P_6 = \frac{P_2}{P_1} \frac{P_4}{P_3} = \lambda_2 \quad (6.35)$$

P_5 and P_6 are not a linear terms these compose of P_1, P_2, P_3 and P_4 therefore, P_5 and P_6 linearized by assigning them λ_1 and λ_2 and all of the other P_i terms must be modified like below, if the unknown parameters are assumed to be linearly dependent non-linear parameters as,

$$P_i = l_i + m_i \lambda_1 + n_i \lambda_2 \quad (6.36)$$

The new objective function will be,

$$\begin{aligned} P_0 f_0 + P_1 f_1 + P_2 f_2 + P_3 f_3 + P_4 f_4 \\ + \lambda_1 P_5 + \lambda_2 P_6 - F = 0 \end{aligned} \quad (6.37)$$

If equation 6.36 is inserted into equation 6.37 and all of the linear and non-linear terms with λ_1 and λ_2 are separated in to three equations, new sets of objective function equations can be written as,

$$\begin{aligned} (l_0 + m_0 \lambda_1 + n_0 \lambda_2) f_0 + (l_1 + m_1 \lambda_1 + n_1 \lambda_2) f_1 \\ + (l_2 + m_2 \lambda_1 + n_2 \lambda_2) f_2 + (l_3 + m_3 \lambda_1 + n_3 \lambda_2) f_3 \\ + (l_4 + m_4 \lambda_1 + n_4 \lambda_2) f_4 + \lambda_1 f_5 + \lambda_2 f_6 - F = 0 \end{aligned} \quad (6.38)$$

$$l_0 f_0 + l_1 f_1 + l_2 f_2 + l_3 f_3 + l_4 f_4 = F \quad (6.39)$$

$$m_0 f_0 + m_1 f_1 + m_2 f_2 + m_3 f_3 + m_4 f_4 = -f_5 \quad (6.40)$$

$$n_0 f_0 + n_1 f_1 + n_2 f_2 + n_3 f_3 + n_4 f_4 = -f_6 \quad (6.41)$$

As each equation has five unknowns, it is possible to find them by re-defining known parameters for five precision points.

$$\begin{aligned}
& \begin{bmatrix} f_0^1 & f_1^1 & f_2^1 & f_3^1 & f_4^1 \\ f_0^2 & f_1^2 & f_2^2 & f_3^2 & f_4^2 \\ f_0^3 & f_1^3 & f_2^3 & f_3^3 & f_4^3 \\ f_0^4 & f_1^4 & f_2^4 & f_3^4 & f_4^4 \\ f_0^5 & f_1^5 & f_2^5 & f_3^5 & f_4^5 \end{bmatrix} \begin{bmatrix} l_0 \\ l_1 \\ l_2 \\ l_3 \\ l_4 \end{bmatrix} = \begin{bmatrix} F_1 \\ F_2 \\ F_3 \\ F_4 \\ F_5 \end{bmatrix}, l_i : i = 0,1,2,3,4 \\
& \begin{bmatrix} f_0^1 & f_1^1 & f_2^1 & f_3^1 & f_4^1 \\ f_0^2 & f_1^2 & f_2^2 & f_3^2 & f_4^2 \\ f_0^3 & f_1^3 & f_2^3 & f_3^3 & f_4^3 \\ f_0^4 & f_1^4 & f_2^4 & f_3^4 & f_4^4 \\ f_0^5 & f_1^5 & f_2^5 & f_3^5 & f_4^5 \end{bmatrix} \begin{bmatrix} m_0 \\ m_1 \\ m_2 \\ m_3 \\ m_4 \end{bmatrix} = \begin{bmatrix} -f_5^1 \\ -f_5^2 \\ -f_5^3 \\ -f_5^4 \\ -f_5^5 \end{bmatrix}, m_i : i = 0,1,2,3,4 \\
& \begin{bmatrix} f_0^1 & f_1^1 & f_2^1 & f_3^1 & f_4^1 \\ f_0^2 & f_1^2 & f_2^2 & f_3^2 & f_4^2 \\ f_0^3 & f_1^3 & f_2^3 & f_3^3 & f_4^3 \\ f_0^4 & f_1^4 & f_2^4 & f_3^4 & f_4^4 \\ f_0^5 & f_1^5 & f_2^5 & f_3^5 & f_4^5 \end{bmatrix} \begin{bmatrix} n_0 \\ n_1 \\ n_2 \\ n_3 \\ n_4 \end{bmatrix} = \begin{bmatrix} -f_6^1 \\ -f_6^2 \\ -f_6^3 \\ -f_6^4 \\ -f_6^5 \end{bmatrix}, n_i : i = 0,1,2,3,4
\end{aligned} \tag{6.42}$$

After the parameters are calculated non-linear terms λ_1 and λ_2 can be found by using equation 6.35 as,

$$\begin{aligned}
& \frac{(l_2 + m_2\lambda_1 + n_2\lambda_2)}{(l_1 + m_1\lambda_1 + n_1\lambda_2)} - \frac{(l_4 + m_4\lambda_1 + n_4\lambda_2)}{(l_3 + m_3\lambda_1 + n_3\lambda_2)} = \lambda_1 \\
& \frac{(l_2 + m_2\lambda_1 + n_2\lambda_2)}{(l_1 + m_1\lambda_1 + n_1\lambda_2)} \cdot \frac{(l_4 + m_4\lambda_1 + n_4\lambda_2)}{(l_3 + m_3\lambda_1 + n_3\lambda_2)} = \lambda_2
\end{aligned} \tag{6.43}$$

After the calculation of λ_1 and λ_2 it is possible to calculate all of the P_i parameters by using equation 6.36 and construction parameters by using equation 6.33

Example: Design a four-bar mechanism that will generate $\phi = \theta^{1.3}$ function between the input interval $30^\circ < \theta < 70^\circ$.

Similar example will be studied with five precision points as in order to reduce the overall error. After this example results obtained from this study and previous studies will be compared in terms of error.

In order to solve given system, 5 precision points are needed to form for the equation system with five equations. These precision points are chosen from the input angle interval by using equal spacing as.

$$\theta_1^1 = 30^\circ = 0.5236 \text{ rad} , \theta_1^2 = 40^\circ = 0.6981 \text{ rad} , \theta_1^3 = 50^\circ = 0.8726 \text{ rad}$$

$$\theta_1^4 = 60^\circ = 1.0472 \text{ rad} , \theta_1^5 = 70^\circ = 1.2217 \text{ rad}$$

Output angles ϕ corresponding to each θ in where $\phi = \theta^{1.3}$,

$$\phi_1^1 = 0.4312 \text{ rad} , \phi_1^2 = 0.6267 \text{ rad} , \phi_1^3 = 0.8377 \text{ rad}$$

$$\phi_1^4 = 1.0617 \text{ rad} , \phi_1^5 = 1.2973 \text{ rad}$$

After defining precision points values, l_i, m_i, n_i and λ_1, λ_2 parameters are calculated to obtain P_i ($i=0,1,2,3,4$).

Using equation 6.42 l_i, m_i, n_i ($i=0,1,2,3,4$) are calculated as,

$$l_0 = 0.9395 , l_1 = -0.1209 , l_2 = -0.1518$$

$$l_3 = -0.0525 , l_4 = -0.1798$$

$$m_0 = 0.5986 , m_1 = 0.9234 , m_2 = -0.3262$$

$$m_3 = 0.2891 , m_4 = -0.0220$$

$$n_0 = 0.9395 , n_1 = -0.1209 , n_2 = -0.1518$$

$$n_3 = -0.0525 , n_4 = -0.1798$$

Also using equation 6.43 non-linear parameter sets are found as,

$$\lambda_1 = -33.6205 , \lambda_2 = -216.058$$

$$\lambda_1 = -0.7126 , \lambda_2 = -0.0704$$

$$\lambda_1 = -1.8229 , \lambda_2 = -1.$$

$$\lambda_1 = 2.0136 , \lambda_2 = -1.$$

$$\lambda_1 = 1.6717 , \lambda_2 = 2.9914$$

After λ_1 and λ_2 pairs were chosen as $\lambda_1 = 1.6717$, $\lambda_2 = 2.9914$ and continued unknown parameters are calculated by using equation 6.33 as,

$$P_0 = 4.7508 , P_1 = 1.0611 , P_2 = -1.1514 , P_3 = 0.2736,$$

$$P_4 = -0.7545 , P_5 = 1.6718 , P_6 = 2.9914$$

Four-bar mechanism's parameters such as link lengths and off-set angle can be calculated by using P_i values. After the unknown parameters are calculated construction parameters can be extracted from them as,

$$\begin{aligned}
a &= 1 / (P_3 \cdot C\theta_0) , \quad b = \sqrt{a^2 + c^2 + 1 - 2P_0acC\theta_0C\phi_0}, \\
c &= 1 / (P_1C\phi_0) , \quad \theta_0 = \text{Arctan}(P_2 / P_1), \\
\phi_0 &= \text{Arctan}(P_4 / P_3)
\end{aligned}
\tag{6.44}$$

$$\begin{aligned}
a &= 5.3913 , \quad b = 2.2335 , \quad c = 2.7636, \\
\theta_0 &= -0.8261 \text{ rad} , \quad \phi_0 = -1.2228 \text{ rad}
\end{aligned}$$

The system found above with resultant link lengths approximate the output angle to the function. This system gives the results with a small error out of precision points, as seen in figure 6.10 at precision points the system generates no errors.

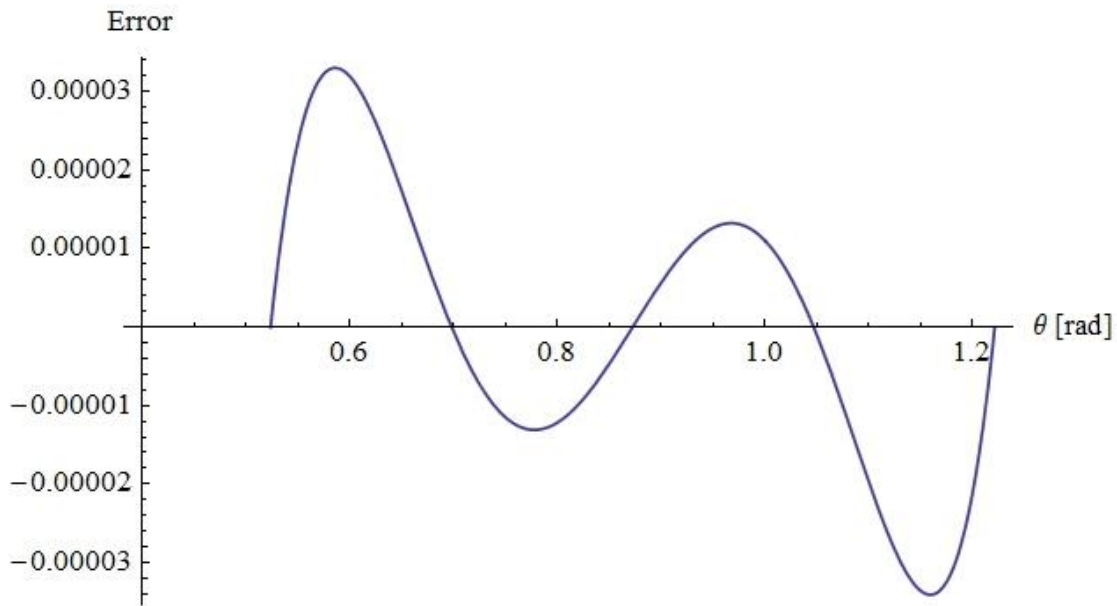


Figure 6.10: Error graph of five precision points synthesis.

Comparison between the results of function generator kinematic synthesis of four-bar mechanisms' error graph is shown in figure 6.11. Using the figure, it can be seen that the errors of function generator synthesis of four-bar with three, four and five precision points. As it is clear from graph the lowest error could be obtained from the study with five precision points.

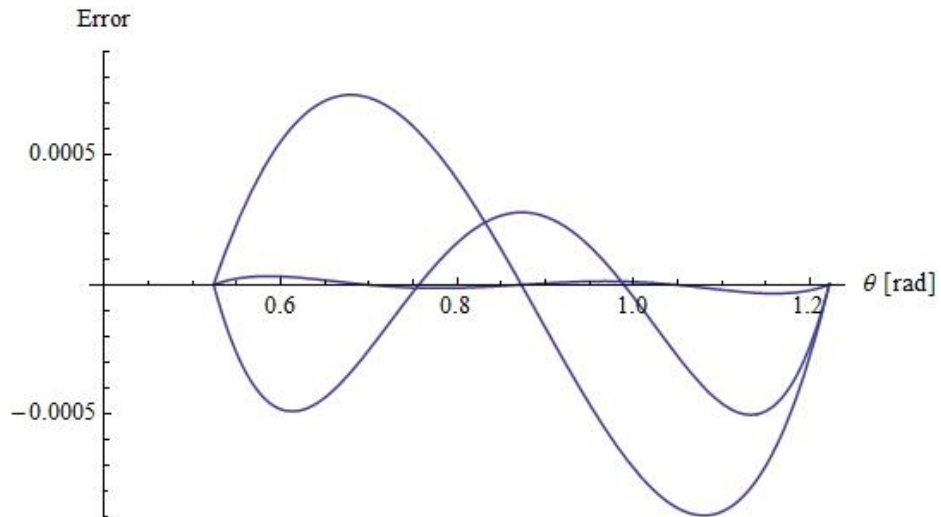


Figure 6.11: Comparison between three, four and five precision points synthesis errors.

6.1.2 Types of approximations

As seen in the previous section error graphs are oscillating into the motion interval, each of negative and positive peaks has different values between precision points for this reason in this section the purpose is to obtain better oscillation of error's.

6.1.2.1 Chebyshev approximation

Chebyshev approximation method will be applied to the function generation kinematic synthesis of four-bar function generator mechanism with five precision points. The output expectation of this study is to obtain an oscillating error output with constant absolute peak points as seen in figure 6.12.

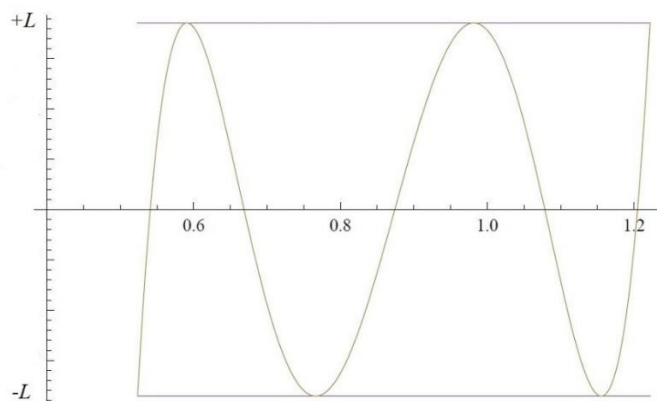


Figure 6.12: Illustration of output of Chebyshev approximation.

$\pm L$ represents the maximized errors. To obtain such an output characteristic we need to modify the objective function of the four-bar mechanism function generator with five precision points generated in previous section equation 6.32.

$$P_0 f_0^j + P_1 f_1^j + P_2 f_2^j + P_3 f_3^j + P_4 f_4^j + P_6 f_6^j + P_7 f_7^j - F = \underbrace{(-1)^{j+1} L}_{-f_5} P_5 \quad (6.45)$$

$$j = 1, 2, \dots, 6$$

$$P_6 = \frac{P_2}{P_1} - \frac{P_4}{P_3} = \lambda_1, \quad P_7 = \frac{P_2}{P_1} \frac{P_4}{P_3} = \lambda_2, \quad P_i = l_i + m_i \lambda_1 + n_i \lambda_2 \quad (6.46)$$

$$i = 1, 2, \dots, 5$$

j represents the number of precision points. L is the additional unknown therefore objective function requires six precision points instead of 5 to be solvable.

$$P_0 \cdot f_0 + P_1 \cdot f_1 + P_2 \cdot f_2 + P_3 \cdot f_3 + P_4 \cdot f_4 + P_5 \cdot f_5 + \lambda_1 \cdot P_6 + \lambda_2 \cdot P_7 - F = 0 \quad (6.47)$$

where,

$$P_0 = \frac{c^2 + a^2 + 1 - b^2}{2caC\theta_0 C\phi_0}, \quad P_1 = \frac{1}{cC\phi_0}, \quad P_2 = \frac{1}{cC\phi_0} \tan \theta_0,$$

$$P_3 = \frac{1}{aC\theta_0}, \quad P_4 = \frac{1}{aC\theta_0} \tan \phi_0, \quad P_5 = L, \quad (6.48)$$

$$P_6 = (\tan \theta_0 - \tan \phi_0), \quad P_7 = \tan \theta_0 \tan \phi_0$$

and,

$$f_0 = 1, \quad f_1 = -C\theta, \quad f_2 = S\theta, \quad f_3 = C\phi, \quad f_4 = -S\phi,$$

$$f_5 = -(-1)^{j+1}, \quad f_6 = S(\theta - \phi), \quad f_7 = C(\theta - \phi), \quad (6.49)$$

$$F = C(\theta - \phi)$$

Open form of objective function with linearized terms,

$$(l_0 + m_0 \lambda_1 + n_0 \lambda_2) f_0 + (l_1 + m_1 \lambda_1 + n_1 \lambda_2) f_1 + (l_2 + m_2 \lambda_1 + n_2 \lambda_2) f_2 + (l_3 + m_3 \lambda_1 + n_3 \lambda_2) f_3 + (l_4 + m_4 \lambda_1 + n_4 \lambda_2) f_4 + (l_5 + m_5 \lambda_1 + n_5 \lambda_2) f_5 + \lambda_1 f_6 + \lambda_2 f_7 - F = 0 \quad (6.50)$$

Now, it is possible to find l_i, m_i and n_i by using objective function.

$$l_0 f_0 + l_1 f_1 + l_2 f_2 + l_3 f_3 + l_4 f_4 + l_5 f_5 = F \quad (6.51)$$

$$m_0f_0 + m_1f_1 + m_2f_2 + m_3f_3 + m_4f_4 + m_5f_5 = -f_6 \quad (6.52)$$

$$n_0f_0 + n_1f_1 + n_2f_2 + n_3f_3 + n_4f_4 + n_5f_5 = -f_7 \quad (6.53)$$

Each equation has four unknown so it is possible to find unknowns by re-defining known parameters for five precision points.

$$\begin{bmatrix} f_0^1 & f_1^1 & f_2^1 & f_3^1 & f_4^1 & f_5^1 \\ f_0^2 & f_1^2 & f_2^2 & f_3^2 & f_4^2 & f_5^2 \\ f_0^3 & f_1^3 & f_2^3 & f_3^3 & f_4^3 & f_5^3 \\ f_0^4 & f_1^4 & f_2^4 & f_3^4 & f_4^4 & f_5^4 \\ f_0^5 & f_1^5 & f_2^5 & f_3^5 & f_4^5 & f_5^5 \\ f_0^6 & f_1^6 & f_2^6 & f_3^6 & f_4^6 & f_5^6 \end{bmatrix} \begin{bmatrix} l_0 \\ l_1 \\ l_2 \\ l_3 \\ l_4 \\ l_5 \end{bmatrix} = \begin{bmatrix} F_1 \\ F_2 \\ F_3 \\ F_4 \\ F_5 \\ F_6 \end{bmatrix} \quad (6.54)$$

$l_i : i = 0,1,2,3,4,5$

are obtained.

By repeating same calculations for m_i ,

$$\begin{bmatrix} f_0^1 & f_1^1 & f_2^1 & f_3^1 & f_4^1 & f_5^1 \\ f_0^2 & f_1^2 & f_2^2 & f_3^2 & f_4^2 & f_5^2 \\ f_0^3 & f_1^3 & f_2^3 & f_3^3 & f_4^3 & f_5^3 \\ f_0^4 & f_1^4 & f_2^4 & f_3^4 & f_4^4 & f_5^4 \\ f_0^5 & f_1^5 & f_2^5 & f_3^5 & f_4^5 & f_5^5 \\ f_0^6 & f_1^6 & f_2^6 & f_3^6 & f_4^6 & f_5^6 \end{bmatrix} \begin{bmatrix} m_0 \\ m_1 \\ m_2 \\ m_3 \\ m_4 \\ m_5 \end{bmatrix} = \begin{bmatrix} -f_6^1 \\ -f_6^2 \\ -f_6^3 \\ -f_6^4 \\ -f_6^5 \\ -f_6^6 \end{bmatrix} \quad (6.55)$$

$m_i : i = 0,1,2,3,4,5$

are obtained. By repeating same calculations for n_i ,

$$\begin{bmatrix} f_0^1 & f_1^1 & f_2^1 & f_3^1 & f_4^1 & f_5^1 \\ f_0^2 & f_1^2 & f_2^2 & f_3^2 & f_4^2 & f_5^2 \\ f_0^3 & f_1^3 & f_2^3 & f_3^3 & f_4^3 & f_5^3 \\ f_0^4 & f_1^4 & f_2^4 & f_3^4 & f_4^4 & f_5^4 \\ f_0^5 & f_1^5 & f_2^5 & f_3^5 & f_4^5 & f_5^5 \\ f_0^6 & f_1^6 & f_2^6 & f_3^6 & f_4^6 & f_5^6 \end{bmatrix} \begin{bmatrix} n_0 \\ n_1 \\ n_2 \\ n_3 \\ n_4 \\ n_5 \end{bmatrix} = \begin{bmatrix} -f_7^1 \\ -f_7^2 \\ -f_7^3 \\ -f_7^4 \\ -f_7^5 \\ -f_7^6 \end{bmatrix} \quad (6.56)$$

$n_i : i = 0,1,2,3,4,5$

are obtained.

There is only one parameter missing to define P_i and it is λ_1 and λ_2 . Two equations are enough to calculate two unknown and these equations are linearization equations of P_6 and P_7 in equation 6.57.

$$\begin{aligned} \frac{(l_2 + m_2\lambda_1 + n_2\lambda_2)}{(l_1 + m_1\lambda_1 + n_1\lambda_2)} - \frac{(l_4 + m_4\lambda_1 + n_4\lambda_2)}{(l_3 + m_3\lambda_1 + n_3\lambda_2)} &= \lambda_1 \\ \frac{(l_2 + m_2\lambda_1 + n_2\lambda_2)}{(l_1 + m_1\lambda_1 + n_1\lambda_2)} \cdot \frac{(l_4 + m_4\lambda_1 + n_4\lambda_2)}{(l_3 + m_3\lambda_1 + n_3\lambda_2)} &= \lambda_2 \end{aligned} \quad (6.57)$$

After the calculation of λ_1 and λ_2 it is possible to calculate all of the P_i parameters.

$$\begin{aligned} P_0 &= l_0 + m_0\lambda_1 + n_0\lambda_2, & P_1 &= l_1 + m_1\lambda_1 + n_1\lambda_2, \\ P_2 &= l_2 + m_2\lambda_1 + n_2\lambda_2, & P_3 &= l_3 + m_3\lambda_1 + n_3\lambda_2, \\ P_4 &= l_4 + m_4\lambda_1 + n_4\lambda_2, & P_5 &= l_5 + m_5\lambda_1 + n_5\lambda_2, \\ & & P_6 &= \lambda_1, & P_7 &= \lambda_2 \end{aligned} \quad (6.58)$$

The calculation of the P_i parameters will be result with the calculation of the construction parameters.

Generally, it is very hard to obtain perfect result in once. It is expected such an error graph that only get closer to $\pm L$ it cannot catch constant absolute peak points between precision points. This situation illustrated in figure 6.13 below.

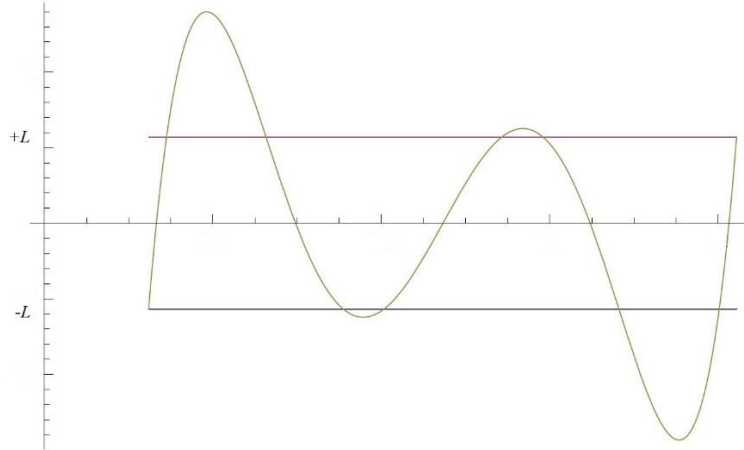


Figure 6.13: Expected first result of Chebyshev approximation.

To obtain better aligned error to the $\pm L$ limits it is taken derivative of objective function with respect to θ and drawn its graphic. Expected graph is shown in figure 6.14 below.

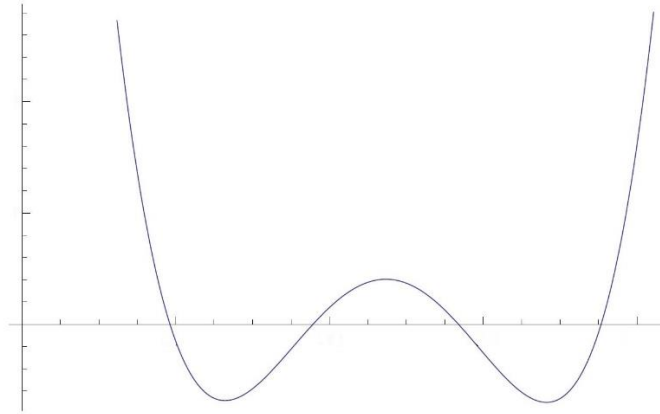


Figure 6.14: Derivative of objective function.

By this figure the points where spline coincidence with horizontal axes, the roots of derived function, is found. These are used as new precision so that make objective function fit better to $\pm L$.

It is important to mention about that the initial and final precision points does not change they are always constant, the points obtained from derived function is replaced with points between initial and final points.

These calculations continued up to find best fitted precision points.

Example: Design a four-bar mechanism that will generate $\phi = \theta^{1.3}$ function for θ input angle in $30^\circ - 70^\circ$ interval.

To solve given system, we need 6 precision points for equation system with six equations.

These points are chosen from input angle interval by using linear spacing.

$$\theta[1] = 30^\circ = 0.5236 \text{ rad} , \theta[2] = 38^\circ = 0.6632 \text{ rad} , \theta[3] = 46^\circ = 0.8028 \text{ rad},$$

$$\theta[4] = 54^\circ = 0.9424 \text{ rad} , \theta[5] = 62^\circ = 1.0821 \text{ rad} , \theta[6] = 70^\circ = 1.2217 \text{ rad}$$

Output angles ϕ corresponding to each θ in where $\phi = \theta^{1.3}$,

$$\phi[1] = 0.4312 \text{ rad} , \phi[2] = 0.5863 \text{ rad} , \phi[3] = 0.7516 \text{ rad},$$

$$\phi[4] = 0.9258 \text{ rad} , \phi[5] = 1.1080 \text{ rad} , \phi[6] = 1.2973 \text{ rad}$$

After defining ϕ and θ values, l_i, m_i, n_i and λ_1, λ_2 parameters are calculated to obtain P_i .

Output of equation 6.54,

$$l_0 = 0.9388, \quad l_1 = -0.1224, \quad l_2 = -0.1515,$$

$$l_3 = -0.0535, \quad l_4 = -0.1799, \quad l_5 = -1.8437 \times 10^{-7}$$

Output of equation 6.55,

$$m_0 = 0.5998, \quad m_1 = 0.9265, \quad m_2 = -0.3259$$

$$m_3 = 0.2911, \quad m_4 = -0.0211, \quad m_5 = -6.3697 \times 10^{-6}$$

Output of equation 6.56,

$$n_0 = 0.9388, \quad n_1 = -0.1224, \quad n_2 = -0.1515,$$

$$n_3 = -0.0535, \quad n_4 = -0.1799, \quad n_5 = -1.8433 \times 10^{-7}$$

Output of equation 2.67,

$$\lambda_1 = -32.3145, \quad \lambda_2 = -206.785$$

$$\lambda_1 = -0.7109, \quad \lambda_2 = -0.0696$$

$$\lambda_1 = -3.4516 \times 10^{-9}, \quad \lambda_2 = -1.$$

$$\lambda_1 = -1.0476 \times 10^{-9}, \quad \lambda_2 = -1.$$

$$\lambda_1 = 1.0476 \times 10^{-9}, \quad \lambda_2 = -1.$$

$$\lambda_1 = 3.4516 \times 10^{-9}, \quad \lambda_2 = -1.$$

$$\lambda_1 = 1.6698, \quad \lambda_2 = 2.9823$$

λ_1, λ_2 pairs were chosen as $\lambda_1 = 1.6698, \lambda_2 = 2.9823$ and continued to calculation with that result.

As mentioned before l_i, m_i, n_i and λ_1, λ_2 parameters calculated to obtain P_i .

Substituting these results into equation 6.58. $P_1, P_2, P_3, P_4, P_5, P_6, P_7$ are found like below,

$$P_0 = 4.7506, \quad P_1 = 1.0597, \quad P_2 = -1.1479,$$

$$P_3 = 0.2730, \quad P_4 = -0.7518, \quad P_5 = -0.00001137,$$

$$P_6 = 1.6698, \quad P_7 = 2.9823$$

Four-bar mechanism's parameters such as link lengths and off-set angle can be calculated by using P_i values.

As,

$$\begin{aligned}
 a &= 1 / (P_3 \cdot C\theta_0) , \quad b = \sqrt{a^2 + c^2 + 1 - 2P_0acC\theta_0C\phi_0}, \\
 c &= 1 / (P_1C\phi_0) , \quad \theta_0 = \text{Arctan}(P_2 / P_1), \\
 \phi_0 &= \text{Arctan}(P_4 / P_3)
 \end{aligned}
 \tag{6.59}$$

link lengths a, b, c, θ_0 and ϕ_0 are found,

$$a = 5.3985 , \quad b = 2.2407 , \quad c = 2.7641 , \quad \theta_0 = -0.8253 \text{ rad} , \quad \phi_0 = -1.2223 \text{ rad}$$

like above.

The system with calculated parameters is expected to give better results in terms of error when compared with previous example. The error graph is shown in figure 6.15. below.

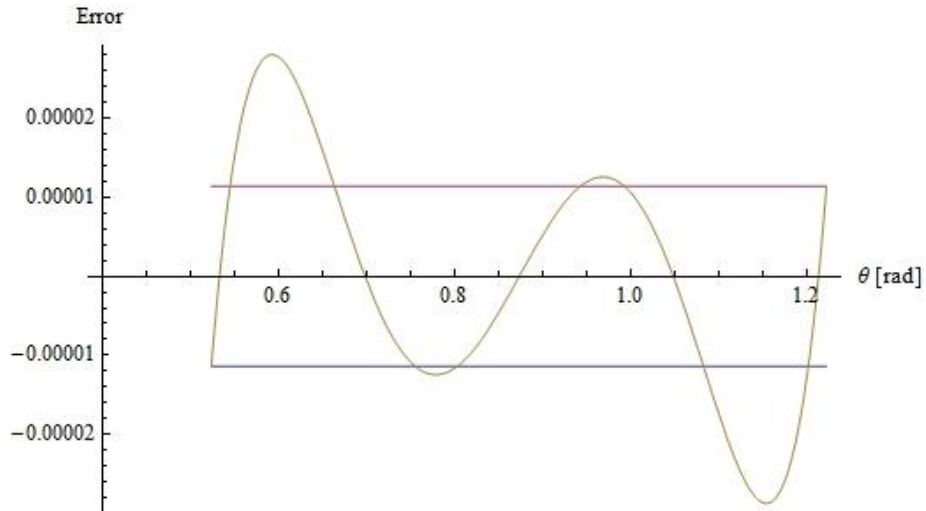


Figure 6.15: Error graph of Chebyshev approximation's first solution.

Red and blue lines on graph represent the calculated value of $\pm L$ and equal to $\pm P_5$. This graph shows us the system obtained from calculations is not suitable yet therefore calculations must be continued up to obtain suitable one.

Next step will begin with the derivative of objective function with respect to θ . Derivation of objective function is to obtain its roots. As mentioned before these roots will be our new precision points. In other words, the system will be tried to fit into $\pm L$ range by means of shifting the precision points. It is important to remember that the roots will replace with the beginning precision points but initial and final precision points will not change.

The graph of derivation of objective function,

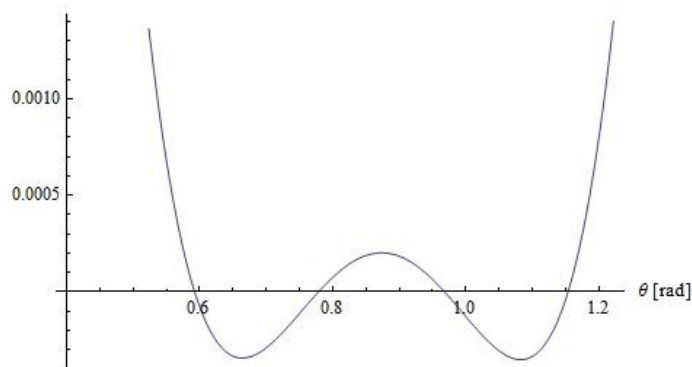


Figure 6.16: Derivative of objective function.

The roots of derivation of objective function,

$$\theta[2] = 0.5925035187403553 \text{ rad} , \theta[3] = 0.7784629695919103 \text{ rad} ,$$

$$\theta[4] = 0.9679585843889184 \text{ rad} , \theta[5] = 1.153460528342797 \text{ rad}$$

New precision points,

$$\theta[1] = 0.52359 \text{ rad} , \theta[2] = 0.5925035187403553 \text{ rad} , \theta[3] = 0.7784629695919103 \text{ rad} ,$$

$$\theta[4] = 0.9679585843889184 \text{ rad} , \theta[5] = 1.153460528342797 \text{ rad} , \theta[6] = 1.22173 \text{ rad}$$

P_i values from new precision points,

$$P_0 = 4.75699594637231 , P_1 = 1.063262218054661 , P_2 = -1.1533919537030743,$$

$$P_3 = 0.27363429223094515 , P_4 = -0.7556602148905295 , P_5 = -0.00001839527738812372$$

$$P_6 = 1.6768026868631336 , P_7 = 2.9956603417412118$$

The error graph of this system is shown below,

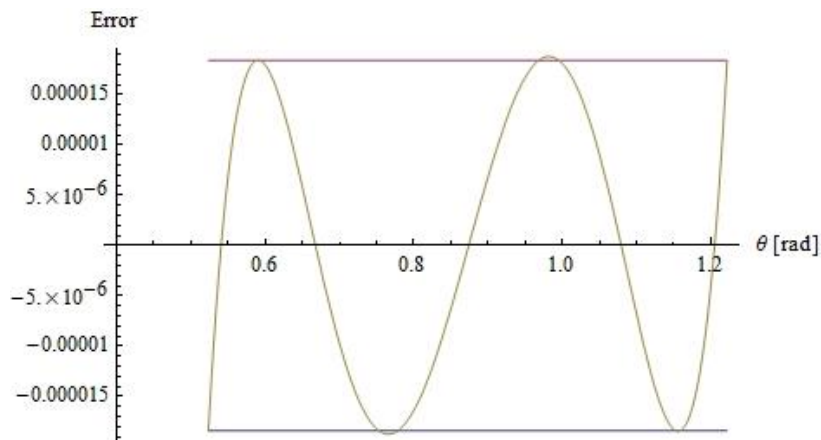


Figure 6.17: Error graph of first iteration.

Although re-defined system error graph shows that the system is not suitable yet therefore second iteration is needed.

Graph of the derivation of the objective function obtained from first iteration is below,

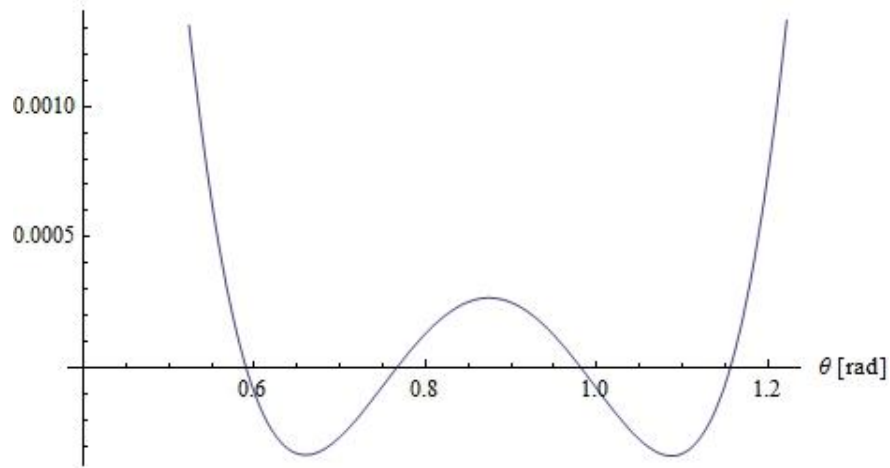


Figure 6.18: Derivative of first iteration's objective function.

The roots of derivation of objective function,

$$\begin{aligned} \theta[2] &= 0.5925035187403551 \text{ rad} , \theta[3] = 0.7784629695919103 \text{ rad}, \\ \theta[4] &= 0.9679585843889184 \text{ rad} , \theta[5] = 1.1534605283428085 \text{ rad} \end{aligned}$$

New precision points,

$$\begin{aligned} \theta[1] &= 0.52359 \text{ rad} , \theta[2] = 0.5925035187403551 \text{ rad} , \theta[3] = 0.7784629695919103 \text{ rad}, \\ \theta[4] &= 0.9679585843889184 \text{ rad} , \theta[5] = 1.1534605283428085 \text{ rad} , \theta[6] = 1.22173 \text{ rad} \end{aligned}$$

P_i values from new precision points,

$$\begin{aligned} P_0 &= 4.756995946367644 , P_1 = 1.0632622180532647 \\ P_2 &= -1.1533919537016244 , P_3 = 0.27363429223096714 \\ P_4 &= -0.7556602148896949 , P_5 = -0.00001839527738797333, \\ P_6 &= 1.6768026868598003 , P_7 = 2.995660341737828 \end{aligned}$$

The error graph of this system is shown below,

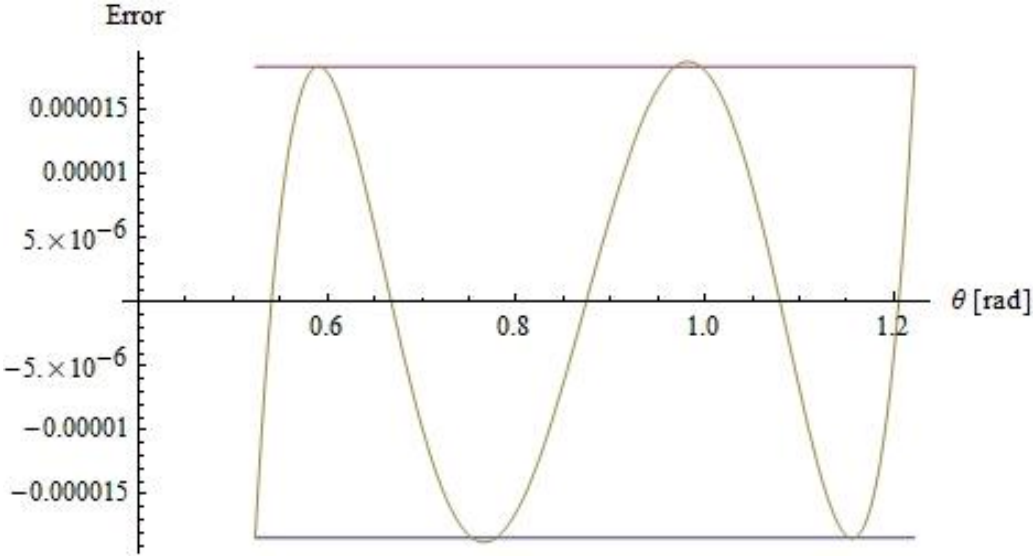


Figure 6.19: Error graph of second iteration.

It is nearly impossible to see any difference between figure 6.17 and figure 6.19. The best way to control the difference between last two results looking for derivation between P_5 values. It can give better understanding about difference between iteration. Because of the inefficient difference in terms of the error one more iteration will be done and system will be redefined.

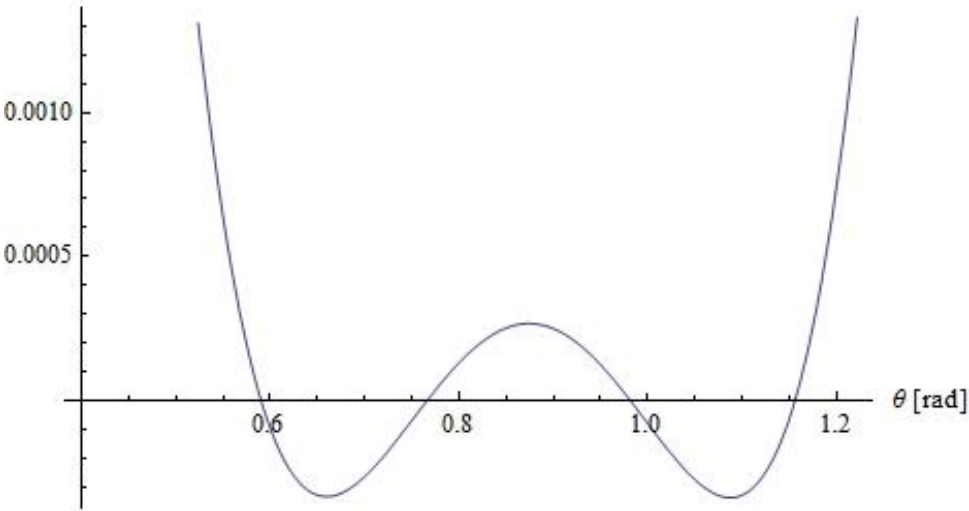


Figure 6.20: Derivative of second iteration's objective function.

The roots of derivation of objective function,

$$\theta[2] = 0.5905748205099249 \text{ rad} , \theta[3] = 0.7657662012570802 \text{ rad},$$

$$\theta[4] = 0.981913161134758 \text{ rad} , \theta[5] = 1.155660009517959 \text{ rad}$$

New precision points,

$$\theta[1] = 0.52359 \text{ rad} , \theta[2] = 0.5905748205099249 \text{ rad}$$

$$\theta[3] = 0.7657662012570802 \text{ rad} , \theta[4] = 0.981913161134758 \text{ rad}$$

$$\theta[5] = 1.155660009517959 \text{ rad} , \theta[6] = 1.22173 \text{ rad}$$

P_i values from new precision points,

$$P_0 = 4.756439204041277 , P_1 = 1.063187835982423,$$

$$P_2 = -1.1531964642816646 , P_3 = 0.2735964175913298,$$

$$P_4 = -0.7555037265409776 , P_5 = -0.000018550772197592263,$$

$$P_6 = 1.676720989305689 , P_7 = 2.9951564149286156$$

The error graph of this system is shown below,

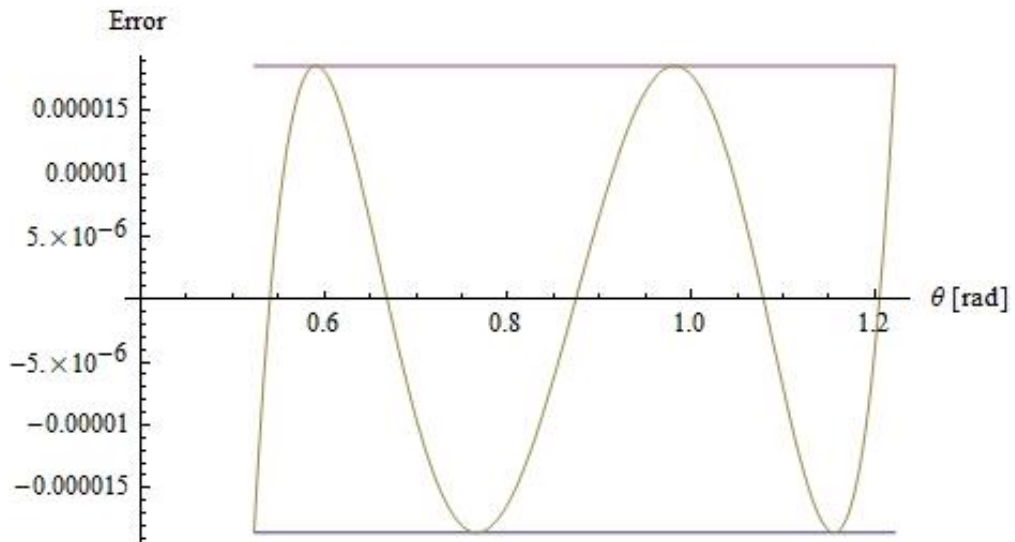


Figure 6.21: Error graph of third iteration.

As shown in graph this result is sufficient in terms of the goal of this study therefore, no other iteration is needed. The roots of this last redefined objective function give as the ultimate precision points.

Ultimate precision points,

$$\begin{aligned}\theta[1] &= 0.5408452288872587 \text{ rad} , \theta[2] = 0.6685467335698574 \text{ rad}, \\ \theta[3] &= 0.8740300954993331 \text{ rad} , \theta[4] = 1.0785188148311473 \text{ rad}, \\ \theta[5] &= 1.2047236102376058 \text{ rad}\end{aligned}$$

6.1.2.2 Least square approximation

In previous section error of objective function with calculated constraint parameters tried to be fitted between two values which is $\pm L$. In this part, another method which is named as Least Square Approximation is applied to the function generator kinematic synthesis of four-bar with 5 precision points. Up to now all of the three of them by changing number of precision points, one of them by adding parameter as L which describes the extremums of oscillating error characteristics, have a similar approach to decrease the error of function generation synthesis. This similarity is that the number of design points is equal to number of unknown parameters. On the other hand in least square approximation case, the number of design points are greater than the number of construction parameters. Least square approximation allows us to describe more design points than number of construction parameters. This method suggests that the best fitting function is reached when sum of squared fitting errors (η) is a minimum [19].

$$\eta = \sum_{i=1}^n \delta^2 \quad (6.60)$$

where n represents the number of design points.

The minimum η is reached when the partial derivations of η with respect to construction parameters P_j are zero.

$$\frac{\partial \eta}{\partial P_j} = \frac{\partial(\delta^2)}{\partial P_j} = 0 \quad (6.61)$$

For this study equation 6.60,

$$\eta = \sum_{i=1}^n (\sum_{j=0}^6 (P_j f_j^i) - F_i)^2 \quad (6.62)$$

When the equation 6.61 is applied to our system, the results will be like below,

$$\delta = P_0 f_0 + P_1 f_1 + P_2 f_2 + P_3 f_3 + P_4 f_4 + P_5 f_5 + P_6 f_6 - F \quad (6.63)$$

$$\eta = \delta^2 = \sum_{i=1}^n (P_0 f_0 + P_1 f_1 + P_2 f_2 + P_3 f_3 + P_4 f_4 + P_5 f_5 + P_6 f_6 - F)^2 \quad (6.64)$$

$$\frac{\partial \eta}{\partial P_{j=1\dots 6}} = \sum_{i=1}^n 2f_j^i (P_0 f_0^i + P_1 f_1^i + P_2 f_2^i + P_3 f_3^i + P_4 f_4^i + P_5 f_5^i + P_6 f_6^i - F_i) \quad (6.65)$$

For example,

$$\begin{aligned} \frac{\partial \eta}{\partial P_0} &= \sum_{i=1}^n 2f_0^i (P_0 f_0^i + P_1 f_1^i + P_2 f_2^i + P_3 f_3^i + P_4 f_4^i + P_5 f_5^i + P_6 f_6^i - F_i) \\ &= 2P_0 \sum_{i=1}^n f_0^i f_0^i + 2P_1 \sum_{i=1}^n f_1^i f_0^i \\ &\quad + 2P_2 \sum_{i=1}^n f_2^i f_0^i + 2P_3 \sum_{i=1}^n f_3^i f_0^i + 2P_4 \sum_{i=1}^n f_4^i f_0^i \\ &\quad + 2P_5 \sum_{i=1}^n f_5^i f_0^i + 2P_6 \sum_{i=1}^n f_6^i f_0^i - 2P_1 \sum_{i=1}^n F f_0^i = 0 \end{aligned} \quad (6.66)$$

to find each $P_j = l_j + m_j \lambda_1 + n_j \lambda_2$, equation 6.51, 6.52, 6.53 would be modified with respect to equation 6.65. By these equations,

$$\begin{aligned} \begin{bmatrix} \sum_{i=1}^n f_0^i f_0^i & \sum_{i=1}^n f_0^i f_1^i & \sum_{i=1}^n f_0^i f_2^i & \sum_{i=1}^n f_0^i f_3^i & \sum_{i=1}^n f_0^i f_4^i \\ \sum_{i=1}^n f_1^i f_0^i & \sum_{i=1}^n f_1^i f_1^i & \sum_{i=1}^n f_1^i f_2^i & \sum_{i=1}^n f_1^i f_3^i & \sum_{i=1}^n f_1^i f_4^i \\ \sum_{i=1}^n f_2^i f_0^i & \sum_{i=1}^n f_2^i f_1^i & \sum_{i=1}^n f_2^i f_2^i & \sum_{i=1}^n f_2^i f_3^i & \sum_{i=1}^n f_2^i f_4^i \\ \sum_{i=1}^n f_3^i f_0^i & \sum_{i=1}^n f_3^i f_1^i & \sum_{i=1}^n f_3^i f_2^i & \sum_{i=1}^n f_3^i f_3^i & \sum_{i=1}^n f_3^i f_4^i \\ \sum_{i=1}^n f_4^i f_0^i & \sum_{i=1}^n f_4^i f_1^i & \sum_{i=1}^n f_4^i f_2^i & \sum_{i=1}^n f_4^i f_3^i & \sum_{i=1}^n f_4^i f_4^i \end{bmatrix} \begin{bmatrix} l_0 \\ l_1 \\ l_2 \\ l_3 \\ l_4 \end{bmatrix} &= \begin{bmatrix} \sum_{i=1}^n f_0^i F_i \\ \sum_{i=1}^n f_1^i F_i \\ \sum_{i=1}^n f_2^i F_i \\ \sum_{i=1}^n f_3^i F_i \\ \sum_{i=1}^n f_4^i F_i \end{bmatrix} \\ l_i : i = 0, 1, 2, 3, 4 & \end{aligned} \quad (6.67)$$

are obtained. By repeating same calculations for n_i ,

$$\begin{aligned} \begin{bmatrix} \sum_{i=1}^n f_0^i f_0^i & \sum_{i=1}^n f_0^i f_1^i & \sum_{i=1}^n f_0^i f_2^i & \sum_{i=1}^n f_0^i f_3^i & \sum_{i=1}^n f_0^i f_4^i \\ \sum_{i=1}^n f_1^i f_0^i & \sum_{i=1}^n f_1^i f_1^i & \sum_{i=1}^n f_1^i f_2^i & \sum_{i=1}^n f_1^i f_3^i & \sum_{i=1}^n f_1^i f_4^i \\ \sum_{i=1}^n f_2^i f_0^i & \sum_{i=1}^n f_2^i f_1^i & \sum_{i=1}^n f_2^i f_2^i & \sum_{i=1}^n f_2^i f_3^i & \sum_{i=1}^n f_2^i f_4^i \\ \sum_{i=1}^n f_3^i f_0^i & \sum_{i=1}^n f_3^i f_1^i & \sum_{i=1}^n f_3^i f_2^i & \sum_{i=1}^n f_3^i f_3^i & \sum_{i=1}^n f_3^i f_4^i \\ \sum_{i=1}^n f_4^i f_0^i & \sum_{i=1}^n f_4^i f_1^i & \sum_{i=1}^n f_4^i f_2^i & \sum_{i=1}^n f_4^i f_3^i & \sum_{i=1}^n f_4^i f_4^i \end{bmatrix} \begin{bmatrix} n_0 \\ n_1 \\ n_2 \\ n_3 \\ n_4 \end{bmatrix} &= \begin{bmatrix} -\sum_{i=1}^n f_0^i f_6^i \\ -\sum_{i=1}^n f_1^i f_6^i \\ -\sum_{i=1}^n f_2^i f_6^i \\ -\sum_{i=1}^n f_3^i f_6^i \\ -\sum_{i=1}^n f_4^i f_6^i \end{bmatrix} \\ n_i : i = 0, 1, 2, 3, 4 & \end{aligned} \quad (6.68)$$

are obtained. Then,

$$\begin{bmatrix}
\sum_{i=1}^n f_0^i f_0^i & \sum_{i=1}^n f_0^i f_1^i & \sum_{i=1}^n f_0^i f_2^i & \sum_{i=1}^n f_0^i f_3^i & \sum_{i=1}^n f_0^i f_4^i \\
\sum_{i=1}^n f_1^i f_0^i & \sum_{i=1}^n f_1^i f_1^i & \sum_{i=1}^n f_1^i f_2^i & \sum_{i=1}^n f_1^i f_3^i & \sum_{i=1}^n f_1^i f_4^i \\
\sum_{i=1}^n f_2^i f_0^i & \sum_{i=1}^n f_2^i f_1^i & \sum_{i=1}^n f_2^i f_2^i & \sum_{i=1}^n f_2^i f_3^i & \sum_{i=1}^n f_2^i f_4^i \\
\sum_{i=1}^n f_3^i f_0^i & \sum_{i=1}^n f_3^i f_1^i & \sum_{i=1}^n f_3^i f_2^i & \sum_{i=1}^n f_3^i f_3^i & \sum_{i=1}^n f_3^i f_4^i \\
\sum_{i=1}^n f_4^i f_0^i & \sum_{i=1}^n f_4^i f_1^i & \sum_{i=1}^n f_4^i f_2^i & \sum_{i=1}^n f_4^i f_3^i & \sum_{i=1}^n f_4^i f_4^i
\end{bmatrix}
\begin{bmatrix}
m_0 \\
m_1 \\
m_2 \\
m_3 \\
m_4
\end{bmatrix}
=
\begin{bmatrix}
-\sum_{i=1}^n f_0^i f_5^i \\
-\sum_{i=1}^n f_1^i f_5^i \\
-\sum_{i=1}^n f_2^i f_5^i \\
-\sum_{i=1}^n f_3^i f_5^i \\
-\sum_{i=1}^n f_4^i f_5^i
\end{bmatrix}$$

$m_i : i = 0, 1, 2, 3, 4$

(6.69)

are obtained.

There is only one parameter missing to define P_i and it is λ_1 and λ_2 . Two equations are enough to calculate two unknowns and these equations are linearization equations of P_5 and P_6 in equation 6.35 which is mentioned in study of four-bar function generator design with five precision points. Beginning and remainder of this study same as in the five-precision points study of four-bar function generator. Main difference shown above. To give better understanding about this study, solution example below can be examined.

Example: Design a four-bar mechanism that will generate $\phi = \theta^{1.3}$ function for θ input angle in $30^\circ - 70^\circ$ interval.

In previous examples we had described precision points between given interval. In least square approximation it is impossible to describe each design point one by one as the number of design points is higher than the number of constraint parameters. Instead of this, equation 6.65 is calculated by using each design points. These design points are used to minimize total error of function generator. 101 design points is used in this study. 101 points between given interval selected by using equal spacing.

$$\frac{\partial \eta}{\partial P_{j=1\dots 6}} = \sum_{i=1}^{101} 2f_j^i (P_0 f_0^i + P_1 f_1^i + P_2 f_2^i + P_3 f_3^i + P_4 f_4^i + P_5 f_5^i + P_6 f_6^i - F_i)$$

Output of equation 6.67,

$$\begin{aligned}
l_0 &= 0.9389, \quad l_1 = -0.1223, \quad l_2 = -0.1515 \\
l_3 &= -0.0534, \quad l_4 = -0.1799
\end{aligned}$$

Output of equation 6.68,

$$n_0 = 0.9389 , n_1 = -0.1223 , n_2 = -0.1515$$

$$n_3 = -0.0534 , n_4 = -0.1799$$

Output of equation 6.69,

$$m_0 = 0.5991 , m_1 = 0.9252 , m_2 = -0.3246$$

$$m_3 = 0.2902 , m_4 = -0.0203$$

Output of equation 6.35. Imaginer outputs are not shown here.

$$\lambda_1 = 1.66914 , \lambda_2 = 2.97169$$

$$\lambda_1 = 0.71268 , \lambda_2 = -0.06961$$

$$\lambda_1 = -32.0816 , \lambda_2 = -205.349$$

λ_1, λ_2 pairs were chosen as $\lambda_1 = 1.66914$, $\lambda_2 = 2.97169$ and continued to calculation with that result.

As mentioned before l_i, m_i, n_i and λ_1, λ_2 parameters calculated to obtain P_i .

Substituting these results into equation 6.36, $P_0, P_1, P_2, P_3, P_4, P_5, P_6$ are found like below,

$$P_0 = 4.7292 , P_1 = 1.0585 , P_2 = -1.1439 , P_3 = 0.2722,$$

$$P_4 = -0.7485 , P_5 = 1.6691 , P_6 = 2.9716$$

Four-bar mechanism's parameters such as link lengths and off-set angle can be calculated by using P_i values. By using P_i , link lengths a, b, c, θ_0 and ϕ_0 are found,

$$a = 5.40874 , b = 2.25187 , c = 2.76422 , \theta_0 = -0.82416 \text{ rad} , \phi_0 = -1.22201 \text{ rad}$$

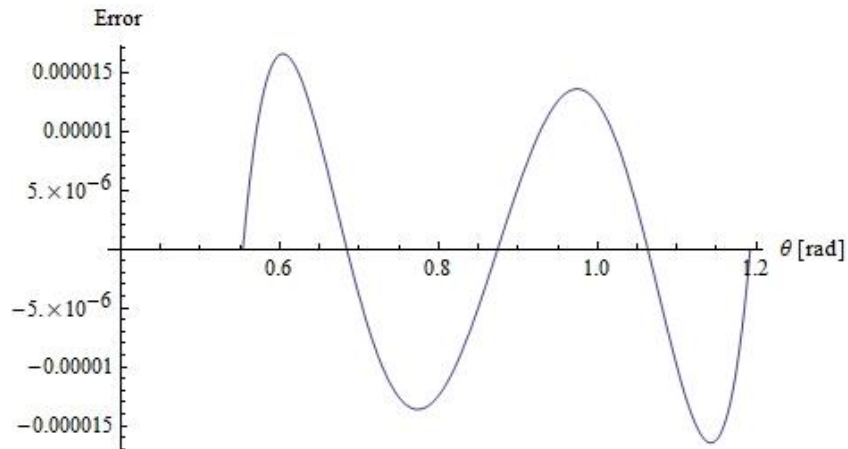


Figure 6.22: Error graph of least square approximation.

Kinematic synthesis of the four-bar function generator has been finished with this study. The five precision points synthesis, five precision synthesis with Chebyshev Approximation and five precision points synthesis with square approximation studies gave the most efficient data. To compare these results the combined error graph can be used.

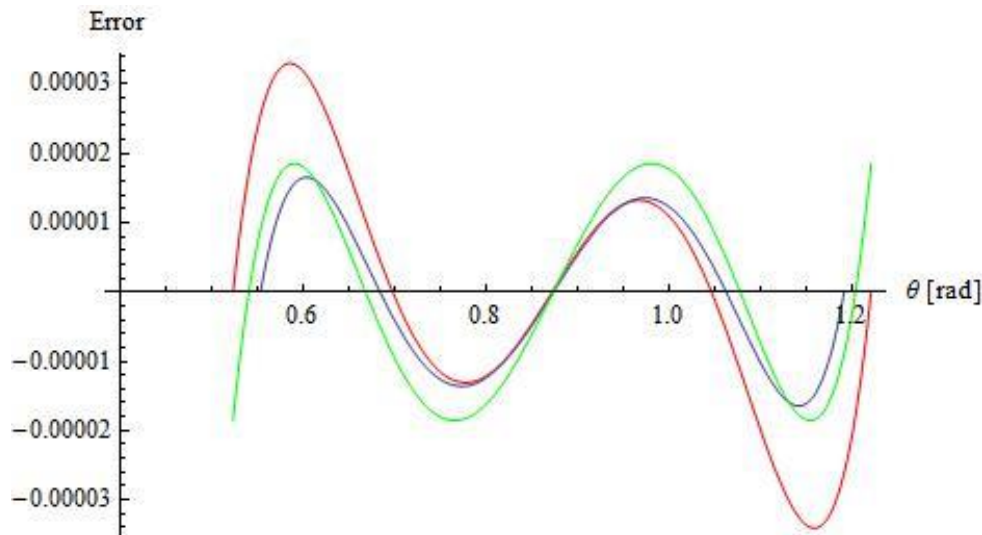


Figure 6.23: Combined error graph.

- — Chebyshev Approximation
- — Least Square Approximation
- — Five precision points

As seen in these graph, minimized error was ensured with Least Square Approximation with 101 design points. As the number of design points getting higher the overall error would be lower.

6.2 Integration of the Function Generation Synthesis into Design of a Collimator Mechanism

Before proceeding further, all of the parameters either they are constant or variable should clearly be defined prior to the kinematic synthesis. As seen in figure 6.24, set of constant construction parameters of an offset slider crank mechanism includes, a_1 ($|OA|$), b_1 ($|AB|$), c_1 ($|BC|$), d ($|DE|$), and e ($|OE|$), while the set of

variable parameters are formed by θ_2, θ_3 , and s_1 . Due to the fact that the vertical distance (d) between the point source and the collimator systems location should be defined with respect to the dimensions of the radiotherapy manipulator along with the horizontal actuator location (e), the only parameters that needs to be calculated become the offset height (a_1) and the link lengths (b_1 , and c_1) of the slider crank mechanism.

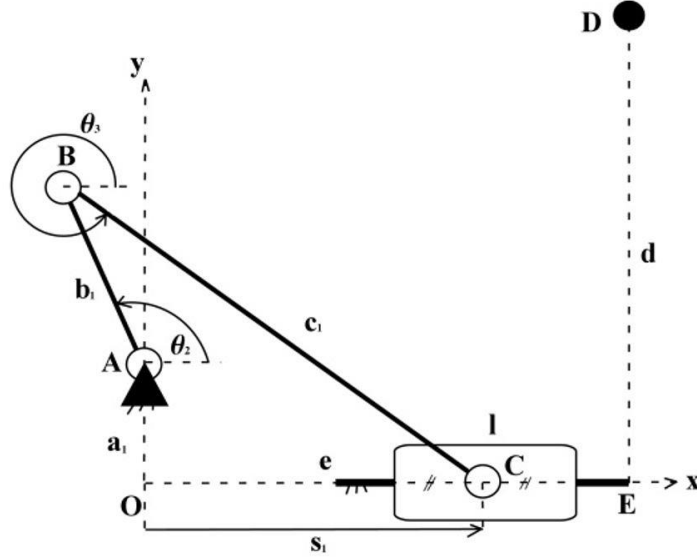


Figure 6.24: Multiple slider crank mechanisms on both sections of the collimator. Leaves that are formed by the sliders on individual sections are controlled by single input.

In order to calculate those parameters with respect to the design constraints, objective function of the system should be formed. Writing the loop closure equation,

$$\begin{aligned} a_1 + b_1 + c_1 &= s_1 \\ a_1 e^{j\theta_1} + b_1 e^{j\theta_2} + c_1 e^{j\theta_3} &= s_1 e^{j\theta_4} \end{aligned} \quad (6.70)$$

and separating equation 6.70 into the real and imaginary parts by considering $\theta_1 = \frac{\pi}{2}$,

and $\theta_4 = 0$,

$$\begin{aligned} c_1 \cos \theta_3 &= s_1 - b_1 \cos \theta_2 \\ c_1 \sin \theta_3 &= -a_1 - b_1 \sin \theta_2 \end{aligned} \quad (6.71)$$

two equation sets can easily be formed. As the study deals with the function generation synthesis between the input θ_2 and the output s of the system, variable parameter θ_3 should be eliminated from equation 6.71. Taking the squares of both sides and adding them together, the objective function in the form of a polynomial can be constructed,

$$P_0 f_0 + P_1 f_1 + P_2 f_2 - F = 0 \quad (6.72)$$

where,

$$P_0 = \frac{a_1^2 + b_1^2 - c_1^2}{2b_1}, f_0 = 1, P_1 = \frac{1}{2b_1}, f_1 = s_1^2, \quad (6.73)$$

$$P_2 = a_1, f_2 = \sin \theta_2, F = s_1 \cos \theta_2$$

It can be easily seen that, equation 6.72 includes three unknown parameters, P_0, P_1 , and P_2 to be solved. Thus, three known precision points (θ_{2i} , and s_{1i} , $i \rightarrow 1, 2, 3$) are needed to evaluate the variable functions f_0, f_1, f_2 and F to form three independent equation sets. As the first leaf of the leaf bank constraints the motions of other leaves, first three sets of precision points can be given freely with respect to the desired collimator opening, and actuator rotation interval. However, it should be noted that one of the precision points for the stroke has to include $s_1 = e - \frac{l}{2}$ due to the fact that all of the leaves should be able to block the beam that travels to the target when the collimator opening is closed. After the evaluation of the variable functions with respect to the given precision points, unknown parameters (P_0, P_1 , and P_2) can be calculated by solving three equations for three unknowns,

$$\begin{bmatrix} \{f_j^1\}_0^2 \\ \{f_j^2\}_0^2 \\ \{f_j^3\}_0^2 \end{bmatrix} \begin{bmatrix} \{P_j\}_0^2 \end{bmatrix}^T = \begin{bmatrix} \{F^j\}_1^3 \end{bmatrix}^T \quad (6.74)$$

where in equation 6.74, f_j^i and F^j are the values of functions f_j and F that will be evaluated by the i^{th} precision point sets θ_{2i} , and s_{1i} . After the solution of equation 6.74, offset height (a) and the link lengths (b and c) of the slider crank mechanism can be calculated by using equations below.

$$a_1 = P_2, \quad b_1 = \frac{1}{2P_1}, \quad c_1 = \sqrt{a_1^2 + b_1^2 - 2b_1P_0} \quad (6.75)$$

In order to proceed further in the design of mechanisms for the collimator layers below, as the leaves of the collimator in individual sides are actuated through a single input, the same precision points with exact amount should be used for the input of the system ($\theta_{2i}, i \rightarrow 1, 2, 3$). Due to the fact that the offsets of the remaining mechanisms are already defined after the kinematic synthesis of the first layer by using the previous calculated offset (a_1) and the thickness of the collimator leaves (t) (figure 5), another unknown should be included into the remaining sections of the mechanism synthesis to be able to use the same number of precision points.

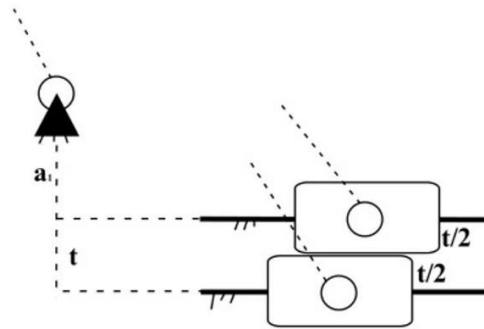


Figure 6.25: Offset of the second collimator layer ($a_2 = a_1 + t$).

For this purpose a new construction parameter was introduced to the system as $\theta_{2,0}^k$ that represents the constant angle between the input links of k^{th} and $(k-1)^{\text{th}}$ mechanisms that are responsible for the actuation of the collimator leaves in related layers (figure 6.26).

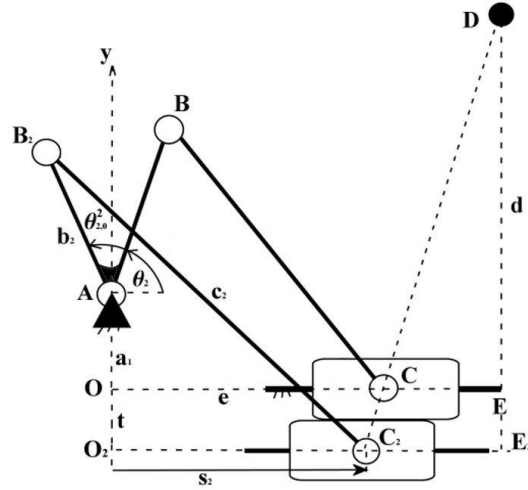


Figure 6.26: Construction and variable parameters of the second layer.

Thus, a new objective function should be formed by substituting $\theta_2 + \theta_{2,0}^k$ into the equation 6.71 in place of θ_2 as,

$$\begin{aligned} c_k \cos \theta_3^k &= s_k - b_k \cos(\theta_2 + \theta_{2,0}^k) \\ c_k \sin \theta_3^k &= -a_k - b_k \sin(\theta_2 + \theta_{2,0}^k) \end{aligned}, (k \rightarrow 2, 3, \dots, n) \quad (6.76)$$

where n is the number of total layers in the vertical stack and $a_k = a_1 + (k-1)t$.

Similarly by taking the squares of both sides and adding them together, the new objective function for the remaining layers in the form of a polynomial can be constructed as equation 6.72, where the polynomial constants and functions become

$$P_0 = \frac{a_k^2 + b_k^2 - c_k^2}{2b_k \cos \theta_{2,0}^k}, f_0 = 1, P_1 = \frac{1}{2b_k \cos \theta_{2,0}^k}, f_1 = s_k^2, P_2 = \tan \theta_{2,0}^k,$$

$$f_2 = a_k \cos \theta_2 + s_k \sin \theta_2, \text{ and } F = s_k \cos \theta_2 - a_k \sin \theta_2.$$

In order to solve the unknown construction parameters $(b_k, c_k, \theta_{2,0}^k)$, three known precision point sets $(\theta_{2i}, \text{ and } s_{ki}, i \rightarrow 1, 2, 3)$ are also needed to evaluate the variable functions f_0, f_1, f_2 and F . On the other hand, it should be noted that as each side of the system will be single degree of freedom and depend on the input angle θ_2 , the same precision points of the first layer should be used for $\theta_{2i} (i \rightarrow 1, 2, 3)$. Knowing

that $s_{k1} = e - \frac{l}{2}$, remaining precision points for s_{ki} ($i \rightarrow 2, 3$) can be calculated by using

triangular geometry on $DC_k E_k$ triangle as,

$$\frac{d}{d + (k-1)t} = \frac{e - s_{1i}}{e - s_{ki}}, \quad i \rightarrow 2, 3, k \rightarrow 2, 3, \dots, n \quad (6.77)$$

After the evaluation of the variable functions with respect to the given and calculated precision points, unknown parameters (P_0, P_1 , and P_3) can be calculated by using equation 6.74. After the solution of polynomial constants, the pole angle $\theta_{2,0}^k$ and the link lengths b_k, c_k of the slider crank mechanism can be calculated by using equations below.

Numerical Example

In the light of the proposed idea, using the existing dimensional constraints of the radiotherapy manipulator designed in the previous project of the authors, a numerical example of a collimator design with three vertical leaf stacks is given below. As seen in table 6.1, defined structural parameters of one side of the collimator system are given by considering existing dimensional constraints.

Table 6.1: Defined structural parameters of the collimator.

<i>Collimator Leaf Thickness (t)</i>	<i>Collimator Leaf Length (l)</i>	<i>Point Source Vertical Distance (d)</i>	<i>Point Source Horizontal Distance (e)</i>
20 mm	160 mm	150 mm	190 mm

In order to calculate the remaining construction parameters ($a_1, b_1, c_1, b_2, c_2, \theta_{2,0}^2, b_3, c_3, \theta_{2,0}^3$) of the collimator with three vertical leaf stacks, three sets of precision points are needed. Utilizing equations 3 through 8, these parameters can easily be calculated after the precision points are determined as shown in table 6.2.

Table 6.2: Precision point sets and calculated parameters.

<i>Set Number</i>	<i>1</i>	<i>2</i>	<i>3</i>
<i>Precision Point Sets</i>	$\theta_{21} = 25^\circ, s_{11} = 110 \text{ mm}$ $\theta_{22} = 55^\circ, s_{12} = 70 \text{ mm}$ $\theta_{23} = 85^\circ, s_{13} = 30 \text{ mm}$	$\theta_{21} = 25^\circ, s_{21} = 110 \text{ mm}$ $\theta_{22} = 55^\circ, s_{22} = 64,67 \text{ mm}$ $\theta_{23} = 85^\circ, s_{23} = 19,33 \text{ mm}$	$\theta_{21} = 25^\circ, s_{31} = 110 \text{ mm}$ $\theta_{22} = 55^\circ, s_{32} = 59,33 \text{ mm}$ $\theta_{23} = 85^\circ, s_{33} = 8,66 \text{ mm}$
<i>Calculated Construction Parameters</i>	$a_1 = 103,02 \text{ mm}$ $b_1 = 35,86$ $c_1 = 141,32$	$b_2 = 35,86 \text{ mm}$ $c_2 = 141,32 \text{ mm}$ $\theta_{2,0}^2 = 2,69^\circ$	$b_3 = 36,65 \text{ mm}$ $c_3 = 179,91 \text{ mm}$ $\theta_{2,0}^3 = 5,91^\circ$

Using these constraint and construction parameters collimator with three vertical leaf stacks was modelled. Planar representation of collimators left section and its motion through three configurations can be seen in figure 6.27.

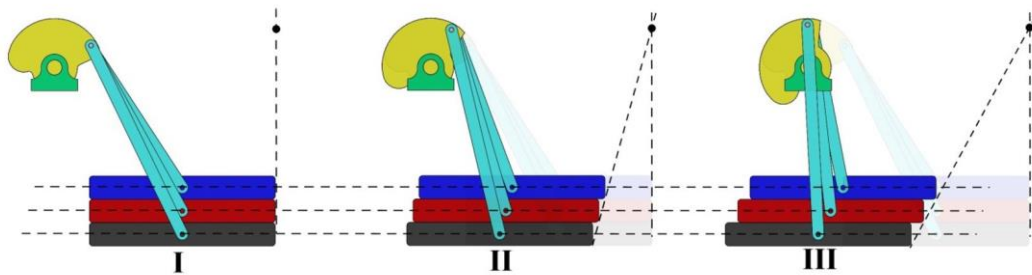


Figure 6.27: Modelled collimator and its motion through three configurations.

It should be remembered that using the same analogy, number of vertical stacks can be increased by the addition of new precision point sets. Furthermore, as mentioned before, if the thicknesses of the leaves are reduced by preserving the overall thickness (increasing number of vertical stacks), finer results in scattering prevention can be accomplished.

7. CONCLUSION

In this thesis Multileaf Collimator that will be utilized in radiation therapy and used with a linear accelerator was designed, simulated and manufactured. The manipulator was designed in 3 different concepts and two of them were manufactured. Components of the collimator mechanism designed by using SolidWorks and Autodesk Inventor CAD software. Before the design of collimator mechanism has been started the maximum beam dimension was taken as 80mm in diameter. Another constraint about the collimator mechanism was the fact that the dimensions and positions of the opening can be changed during treatment.

The first collimator design was four degrees of freedom decoupled mechanism that works in the Cartesian coordinate system. The first design was modified so as to decrease the footprint of the devices by changing upper jaws motion concepts by the modification of the system that works in polar coordinates. This modification also became advantageous in terms of better alignment between the beam angle and jaw surface thus, the scattering and end leaf transmission has been decreased in one axis of 2D planar projection of the contour that has been generated by Multileaf Collimator. After the design was completed prototypes were manufactured and assembled. Examinations and tests on this system emerged new ideas and new design constraints and goals were decided. In the light of new design constraints and goals second modification stage was performed.

One of the most important subjects of the second modification was to obtain as compact as possible design. Components numbers, connector numbers, loads, mass and footprint were critically reduced without changing workspace of the Collimator. Thanks to the rapid prototyping devices and modern design approach 116.71kg mass reduction and 4324.06cm² footprint reduction was ensured when compared with the first prototype. Vibrations caused by the mass moment of inertia of the moving jaws was reduced by lowering the number of connectors, optimizing center of mass and

decreasing weight of all jaws. Mass reduction amount of one upper jaw was 1.78 kg and one lower jaw was 7.39 kg.

At the end of the thesis, lower jaw modification was also done so as to obtain higher performance in terms of the decreased scattering.

In this part function generation synthesis was tried to be implemented in the partial design of a multi-leaf collimator that are being used in radiation therapy to guide the beams through the adjustable beam gap during the treatment period.

Due to the fact that scattering issues are one of the most important problems to be solved in the field, a collimator design with vertically stacked leaves was proposed for kinematic synthesis implementation. In this design it is clear that when the number of leaves is increased in the vertical stack at the same time while reducing the thickness of them by preserving the total amount of shielding thickness, finer adjustments and better scattering reduction will be possible. On the other hand, as the leaf number increases, number of independent actuations that are needed to control the individual leaves should also be increased to adjust the beam gap. In order to reduce the amount of these actuations, proper motion of the vertically stacked leaves was verified to reduce the scattering issues. As the motions of the leaves on each sides of the system should be functionally dependent on each other to form the geometrical constraints, control possibility of the leaves on individual sides by a single actuation was also verified. In the light of this, kinematic synthesis solution was demonstrated in two degrees of freedom planar system with a point source by only considering adjustment of the beam geometry in single plane.

Throughout the section procedural approaches were explained in detail and the required objective functions were introduced to carry out the function generation synthesis. Also in order to verify the proposed synthesis equations and their solutions a numerical example was given to design a collimator with three stacks of vertical leaves. Acquired results were used to model the mechanism and the desired motion was successfully simulated in a software environment. It is concluded that the integration possibility of function generation synthesis into the multi leaf collimator design have promising results and potential benefits for the related field.

REFERENCES

1. Lawrence TS, Ten Haken RK, Giaccia A. *Principles of Radiation Oncology*. In: DeVita VT Jr., Lawrence TS, Rosenberg SA, editors. *Cancer: Principles and Practice of Oncology*. 8th ed. Philadelphia: Lippincott Williams and Wilkins, 2008.
2. National Cancer Institute. (2010). *Radiation Therapy for Cancer Treatment*, Retrieved January 05,2016, from cancer.gov: <https://www.cancer.gov/about-cancer/treatment/types/radiation-therapy/radiation-fact-sheet#r1>
3. American Cancer Society, (n.d). *Radiation Therapy Methods*, Retrieved January 05,2016, from cancer.org: <https://www.cancer.org/treatment/treatments-and-side-effects/treatment-types/chemotherapy.html?print=true&ssDomainNum=5c38e88&ssDomainNum=5c38e88>
4. Cancer Treatment Centers of America. (n.d.). *What is Brachytherapy*. Retrieved May 03, 2016, from brachytherapy.com: <https://www.cancer.org/treatment/treatments-and-side-effects/treatment-types/chemotherapy.html?print=true&ssDomainNum=5c38e88&ssDomainNum=5c38e88>
5. AAPM Radiation Therapy Committee, & Boyer, A. (2001). *Basic applications of multileaf collimators*. Madison: American Association of Physicists in Medicine.
6. de Oliveira, A. C. H., Vieira, J. W., & Lima, F. R. A. (2015). Monte Carlo modeling of multileaf collimators using the code Geant4. *Brazilian Journal of Radiation Sciences*, 3(1A).
7. *Treatment Delivery System Technical Specifications* [Brochure]. (n.d.). Cyberknife®
8. Echner, G. G., Kilby, W., Lee, M., Earnst, E., Sayeh, S., Schlaefer, A., ... & Lessard, E. (2009). The design, physical properties and clinical utility of an iris collimator for robotic radiosurgery. *Physics in medicine and biology*, 54(18), 5359.

9. Kathriarachchi, V., Shang, C., Evans, G., Leventouri, T., & Kalantzis, G. (2016). Dosimetric and radiobiological comparison of CyberKnife M6™ InCise multileaf collimator over IRIS™ variable collimator in prostate stereotactic body radiation therapy. *Journal of Medical Physics/Association of Medical Physicists of India*, 41(2), 135.
10. Jeraj, M., & Robar, V. (2004). Multileaf collimator in radiotherapy. *Radiol Oncol*, 38(3), 235-40.
11. Jabbari, K., Akbari, M., Tavakoli, M. B., & Amouheidari, A. (2016). Dosimetry and evaluating the effect of treatment parameters on the leakage of multi leaf collimators in ONCOR linear accelerators. *Advanced biomedical research*, 5.
12. Isabelle M. Germano (Ed.). (2000). *Linac and gamma knife radiosurgery*. Thieme.
13. Gammaknife. (n.d.). *Radiation delivery systems*. Retrieved. January 06, 2018. From gammaknife.com: <https://gammaknife.com/what-is-gamma-knife/>
14. Jochen et al, Linear accelerator with x-ray imaging elements mounted on curved support, United States Patent, PN: US 20050281389 A1, June 8, 2004
15. SIEMENS, (n.d.). *Surgical c-arms*. Retrieved. January 06, 2018. From [www.healthcare.siemens.com](http://www.healthcare.siemens.com/surgical-c-arms-and-navigation/mobile-c-arms/cios-spin): <https://www.healthcare.siemens.com/surgical-c-arms-and-navigation/mobile-c-arms/cios-spin>
16. Pinterest, (n.d.). *Beam delivery systems*. Retrieved January 07, 2018. From <https://tr.pinterest.com/>: <https://tr.pinterest.com/pin/567523990515020775/>
17. Jang, J., Kang, Y. N., Choi, B. O., Choi, I. B., Kim, M. C., Shin, D. O., ... & Kwon, S. I. (2007). Evaluation of the Accuracy of the CyberKnife. In *World Congress on Medical Physics and Biomedical Engineering 2006* (pp. 2024-2027). Springer, Berlin, Heidelberg.
18. Cyberknife. (n.d.). *Beam delivery systems*. Retrieved January 07, 2018. From <http://www.cyberknife.com/>: <http://www.cyberknife.com/technology>
19. Y. Kamino, S. Miura, M. Kokubo, I. Yamashita, E. Hirai, M. Hiraoka, and J. Ishikawa. Development of an Ultrasmall C-band Linear Accelerator Guide For a Four-dimensional Image-guided Radiotherapy System With a Gimbaled X-ray Head. *Medical Physics*, 34(5):1797–1808, May 2007.
20. J.M. Balter and Y. Cao. Advanced Technologies in Image-Guided Radiation Therapy. *Seminars in Radiation Oncology*, 17(4):293–297, 2007.
21. Wikipedia. (n.d.). *Linear particle accelerator*. Retrieved May 29,2016. From www.en.wikipedia.org: http://en.wikipedia.org/w/index.php?title=Linear_particle_accelerator&redirect=no#Medical_linacs

22. Weinmann, A. L., Hruska, C. B., & O'Connor, M. K. (2009). Design of optimal collimation for dedicated molecular breast imaging systems. *Medical physics*, 36(3), 845-856.
23. Talat, D., & Guvenis, A. (2016). Design and Evaluation of a Breast-Specific Collimator Using Response Surface Methodology and Monte Carlo Simulations. *IEEE Transactions on Nuclear Science*, 63(1), 98-107.
24. Jaszczak, R. J., et al. "Pinhole collimation for ultra-high-resolution, small-field-of-view SPECT." *Physics in medicine and biology* 39.3 (1994): 425.
25. Molazadeh, M., Zeinali, A., Robotjazi, M., Shirazi, A., & Geraily, G. (2017). Dosimetric characteristics of LinaTech DMLC H multi leaf collimator: Monte Carlo simulation and experimental study. *Journal of applied clinical medical physics*, 18(2), 113-124.
26. Zhou, D., Zhang, H., & Ye, P. (2016). Lateral penumbra modelling based leaf end shape optimization for multileaf collimator in radiotherapy. *Computational and mathematical methods in medicine*, 2016.
27. Ling, C. C., Zhang, P., Archambault, Y., Bocanek, J., Tang, G., & LoSasso, T. (2008). Commissioning and quality assurance of RapidArc radiotherapy delivery system. *International Journal of Radiation Oncology* Biology* Physics*, 72(2), 575-581.
28. Bohn, Multileaf Collimator and Radiation Therapy Device, United States Patent, PN: US 7,792,252 B2, Sep. 7, 2010
29. Ciscato et al, Collimator for Radiation Therapy, United States Patent, PN: 5,745,279, Apr.28, 1998
30. Pastyr et al, Contour Collimator for Radiation Therapy, United States Patent, PN: 4,794,629 Dec. 27, 1988
31. Pastyr et al, Contour Collimator for Radiation Therapy, United States Patent, PN: US 6,188,748 B1, Feb. 13, 2001
32. Swerdloff et al. Dynamic Collimator for Radiation Therapy, United States Patent, PN: 5,442,675, Aug. 15, 1995
33. JI et al. Collimator Device for Radiotherapy and Radiotherapy Apparatus Using the Same, United States Patent, PN: US 2009/0220046 A1, Sep.3, 2009
34. Green at al. Adjustable Collimator for Radiation Therapy, United States Patent, PN: 2,959,680, Nov. 8, 1960
35. Nunan, Multileaf Collimator for Radiotherapy Machines, United States Patent, PN: 4,868,844, Sep. 19, 1989

36. Kasper et al. Leave Collimator for Radiation Therapy, United States Patent, PN: US 7,386,099 B1, Jun. 10, 2008
37. Hartenberg, R. S., & Denavit, J. (1964). *Kinematic synthesis of linkages*. McGraw-Hill.

CURRICULUM VITAE



Name Surname: Mustafa Volkan YAZICI

Place and Date of Birth: ISPARTA 07.06.1993

Address: İzmir Katip Çelebi Üniversitesi Mühendislik ve Mimarlık Fakültesi, Mekatronik Mühendisliği Bölümü, Balatçık Kampüsü, Çiğli/İzmir, Türkiye

E-Mail: mustafa.v.yazici@gmail.com

B.Sc.: Mechanical Engineering

List of Completed Projects:

Design and development of a collimator mechanism that will be utilized in radiation therapy, International research project between Turkey IKCU (İzmir Katip Çelebi Üniversitesi) and South Korea DGIST (Daegu Gyeongbuk Institute of Science & Technology)

List of Publications:

Gezgin E. and Yazıcı M.V., Integration of the Function Generation Synthesis into the Design of a Multi-Leaf Collimator Journal of Mechanisms and Robotics (Under Review)